GEODESIC NETS WITH FEW BOUNDARY POINTS

BY

FABIAN PARSCH

A thesis submitted in conformity with
the requirements for the degree of
Doctor of Philosophy
Graduate Department of Mathematics
University of Toronto

ABSTRACT

Geodesic Nets with Few Boundary Points
Fabian Parsch
Doctor of Philosophy
Graduate Department of Mathematics
University of Toronto
2019

Geodesic nets on Riemannian manifolds form a natural class of stationary objects generalizing geodesics. Yet almost nothing is known about their classification or general properties even when the ambient Riemannian manifold is the Euclidean plane or the round 2-sphere.

We survey some results and open questions (old and new) about geodesic nets on Riemannian manifolds. A particular focus will be put on the question if the number of inner vertices (balanced vertices) in a geodesic net can be bounded by the number of boundary points (unbalanced vertices) or the total imbalance.

We prove that a geodesic net with three unbalanced vertices on a non-positively curved plane has at most one balanced vertex. We do not assume any a priori bound for the degree of unbalanced vertices. The result seems to be new even in the Euclidean case.

We demonstrate by examples that the result is not true for metrics of positive curvature on the plane, and that there are no immediate generalizations of this result for geodesic nets with four unbalanced vertices which can have a significantly more complicated structure. In particular, an example of a geodesic net with four unbalanced vertices and sixteen balanced vertices that is not a union of simpler geodesic nets is constructed. The previously known irreducible geodesic nets with four unbalanced vertices have at most two balanced vertices.

We provide a partial answer for a related question, namely a description of a new infinite family of geodesic nets on the Euclidean plane with 14 unbalanced vertices and arbitrarily many balanced vertices of degree ≥ 3.

To my grandparents, Franz, Hildegard, Renate and Siegfried,
who like so many of our grandparents worked tirelessly,
so that we can pursue our dreams today.

Meinen Großeltern, Franz, Hildegard, Renate und Siegfried,
die wie so viele unserer Großeltern unermüdlichen Einsatz erbrachten,
damit wir heute unseren Träumen folgen können.

To my parents, Marion and Werner,
who give advice at any time, but never ask for anything,
without whom I would not be the independent person that I am today,
and who are proof that in the uncountably infinite set of possible parents,
at least two maximal elements do exist.

Meinen Eltern, Marion und Werner,
die jederzeit Rat geben, aber nie etwas verlangen,
ohne die ich nicht der unabhängige Mensch wäre, der ich heute bin,
und die Beweis dafür sind, dass in der überabzählbar unendlichen Menge
möglicher Eltern mindestens zwei maximale Elemente existieren.

ACKNOWLEDGEMENTS

Doing a PhD would be impossible without great questions to work on. I want to thank my advisor Alexander Nabutovsky for his resourcefulness in coming up with many such questions until I found one that worked for me. Thank you for your inspiration, for your patience, for countless conversations, and for always keeping me motivated.

Many members of the Department of Mathematics faculty supported me on my way to the finish line. I want to particularly thank Almut Burchard for many productive conversations, Mary Pugh for sheer endless advice, and Bernardo Galvão-Sousa whose inspiration made it possible that I will soon be able to call these amazing people colleagues of mine.

I want to thank the great and truly indispensable staff of the Department, in particular Ida Bulat, who is missed by many every day. Without her encouragement, I would have never taken the leap to join the PhD program. And I want to thank Jemima Merisca. Your helpfulness and cheerfulness plays an essential part in every graduate student's success.

The Government of Canada very generously funded my research with a Vanier Canada Graduate Scholarship.

I would have never ended up in Canada if it weren't for Salma Kuhlmann. Thank you for encouraging me to give Toronto a try. I obviously didn't regret it.

Working on and – in particular – finishing a PhD would be impossible without your fellow graduate students. I want to thank Asif Zaman, Dan Soukup, James Mracek, Jeremy Lane and Jerrod Smith for being amazing friends. Thank you for your support and for enduring my rants, be they about grad school, politics or the imperial "system" of measurements.

Supporting my company while working on my PhD was always exciting thanks to Ewa Kurcinak, Hermann Lensch, Nora Finck, Ralf Bentien, Theresa Hunger and Tina Kirchhoff. Thank you for being such great colleagues.

Life is much more fun if people join you for the ride. Allen Chien, Constence Hsu and Stephanie Ma, thank you for making this ride much more exciting. Colleen Kurcinka and Carl Nagy, thank you for being not just great roommates but also great friends. Christoph Schiller, thank you for our hangouts and a lot of mutual career advice. Vanessa Foster, thanks to you I have been feeling at home in Canada from day one. Thank you for being my fellow Germanadian. Kevin Sieg, thank you for our many adventures since literally the first of our university days. I can't wait for the next one.

My family in Wössingen, Stuttgart, Jork, Neuenfelde and Weddingstedt is the best family I could have ever asked for. I am very grateful for having each and every one of you in my life. I want to particularly thank my brother and sister, Frederik and Yvonne. Growing up with you was a privilege. You have no clue how much you helped and inspired your little brother to become the person that he is today.

Most importantly, I want to thank my grandparents and my parents. Dedicating this thesis to you is my futile attempt at doing justice to your support.

PUBLICATIONS

Parts of this thesis have been or will be published in other places as follows:

The content of Chapter 3 as well as two of the examples presented in Chapter 4 are based on [Par19b] (accepted for publication in the *Journal of Differential Geometry* and available on the arXiv).

The example of an irreducible geodesic net in Chapter 4 was previously described in [Par19a] (submitted for publication and available on the arXiv).

Parts of the survey in Chapter 2 as well as the "star example" constructed in Chapter 5 also appear in [NP19] (submitted for publication and available on the arXiv).

CONTENTS

1 INTRODUCTION AND OVERVIEW 1
- 1.1 Geodesic Nets: Two Equivalent Definitions . . . 1
- 1.2 Geodesic Multinets . . . 2
- 1.3 Terminology and Conventions . . . 2
- 1.4 Chapter Overview . . . 3

2 QUESTIONS, ANSWERS AND OPEN PROBLEMS 5
- 2.1 Geodesic Nets in Euclidean Spaces . . . 5
- 2.2 Steiner Trees and Locally Minimal Geodesic Nets . . . 7
- 2.3 Survey Overview . . . 9
- 2.4 Closed Geodesic Nets and Multinets . . . 9
- 2.5 Three Unbalanced Vertices . . . 12
- 2.6 Four Unbalanced Vertices . . . 15
- 2.7 Bounding the Number of Balanced Vertices . . . 18
- 2.8 Gromov's Conjecture . . . 19

3 GEODESIC NETS WITH THREE BOUNDARY VERTICES 22
- 3.1 Structure of the Proof . . . 24
- 3.2 Local Properties . . . 25
- 3.3 Global Properties on the Flat Plane . . . 33
- 3.4 Main Proof on the Flat Plane . . . 46
- 3.5 The Case of Nonpositive Curvature . . . 50

4 CONSTRUCTION OF EXAMPLES 57
- 4.1 Four Vertices in the Plane . . . 57
- 4.2 An Irreducible Geodesic Net That is Not a Tree . . . 61
- 4.3 Three Vertices on a Surface of Positive Curvature . . . 68

5 THE STAR 70
- 5.1 Construction Toolbox . . . 71
- 5.2 The Iterative Construction . . . 75
- 5.3 Analyzing the Non-Deviated Construction . . . 86
- 5.4 Edges Under Deviation . . . 87
- 5.5 Studying the Sequence $\varphi_i'(0)$ . . . 92
- 5.6 Finding the Formulas for the Sequence $\varphi_i'(0)$ . . . 94

1 INTRODUCTION AND OVERVIEW

In this thesis, we will study geodesic nets and geodesic multinets, shedding light on some of their properties, both through theorems and important (counter)examples. This introduction will describe the notion of a geodesic (multi)net, using two equivalent definitions: one of a more variational nature, one with a more combinatorial viewpoint.

1.1 GEODESIC NETS: TWO EQUIVALENT DEFINITIONS

Consider a Riemannian manifold M. Geodesic nets on M are critical points[1] of the length functional on the space of embedded multigraphs[2] into M, where a certain subset of the set of vertices must be mapped to prescribed points of M. More formally, they can be defined as follows:

Definition 1.1 (Geodesic Net, Variational Perspective)**.** Let S be a finite (possibly empty) set of points in a Riemannian manifold M, and G a finite multigraph (or, more formally, a finite 1-dimensional cell complex). A *geodesic net modelled on G with boundary vertex set S* is a smooth embedding $f : G \hookrightarrow M$ such that:

(i) Every point of S is the image under f of a vertex of G, and

(ii) For any 1-parametric flow Φ_t, $t \in (-\epsilon, \epsilon)$ of diffeomorphisms of M that fixes the points of S, $\Phi_0 = \mathrm{Id}$ is a critical point of the function $l(t)$ defined as the length of $\Phi_t(f(G))$.

The simplest example of geodesic nets arises when $S = \{x, y\}$ is a set of two points, and $G = [0, 1]$ is the graph with two vertices and one edge. In this case, the geodesic nets modelled on G with boundary vertices x, y are precisely non-self-intersecting geodesics in M connecting x and y.

Applying the first variation formula for the length functional, we see that the above definition of a geodesic net is equivalent to the following:

1 but not necessarily local minima

2 graphs with possibly multiple edges between two vertices

Definition 1.2 (Geodesic Net, Combinatorial Perspective)**.** Let S be a finite (possibly empty) set of points in a Riemannian manifold M. A *geodesic net on M with boundary vertex set S* consists of a finite set V of points of M (called vertices) that includes S and a finite set E of non-constant geodesics between vertices (called edges) such that:

(i) Edges do not intersect or self-intersect, except possibly at endpoints.

(ii) For every vertex $v \in V \setminus S$, the following *balancing condition* holds: Consider the unit tangent vectors at v to all edges incident to v. Direct each unit tangent vector from v towards the other endpoint of the edge. Then the sum of all these unit tangent vectors must be equal to $0 \in T_v M$.

Note that, in particular, we are not considering geodesic rays. Edges must begin and end at a (balanced or unbalanced) vertex.

1.2 GEODESIC MULTINETS

In the above definitions, we do not allow edges in M to intersect. In particular, we are excluding the possibility that some edges coincide.

We could modify Definition 1.1 by allowing f to be only an immersion on the union of interiors of edges. In other words, one may allow edges to self-intersect and to intersect each other. In particular, we are allowing that two different edges between the same pair of vertices might have the same image.

As a result, the images of edges of G in M acquire multiplicities that can be arbitrary positive integer numbers. In this thesis, if a geodesic net is defined using immersions rather than embeddings of multigraphs, we call it a *geodesic multinet*. Note that self-intersecting geodesics connecting two points are examples of geodesic multinets.

We could also modify Definition 1.2 to allow an equivalent description of geodesic multinets as follows:

(i) Edges are allowed to intersect and self-intersect.

(ii) Each edge is endowed with a positive integer multiplicity. The unit tangent vector to an edge then enters the sum in the balancing condition at each endpoint with the multiplicity equal to that of the corresponding edge.

1.3 TERMINOLOGY AND CONVENTIONS

Working with the above definitions necessitates some additional terminology which will be used as follows throughout this thesis:

- Vertices in S as given by the above definitions are called *boundary vertices* or *unbalanced vertices*[3].
- Vertices in $V \setminus S$ are called *inner*, or *free*, or *balanced* (as the balancing condition must hold only at each vertex in $V \setminus S$).
- If v is an unbalanced vertex, then the sum of all unit tangent vectors to edges incident to v need not be equal to the zero vector. We call this sum the *imbalance vector at* v, $\mathrm{Imb}(v)$, and its norm the *imbalance at* v, $\mathrm{imb}(v)$. It is convenient to define $\mathrm{Imb}(v)$ also at balanced vertices as zero vectors in $T_v M$.
- The sum of imbalances $\sum_{v \in S} \mathrm{imb}(v)$ over the set of all unbalanced points is called the *total imbalance* of the geodesic net.

In the following, we will classify geodesic (multi)nets and consider many quantitative aspects. To do so, it is necessary to introduce some conventions:

- We are going to consider only *connected* geodesic (multi)nets, as the classification of disconnected nets obviously reduces to classification of their connected components.
- In particular, we require that no balanced vertex is isolated.
- As the degree of a balanced vertex clearly cannot be one, we see that the minimal degree of a balanced vertex becomes two. The balancing condition implies that for any balanced vertex of degree 2, its two incident edges can be merged into a single geodesic. Conversely, we can subdivide each edge of a geodesic net by inserting as many new balanced vertices of degree 2 as we wish. As now the role of balanced vertices of degree 2 in the classification of geodesic (multi)nets is completely clear, we are going to consider below only geodesic (multi)nets where *all balanced vertices have degree at least* 3.
- It is clear that we can add or remove geodesics connecting unbalanced vertices at will without affecting the balancing condition at a balanced vertex. Therefore, we agree that all considered geodesic (multi)nets *do not contain edges between unbalanced vertices.*

1.4 CHAPTER OVERVIEW

We will proceed as follows: Chapter 2 provides an overview of questions and problems surrounding geodesic nets and geodesic multinets, both solved and unsolved. It also includes examples illustrating many important behaviours.

3 We will observe later that unbalanced vertices do in fact not always have to be on the boundary of the convex hull of all vertices, making *unbalanced* vertices the more general choice of words.

Some of the answers and examples provided will be proved and constructed in this thesis: In Chapter 3, we will prove a theorem that a geodesic net with three boundary vertices on the plane endowed with a Riemannian metric of nonpositive curvature has at most one balanced vertex. Examples of geodesic nets will be constructed in Chapter 4, including those illustrating that the aforementioned theorem does not generalize to geodesic nets with four boundary vertices or to the case of positive curvature.

Finally, Chapter 5 will describe the construction of an example we call "the star", which is suggested as an example of a geodesic net with a bounded number of unbalanced vertices but an arbitrarily large number of balanced vertices. The chapter finishes with a conjecture that is strongly supported by numerical evidence suggesting that this example is in fact a geodesic net and not a geodesic multinet.

2

QUESTIONS, ANSWERS AND OPEN PROBLEMS

In this chapter, we will consider geodesic nets and multinets in the context of different ambient spaces. We will first consider fundamental properties of geodesic nets and their vertices with an initial focus on nets in Euclidean space. We continue with observing the similarities with and differences to the study of minimal networks (also known ass Steiner trees).

The main part will be a survey of nets both in Euclidean space and in other Riemannian manifolds, in particular closed Riemannian manifolds. Several of the Questions and Problems raised in this survey will be solved in the subsequent chapters.

2.1 GEODESIC NETS IN EUCLIDEAN SPACES

A significant part of this thesis will be devoted to geodesic nets in Euclidean spaces, in particular in the Euclidean plane. In this case it follows from Definition 1.2 that, given a finite[1] set of points S in $\mathbb{R}^n$, a geodesic multinet is a graph $G = (V, E)$ in $\mathbb{R}^n$ such that

(i) S is a subset of the set of vertices V,

(ii) each edge e is a straight line segment between its endpoints, and is endowed with a positive integer multiplicity $n(e)$, and

(iii) for each vertex $v \in V \setminus S$, there is zero imbalance, i.e. if $I(v)$ denotes the set of edges incident to v, then $\sum_{e \in I(v)} n(e) \frac{e}{\|e\|} = 0$, where e denotes an edge regarded as the vector in $\mathbb{R}^n$ directed from v towards the other endpoint.

For geodesic nets (instead of multinets), each $n(e)$ must be equal to 1, and, in addition, different edges are not allowed to intersect.

Figure 2.1 depicts examples of balanced vertices of degrees 3, 4 and 7 in $\mathbb{R}^2$. The following are easy to see:

- The angles between edges incident to a balanced vertex of degree 3 are always equal to 120°. This will be true not only for $\mathbb{R}^2$ but for all ambient Riemannian manifolds M.

1 Technically, we still allow S to be empty, but it is immediate that in Euclidan space, every nonempty geodesic net must have boundary vertices, so the case $S = \emptyset$ is of no interest.

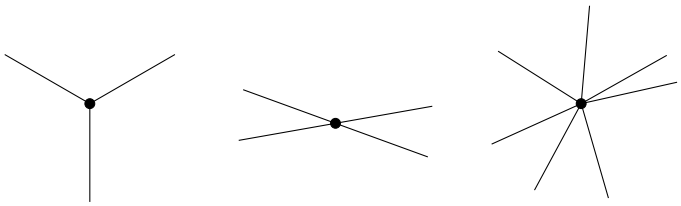

Figure 2.1: Examples for balanced vertices of degree 3, 4 and 7. Note that all edges have weight one.

- A balanced vertex v of degree 4 in the Euclidean plane is a point of intersection of two straight line segments formed by two pairs of incident edges at v. For arbitrary ambient Riemannian manifolds M, this generalizes to a transversal intersection between two geodesics.

Here are some other easily verified facts about geodesic (multi)nets in Euclidean spaces:

- Each geodesic multinet is contained in the convex hull of its unbalanced points.
- As a corollary each geodesic (multi)net with two boundary points is simply the straight line segment connecting these points (that can be endowed with any positive integer multiplicity in the case of geodesic multinets). Therefore, the interesting part of the classification of geodesic (multi)nets in the Euclidean plane begins with the case of three boundary points.
- For each geodesic (multi)net in $\mathbb{R}^n$, we can consider $\mathrm{Imb}(v)$ as vectors in the ambient space $\mathbb{R}^n$. Therefore, in this case one can also define the total imbalance vector. Yet this vector is always zero:

$$\sum_{v\in S} \mathrm{Imb}(v) = \sum_{v\in V} \mathrm{Imb}(v) = 0 \tag{2.1}$$

  Indeed, the second sum can be represented as the sum of contributions of individual edges. Each edge contributes two oppositely directed vectors that enter sums in the definition of imbalance vectors at its endpoints. Therefore, the sum over all edge contributions is zero.
- For a geodesic (multi)net G in a Euclidean space its length $L(G)$ is given by the following formula:

$$L(G) = -\sum_{v\in S} \langle v, \mathrm{Imb}(v)\rangle. \tag{2.2}$$

  On the right hand side we perform the summation over the set of all unbalanced vertices. Each vertex is also regarded as a vector in $\mathbb{R}^n$.

Proof of length formula (Equation 2.2). First observe that the right hand side does not change when we change the origin of the coordinate system in $\mathbb{R}^n$ (this easily follows from Equation 2.1). Therefore, we can assume that the origin is not on the net.

For each positive r, let D_r denote the ball of radius r centred at the origin, ∂D_r its boundary and $E(r)$ the set of edges of the net intersecting ∂D_r. For each $e \in E(r)$, let $e(r)$ denote the point of intersection of e and ∂D_r. Equation 2.2 is an immediate corollary of the following formula, when it is applied to very large values of r.

$$L(G \cap D_r) = \sum_{e \in E(r)} \left\langle e(r), \frac{e}{\|e\|} \right\rangle - \sum_{v \in D_r} \langle v, \mathrm{Imb}(v) \rangle \tag{2.3}$$

In this formula, we regard each edge e also as a vector in $\mathbb{R}^n$. We choose its direction from $e(r)$ towards the interior of D_r. This formula obviously holds when r is small, as both sides are equal to zero.

Define *special values* of r as those where ∂D_r is either tangent to one of the edges or passes through one of the vertices. There are only finitely many special values of r. Our next observation is that the right hand side of Equation 2.3 changes continuously when r passes through its special value. Obviously, one needs only to check what happens if ∂D_r passes through a balanced or an unbalanced vertex.

We conclude that it is sufficient to check that the derivatives of the right hand side and the left hand side with respect to r at each non-special point coincide. Each of these derivatives will be a sum over edges in $E(r)$ (a set that doesn't change away from non-special points).

To complete the proof, it is sufficient to verify that the contributions of each edge to both sides are the same. Each such edge e contributes $\frac{1}{\cos\theta_e(r)}$ to the derivative of the left hand side, where $\theta_e(r)$ denotes the angle between e and the position vector of $e(r)$. Its contribution to the right hand side is $(r\cos\theta_e(r))' = \cos\theta_e(r) - r\sin\theta_e(r)\theta_e'(r) = \frac{1}{\cos\theta_e(r)}$, as a trigonometric argument implies that $\theta_e'(r) = -\frac{\tan\theta_e(r)}{r}$.

This completes the proof of Equation 2.3 and therefore Equation 2.2. □

2.2 STEINER TREES AND LOCALLY MINIMAL GEODESIC NETS

The study of geodesic nets was originally motivated by the following question posed by Gauß: Given a set of points on the plane, connect them by means of a graph of the minimal possible length.

It is easy to see that this graph is always a geodesic net modelled on a tree (called the Steiner tree) where the given points are unbalanced

points. It typically also contains new balanced vertices. It is easy to prove that all balanced vertices of a Steiner tree have degree 3. The first and most fundamental example is the case of three points A, B, C on the plane forming a triangle with angles $< 120°$. In this case, there exists the (unique) point F in the triangle ABC, called the *Fermat Point*, such that the angles between any two of A, B, C at F are all equal to $120°$. The Steiner tree will consist of three edges FA, FB and FC (see Figure 2.2). The Steiner tree on four given (unbalanced) vertices might involve two extra (balanced) vertices (see Figure 2.2).

A geodesic net (in a Riemannian manifold) is called *locally minimal* if its intersections with all sufficiently small balls are Steiner trees (connecting the unbalanced points inside the ball with the points of intersection between the geodesic net and the boundary sphere). For geodesic nets in the Euclidean plane, the local minimality is equivalent to the requirement that all balanced points have degree 3. The locally minimal geodesic nets in Euclidean spaces and, more generally, Riemannian manifolds were extensively investigated by A. Ivanov and A. Tuzhilin (cf. [IT94], [IT16]).

Note that although general geodesic nets are not locally minimal with respect to this condition, they are locally minimal in the following less restrictive sense: For each point p on the net and all sufficiently small r, the intersection of the net with the ball of radius r provides the global minimum of the length among all trees *of the same shape* (i.e. star-shaped with the same number of edges) connecting the boundary points.

With this in mind, the idea of minimization of length might seem useful to find geodesic nets as follows: Assume we want to construct a geodesic net with the set S of boundary points modelled on a given graph G, say, in the Euclidean plane. Consider embeddings of G in the plane such that all edges are mapped into straight line segments, and a certain set of vertices is being mapped to S. Yet the positions of other vertices are variable, and we do not insist on the balancing condition at any vertex. Now we are

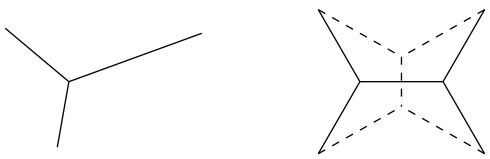

Figure 2.2: On the left, a geodesic net with 3 unbalanced vertices and 1 balanced vertex (the *Fermat Point*). This is in fact the maximal number of balanced vertices when only given 3 unbalanced vertices on the plane with a metric of nonpositive curvature (see Theorem 3.2). On the right, the two Steiner trees for four points are not maximal regarding the number of balanced vertices of a geodesic net with four unbalanced vertices (see examples in Chapter 4).

going to minimize the total length of all edges of the graph over the set of such embeddings. It is easy to see that the total length will be a convex function and has a unique minimum. Moreover, one can start with an arbitrary allowed embedding of G and use an easy algorithm based on gradient descent that numerically finds this minimum. This minimum will always be a geodesic net.

The problem is that in the process of gradient descent different vertices or edges can merge, and some edges can shrink to a point. In this case, the resulting graph will not be isomorphic to G anymore. In fact, our numerical experiments seem to indicate that if one starts from a random allowed embedding of G, one typically ends up with very simple geodesic nets such as, for example, the geodesic net with just one extra (balanced) vertex in the centre.

Furthermore, since not all geodesic nets are such local minima but often just critical points of the length functional, we run into the risk that numerical experiments overlook important examples. This makes finding more intricate examples of geodesic nets, like the ones in Chapter 4, such an interesting endeavour.

2.3 SURVEY OVERVIEW

We will now provide a survey of known results and conjectures regarding geodesic nets. In Section 2.4, we survey closed geodesic nets in closed Riemannian manifolds. In Section 2.5 and Section 2.6, we survey geodesic nets in Euclidean spaces and Riemannian surfaces respectively. We will emphasize the (im)possibility to majorize the number of balanced points in terms of the number of unbalanced points (and possibly also the total imbalance).

2.4 CLOSED GEODESIC NETS AND MULTINETS

Geodesic nets with $S = \emptyset$, i.e. no unbalanced vertices, are called *closed geodesic nets*. The simplest examples of closed geodesic nets are periodic geodesics (that can be modelled on any cyclic graph or the graph with one vertex and one loop-shaped edge) or, more generally, unions of periodic geodesics.

We could, for example, take the union of a finite number of great circles on the round 2-sphere, getting a closed geodesic net with an arbitrarily large number of intersections, each of which is a balanced vertex.

The simplest example of a closed geodesic net not containing a non-trivial periodic geodesic is modelled on the θ-graph with 2 vertices con-

nected by 3 distinct edges. The corresponding closed geodesic net consists of two vertices connected by 3 distinct geodesics, so that all angles between each pair of geodesics at each of the two vertices are equal to 120°.

J. Hass and F. Morgan [HM96] proved that for each convex Riemannian S^2 sufficiently close to a round metric, there exists a closed geodesic net modelled on the θ-graph. It is remarkable that this is the only known result asserting the existence of closed geodesic nets not composed of periodic geodesics on an open (in C^2 topology) set of Riemannian metrics on a closed manifold. In other words, the following problem is wide open.

Problem 2.1. Is it true that each closed Riemannian manifold contains a closed geodesic multinet not containing a non-trivial periodic geodesic?

The standard Morse-theoretic approach to constructing periodic geodesics fails when applied to constructing closed geodesic nets, as any gradient-like flow might make the underlying multigraph collapse to one or several closed curves and, thus, yields only a periodic geodesic.

A classification of shapes of closed geodesic nets on specific closed Riemannian surfaces is aided by the Gauß-Bonnet theorem and the obvious observation that if a geodesic net on, say, a Riemannian S^2 is modelled on a graph G, then G must be planar. Using these observations A. Heppes [Hep64] classified all closed geodesic nets on the round S^2, where all vertices have degree 3 (there are just nine possible shapes). On the other hand, we are not aware of any restrictions on shapes in closed Riemannian manifolds of dimension > 2.

The first question one might ask about closed geodesic nets in Riemannian manifolds of dimension ≥ 3 is the following:

Problem 2.2. Classify all 3-regular graphs G such that the round 3-sphere has a geodesic net modelled on G.

Another reasonable question (which, of course, can also be asked for surfaces) is:

Problem 2.3. Is it true that each closed Riemannian manifold of dimension ≥ 3 has a θ-graph shaped closed geodesic net?

To the best of our knowledge, nothing else is known about classification of geodesic nets on round S^2. In particular, the answer for the following problem posed by Spencer Becker-Kahn [BK] is not known even when M is the round 2-sphere.

Problem 2.4 (Becker-Kahn)**.** Let M be a closed Riemannian manifold. Is there a function f_M (depending on geometry and topology of M) such that each closed geodesic net on M of length L has at most $f_M(L)$ (balanced) vertices?

As we already noticed, the set of closed geodesic nets include periodic geodesics as well as their unions. Yet the standard "folk" argument involving the compactness of the set of closed curves of length $\leq x$ parametrised by the arclength on a closed Riemannian manifold, and a quantitative (Yomdin-style) version of the Sard-Smale theorem that implies that the set of non-constant periodic geodesics on a generic closed Riemannian manifold is countable, also implies the set of closed geodesic nets is countable as well. So, closed geodesic nets are also "rare". This fact might be at least partially responsible for the scarcity of examples of closed geodesic nets not containing periodic geodesics.

Surprisingly, many extremely hard open problems about periodic geodesics can be solved when asked about closed geodesic nets. Here are some results about the existence of closed geodesic nets with interesting properties:

- A. Nabutovsky and R. Rotman [NR07] proved the existence of a constant $c(n)$ such that each closed Riemannian manifold M^n contains a closed geodesic multinet of length $\leq c(n)vol(M^n)^{\frac{1}{n}}$. It also contains a closed geodesic multinet of length $\leq c(n)$ diameter(M^n). R. Rotman [Rot11] later improved this result and proved that one can choose a closed geodesic multinet satisfying these estimates that has the shape of a flower, i.e. consist of (possibly) multiple geodesic loops based at the same point (vertex).[2]
- Recently, L. Guth and Y.Liokumovich [GL] proved that for a generic closed Riemannian manifold, the union of all closed geodesic multinets must be a dense set.

Note that these results do not shed any light on the existence of closed geodesic nets that do not include any periodic geodesic on closed manifolds as all closed geodesic nets in these theorems might be just periodic geodesics. Yet, in dimensions > 2, it is completely unknown if either of the quoted results from [NR07] and [GL] holds for periodic geodesics instead of geodesic multinets.

Finally, note that closed geodesic multinets can be a useful tool to study other minimal objects on general closed Riemannian manifolds. For example, recently R. Rotman [Rot] proved that for each closed Riemannian manifold M^n and positive ϵ, there exists a "wide" geodesic loop on M^n with the angle greater than $\pi - \epsilon$ so that its length is bounded only in terms of n, ϵ and the volume of M^n. Alternatively, one can also use the diameter of M^n instead of its volume. The proof involves demonstrating the existence of closed geodesic multinets with certain properties. Yet these

2 Of course, the balancing (stationarity) condition at this point must hold.

nets can turn out to be a periodic geodesic in which case the short wide geodesic loop will be a short periodic geodesic as well.

Our last remark about closed geodesic multinets is that in some sense they can be considered a better 1-dimensional analog of minimal surfaces in higher dimensions than periodic geodesics. Indeed, minimal surfaces tend to develop singularities. Their existence is frequently proven through a version of Morse theory on spaces of cycles, where the resulting minimal surface first arises as a stationary varifold. Similar arguments using the space of 1-cycles lead to proofs of existence of closed geodesic multinets that can be regarded as a particularly nice class of stationary 1-varifolds.

We refer the reader to [AA76] for properties of stationary 1-varifolds including a version of Equation 2.2 ("monotonicity formula") valid for stationary 1-varifolds, and, therefore, closed geodesic multinets on Riemannian manifolds.

2.5 THREE UNBALANCED VERTICES ON THE EUCLIDEAN PLANE AND MORE GENERAL RIEMANNIAN SURFACES

Recall the convention in Section 1.3 to consider only connected geodesic (multi)nets with balanced vertices of degree ≥ 3 and without edges running between unbalanced points.[3]

We are going to start from the description of the following example (see Figure 2.3):

Example 2.5. Let $A_1A_2A_3$ be a triangle. Denote its angle at A_i by α_i. Assume that for each $i = 1, 2, 3$, $\cos\frac{\alpha_i}{2}$ is a rational number.

It is easy to produce an infinite set of such triples of angles using Pythagorean triples of integers. For example, we can take $\alpha_1 = \alpha_2 = 2\arccos(\frac{12}{13})$, and $\alpha_3 = \pi - \alpha_1 - \alpha_2$. Any choice of angles α_i determines the triangle $A_1A_2A_3$ up to a similarity. The exact choice of its side lengths is not important to us.

As $\cos\frac{\alpha_i}{2}$ is rational, it can be written as $\frac{m_i}{n_i}$ for positive integer m_i and n_i. Let N denote $n_1n_2n_3$ and N_i denote the integer $\frac{m_iN}{n_i}$. Further, let $0 < r_1 < r_2 < \ldots < r_k < 1$ and let O denote the point of intersection of bisectors of angles α_i.

The set of vertices of a geodesic multinet that we are going to describe looks as follows: It has three unbalanced vertices A_1, A_2 and A_3. To describe its set of balanced vertices consider k homotheties of $A_1A_2A_3$ with center O using ratios $r_1, \ldots, r_k$. Denote the corresponding vertices of the homothetic triangles by $A_1^jA_2^jA_3^j$, $j \in \{1, \ldots, k\}$.

3 However, it is still possible that the union of two or more edges forms a segment between two unbalanced points; of course, this segment will not be an edge.

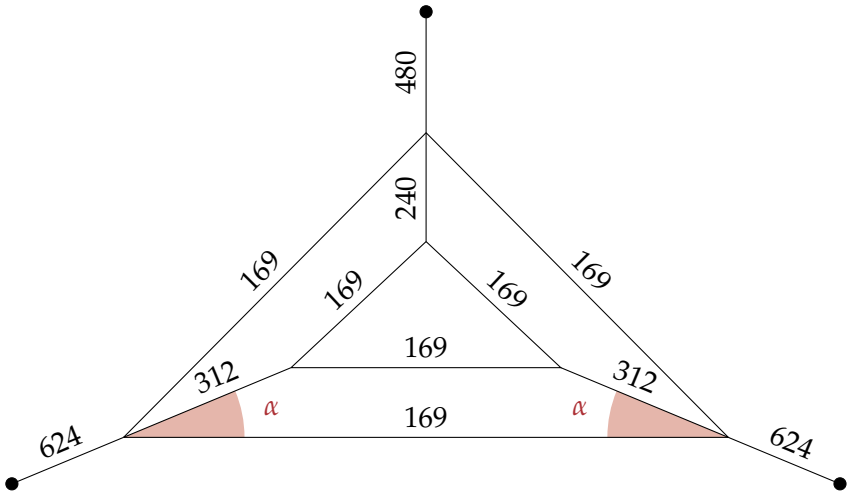

Figure 2.3: An example of a geodesic *multi*net with three unbalanced vertices and six balanced vertices. Through continuous nesting, the number of balanced vertices can be increased arbitrarily. However, this is at the expense of additional imbalance at the three unbalanced vertices. In this example, $\cos\alpha = 12/13$ and $\sin\alpha = 5/13$

The set of balanced vertices of the geodesic multinet will include all vertices A_i^j. Observe that for each $i = 1, 2, 3$, the vertices A_i^j will subdivide $A_i^1 A_i$ into k segments. We are going to denote these segments by e_i^j, $j = 1, \ldots, k$ where the numeration by superscripts j goes in the order from A_i^1 to A_i, so that $e_i^1 = A_i^1 A_i^2$ and $e_i^k = A_i^k A_i$. All these segments e_i^j will be edges of the geodesic multinet; the weight of e_i^j will be equal to $2jN_i$.

The set of edges of the multinet will also include the three sides of each triangle $A_i^j A_2^j A_3^j$, all these edges will be endowed with the same weight N.[4] Now an easy calculation confirms that we, indeed, constructed (an uncountable family of) geodesic multinets with 3 unbalanced points and $3k$ balanced points, where k can be arbitrarily large.

However, we would like to make the following observations:

- The weights of at least some of the edges (e.g. $A_i^k A_i$) become unbounded, as $k \longrightarrow \infty$.
- In fact, the total imbalance will increase linearly with k, as $k \longrightarrow \infty$.
- The condition of rationality of the trigonometric functions of $\frac{\alpha_i}{2}$ is very restrictive. We were able to carry out our construction only for a set of triples of points A_1, A_2, A_3 of measure 0 in the space of all vertices of triangles in the Euclidean plane.

4 Of course, in the end, we can divide all weights by their gcd, if it is greater than 1

Looking at this example, one might be led into thinking that the constructed geodesic multinets with 3 unbalanced vertices and arbitrarily many balanced vertices can be converted into a geodesic net by some sort of a small perturbation, where the balanced vertices are replaced by “clouds" of nearby points (with some extra edges inside each cloud), and all multiple edges are replaced by close but distinct edges running between chosen nearby “copies" of their former endpoints. It is easy to believe that such a perturbation plus, maybe, some auxiliary construction will be sufficient to construct examples of geodesic nets in the plane with 3 unbalanced vertices and an arbitrary number of balanced vertices.

Yet all such hopes are shattered by the following theorem that we will prove in Chapter 3.

Theorem 2.6. *A geodesic net with* 3 *unbalanced vertices* A_1, A_2, A_3 *in the Euclidean plane has exactly one balanced vertex* F *at the Fermat point of the three unbalanced vertices and three edges* FA_i. *Moreover, this assertion is true for geodesic nets with* 3 *unbalanced vertices on* $\mathbb{R}^2$ *endowed with any non-positively curved Riemannian metric.*[5]

Note that Section 4.3 contains an example demonstrating that this assertion is no longer true without the sign restriction on the curvature of the Riemannian plane. Yet it is not known if the assertion is still true if the integral of the positive part of the curvature is sufficiently small. The example for positive curvature constructed in Section 4.3 requires total curvature at least π.

The striking contrast between Example 2.5 of geodesic multinets with 3 unbalanced vertices and the extreme rigidity of geodesic nets with three unbalanced vertices on the Euclidean plane leads to some intriguing open questions such as the following.

Problem 2.7. Let Σ be the set of all triples S of points of the Euclidean plane such that there exist geodesic multinets with 3 unbalanced vertices at S and arbitrarily many balanced vertices. Is it true that Σ is a set of measure zero in $(\mathbb{R}^2)^3$?

Problem 2.8. Is there a function $f(n)$ such that for each geodesic multinet with three boundary vertices in the Euclidean plane such the that multiplicities of all edges do not exceed n the number of balanced vertices does not exceed $f(n)$?

Problem 2.9. Classify all geodesic multinets in the Euclidean plane with 3 unbalanced vertices.

5 Note that there are additional trivial cases if we allow edges between two unbalanced vertices. We excluded those earlier, see conventions in Section 1.3

2.6 FOUR UNBALANCED VERTICES IN THE EUCLIDEAN PLANE AND EUCLIDEAN 3-SPACE

Consider the following definition: Given several points $A_1, \ldots, A_k$ in the Euclidean space $\mathbb{R}^n$, there is always the unique point $F \in \mathbb{R}^n$ (which we also call Fermat point) such that at F, the sum of distances $\sum_{i=1}^{k} \operatorname{dist}(x, A_i)$ attains its global minimum.[6]

As explained previously, for three points forming a triangle with the angles $< 120°$, F is the point such that all three angles between any two points at F are equal to $120°$. For four points in the plane at the vertices of a convex quadrilateral, F is the point of intersection of the two diagonals. For four vertices of a regular tetrahedron, F is its centre. If F is not one of the points A_i, then the star-shaped tree formed by all edges FA_i is a geodesic net with unbalanced vertices $A_1, \ldots, A_k$ and the only balanced vertex at F.

If A_1, A_2, A_3, A_4 are, say, vertices of a square or a rectangle close to a square one has two other well-known and "obvious" geodesic nets with unbalanced vertices at A_i. Both these nets are $\rangle\!\!-\!\!\langle$ shaped (see Figure 2.2): They have two new balanced vertices F_1 and F_2 connected by an edge. Each balanced vertex is connected by edges with a pair of unbalanced vertices, so that all three angles at each of F_1 and F_2 are 120 degrees, and each of the four unbalanced vertices is connected with exactly one balanced vertex. There are three ways to partition a set of four vertices into two unordered pairs, yet only those where the unbalanced vertices in each pair are connected by a side of the convex quadrilateral can "work". Of course, the locations of balanced points F_1, F_2 will be different for the two ways to partition the set of four sides of the quadrilateral into pairs. Note that exactly the same idea works for the regular tetrahedron: Each of three pairs of opposite edges gives rise to a $\rangle\!\!-\!\!\langle$ shaped geodesic net with two balanced vertices.

The example constructed in Section 4.1 shows that given vertices $A_1, \ldots, A_4$ of a convex quadrilateral close to a square but in general position, one can combine the star-shaped net with one balanced point at the point of intersection of diagonals, the two $\rangle\!\!-\!\!\langle$ shaped nets and four star-shaped geodesic nets with unbalanced points at the vertices of each of 4 triangles formed by all triples of four vertices A_i. This way, one obtains a geodesic net with 28 balanced vertices (see Figure 2.4)[7]. This example might seem like a strong indication that no analog of Theorem 2.6 for geodesic nets with 4 unbalanced vertices is possible.

---

6 This fact is an immediate corollary of the convexity of the function $\sum_i \operatorname{dist}(A_i, x)$.

7 This number includes some extra balanced vertices at points of intersection of edges of geodesic nets that are being combined

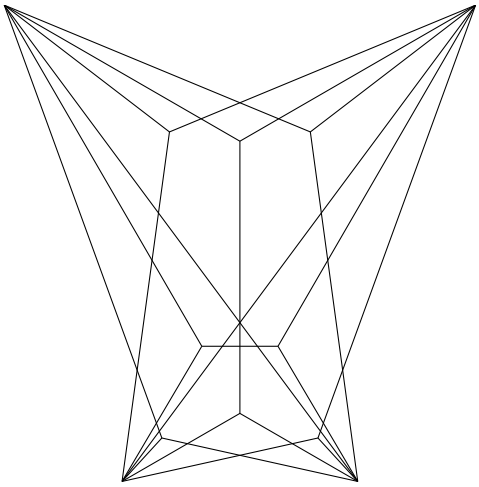

Figure 2.4: A geodesic net in the plane with four unbalanced vertices which is an "overlay" of trees, as constructed in Section 4.1

At the same time, however, note that this example is – as explained above – an overlay of trees. This motivates the definition of *irreducible* geodesic nets on a given set S of unbalanced vertices as geodesic nets such that no subgraph formed by a proper subset of the set of edges (with all incident vertices) is a geodesic net with unbalanced vertices in S. It is clear that classification of geodesic nets boils down to the classification of irreducible nets. As so far we have only two "obvious" isomorphism types of geodesic nets with 4 unbalanced vertices (namely, χ shaped and $\bowtie$ shaped trees), one might still suspect that there exists an easy classification of geodesic nets with 4-vertices on the Euclidean plane.

Yet the situation changed (at least for us) after we discovered a new example of an irreducible geodesic net with 4 unbalanced vertices at four vertices of the square and 16 balanced vertices (see Figure 2.5) A detailed description of this example can be found in Section 4.2. Now a natural next step in classification of geodesic nets on 4 vertices in the plane would be the following problem:

Problem 2.10. Find an irreducible geodesic net with 4 unbalanced vertices in the Euclidean plane with more than 16 vertices (or prove that such a geodesic net does not exist.)

In fact, we believe the following:

Conjecture 2.11. *There exist geodesic nets in the Euclidean plane with* 4 *unbalanced vertices and an arbitrarily large number of balanced points. (Moreover, we would not be surprised if this assertion is already true in the case when the set of unbalanced vertices coincides with the set of vertices of a square).*

Note that we are not aware of any analogs of this geodesic net with 4 unbalanced and 16 balanced vertices when 4 unbalanced vertices are non co-planar points in the Euclidean 3-space, e.g. the vertices of the regular tetrahedron. Yet in this case there exists a geodesic net with 4 unbalanced vertices A_i and 7 balanced vertices obtained as follows (see Figure 2.6):

Start from the star-shaped geodesic net with the balanced vertex at the center of the regular tetrahedron. For each of 6 triangles A_iA_jO – where i, j run over the set of all unordered distinct pairs of numbers $1, 2, 3, 4$ – attach the Y-shaped geodesic net with unbalanced vertices at A_i, A_j and O and a new balanced vertex at the center of the triangle A_iA_jO.

Nevertheless, it seems that it is harder to construct irreducible nets with unbalanced vertices at the vertices of a regular tetrahedron than at the vertices of a square. We would not be surprised if the answer for the following question turns out to be positive, which is the three-dimensional analog of Theorem 2.6.

Problem 2.12. Is there a number N such that each irreducible geodesic net with unbalanced vertices at all vertices of a regular tetrahedron has at most N balanced vertices?

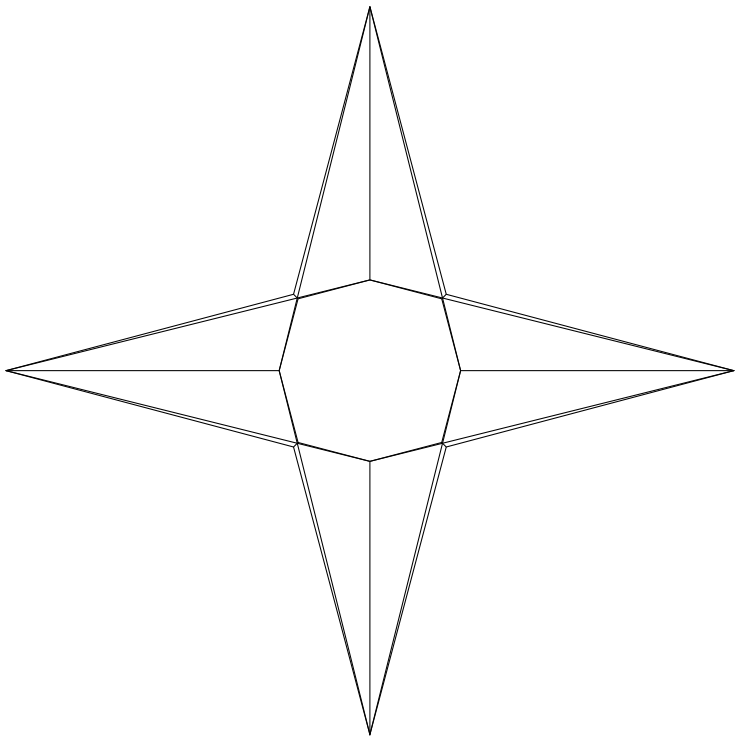

Figure 2.5: An irreducible geodesic net with four unbalanced vertices that is not a tree, as constructed in Section 4.2

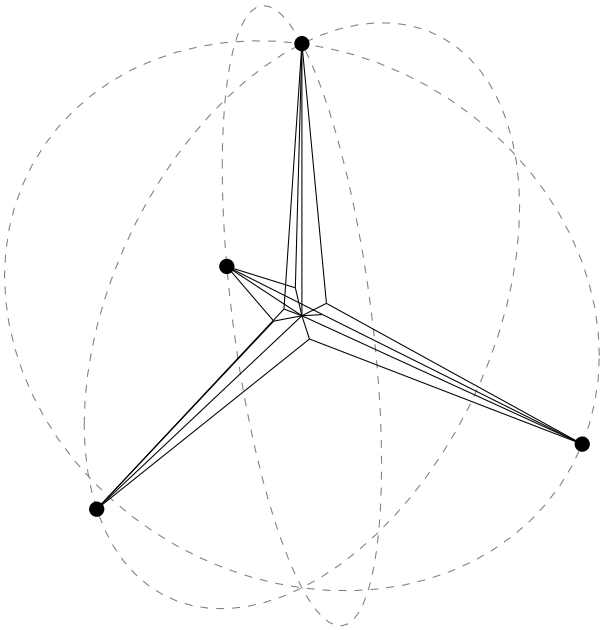

Figure 2.6: A geodesic net in Euclidean three-space, with four unbalanced and seven balanced vertices

2.7 GEODESIC NETS IN THE PLANE: BOUNDING THE NUMBER OF BALANCED VERTICES IN TERMS OF THE NUMBER OF UNBALANCED VERTICES

We cannot solve Problem 2.10. Yet in Chapter 5, we are going to describe a construction of a certain family of irreducible geodesic multinets $G_n(\varphi)$ with 14 unbalanced vertices (7 of which are fixed and 7 of which are variable) and arbitrarily many balanced vertices. We *believe* that these geodesic multinets are, in fact, geodesic nets. Our faith is based on the following facts:

- Numerical evidence suggests that the first 100 geodesic multinets from our list are, indeed, geodesic nets. The number of balanced vertices of $G_n(\varphi)$ is greater or equal than $7n$.
- We constructed a sequence of functions φ_i of one real variable φ. If for each N, some N functions $\varphi_i(\varphi)$ are pairwise distinct in a neighbourhood of 0, then our construction indeed produces geodesic nets with at least $7N$ balanced vertices. The functions $\varphi_i(\varphi)$ are presented by an explicit, yet very complicated set of recurrent relations. Whenever there seem to be no reason for any pair of these functions to coincide, the formulae are so complicated that the proof of this fact eludes us.

Note that while the imbalances at the seven constant vertices are unbounded, the imbalance at 7 variable vertices remain bounded. This leads us to a belief that some modification of our construction might lead to elimination of several variable unbalanced points leaving us only with seven constant unbalanced points. Moreover, we believe that it is possible that our construction will "survive" small perturbations of the seven constant unbalanced points. As a result we find that the following conjecture is very plausible:

Conjecture 2.13. *There exist N_0 and an N_0-tuple S such that for each N there exists a geodesic net with S being its set of unbalanced vertices and the number of balanced vertices greater than N.*

Furthermore, there exist not merely one such N_0-tuple S but a subset of $(\mathbb{R}^2)^{N_0}$ of positive measure (or even a non-empty open subset) of such N_0-tuples.

2.8 GROMOV'S CONJECTURE

As we saw, even for the simplest geodesic multinets in the Euclidean plane, there is no upper bound for the number of balanced vertices in terms of the number of unbalanced vertices. The example mentioned in section Section 2.7 and explained in detail in Chapter 5 strongly suggests, that such a bound does not exist already for geodesic nets. The length of a geodesic net cannot be of great help either, as we can rescale any geodesic net to an arbitrarily small (or large) length without changing its shape. One appealing conjecture due to M. Gromov is the following:

Conjecture 2.14 (M. Gromov)**.** *The number of balanced vertices of a geodesic net in the Euclidean plane can be bounded above in terms of the number of unbalanced vertices and the total imbalance.*

In fact, we do not see any reasons why this conjecture could not be extended to geodesic multinets.

Note that the following example demonstrates that one cannot majorize the number of balanced points only in terms of the total imbalance without using the number of unbalanced vertices (see Figure 2.7): Take a copy of a regular N-gon, and obtain a second copy by rotating it by $\frac{\pi}{N}$ about its center. Take a geodesic net obtained as the union of these two copies of the regular N-gon. The set of unbalanced vertices will consist of $2N$ vertices of both copies. Yet as sides of two copies intersect, we are going to obtain also $2N$ balanced vertices that arise as points of intersections of various pairs of sides. The imbalance at each unbalanced vertex is $2\sin\frac{\pi}{N}$, so the total imbalance is $4N\sin\frac{\pi}{N} < 4\pi$. We see that when $N \longrightarrow \infty$, the number of balanced points also tends to ∞, yet the total imbalance remains uniformly bounded.

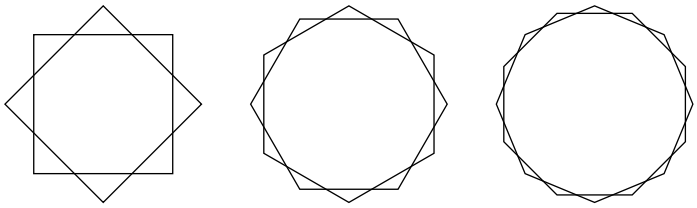

Figure 2.7: This construction shows that there is a sequence of nets with bounded imbalance, but arbitrarily many balanced vertices

It is worth pointing out that this example matches the length formula in Equation 2.2: Assuming the unbalanced points are arranged on a unit circle, both the imbalance and the length of the geodesic net approach 4π.

The above conjecture by Gromov was published in the paper by Y. Memarian [Mem15] for geodesic nets such that all imbalances are equal to one (in our terms).

Since in this case the total imbalance is equal to the number of unbalanced vertices, the conjecture is that the number of unbalanced vertices does not exceed the value of some function of the number of balanced vertices. Note also that [Mem15] contains the proof of this restricted version of the conjecture in cases, when the degrees of all balanced vertices are either all equal to 3, or all are equal to 4.

Yet, the following simple observation implies that the restricted form (with imbalances equal to 1 at each unbalanced vertex) is, in fact, equivalent to the full Conjecture 2.14.

The observation is that if v is an unbalanced vertex, then it can be extended by adding less than $\operatorname{imb}(v) + 3$ new edges starting at v so that v becomes balanced. Applying this trick to all imbalanced vertices we replace our original geodesic net by a new one, with the number of vertices not exceeding the sum of the total imbalance and twice the number of unbalanced vertices such that the imbalance of each unbalanced vertex is equal to one. Thus, the restricted version of the conjecture implies the general version.

We are going to explain this observation in the case when $\operatorname{imb}(v) \in (0,1)$, leaving the general case to the reader. In this case we need to find three new edges starting at v such that their angles α_1, α_2 and α_3 with the imbalance vector $\operatorname{Imb}(v)$ satisfy the balancing condition that can be written in the scalar form as a system of two equations: $\sum_{i=1}^{3} \cos\alpha_i = \operatorname{imb}(v)$ and $\sum_{i=1}^{3} \sin\alpha_i = 0$. It is clear that this system has an uncountable set of solutions. This fact enables us to ensure that none of the new edges coincide with already existing edges incident to v.

Note that Equation 2.2 implies that the length of a geodesic net does not exceed the product of its total imbalance and the diameter (which

for geodesic nets in the Euclidean space is always equal to the maximal distance between two unbalanced points). Further, we can always rescale a geodesic net in the plane so that its diameter becomes equal to 1. In this case its length becomes equal to $\frac{L}{D}$, where L and D are the values of the length and the diameter before rescaling. Therefore, Conjecture 2.14 would follow from the validity of the following conjecture:

Conjecture 2.15. *There exists a function f such that each geodesic multinet in the Euclidean plane with n unbalanced vertices, diameter D, and total length L has less than $f\left(\frac{L}{D}, n\right)$ balanced vertices.*

Now we would like to combine this conjecture with the Becker-Kahn Problem 2.4 and extend it to all Riemannian manifolds. Before doing so, consider the example of a complete non-compact Riemannian manifold which is a disjoint union of (smooth) capped cylinders that have a fixed length but are getting thinner. More specifically, the cylinders have radii $\frac{1}{n}$ for all positive integers n but fixed diameter of 1. On any of these cylinders, we can now add N closed geodesics around the waist of the cylinder, connecting all of them with a single closed geodesic that travels twice along the diameter of the manifold. Such a net will have $2N$ balanced vertices and fixed diameter $D = 1$, but as long as N/n is small enough, the length of the net L gets arbitrarily close to 2. So both L/D and L stay bounded whereas the number of balanced vertices can be chosen to be arbitrarily large. Note that we could make this manifold connected by connecting consecutive cylinders by thinner and thinner tubes of length 1.

This example shows that for general Riemannian manifolds, we can't bound the number of unbalanced vertices in terms of L/D, L, and the number of balanced vertices. So we must either bound the injectivity radius of our Riemannian manifold M from below, or, more generally, adjust the length as follows: The *adjusted total length* $\tilde{L}$ of a geodesic net is the sum of integrals over all edges e_i (parametrized by their respective arclengths) of $\frac{1}{\mathrm{inj}(e_i(s))}$, where $\mathrm{inj}(e_i(s))$ denotes the injectivity radius of the ambient Riemannian manifold at $e_i(s)$. If M is a Riemannian manifold with a positive injectivity radius inj, then $\tilde{L} \leq \frac{L}{\mathrm{inj}}$. Now we can state our most general conjecture.

Conjecture 2.16 (Boundedness conjecture for geodesic nets on Riemannian manifolds)**.** *Let M be a complete Riemannian manifold. There exists a function f_M which depends on M, but is invariant with respect to rescalings of M, with the following property: Let G be a geodesic net on M with total length L, adjusted length $\tilde{L}$ and diameter D that has n unbalanced vertices. Then its number of balanced vertices does not exceed $f_M\left(\tilde{L}, \frac{L}{D}, n\right)$. In particular, if M has injectivity radius* $\mathrm{inj} > 0$*, then the number of balanced vertices does not exceed $f_M\left(\frac{L}{\mathrm{inj}}, \frac{L}{D}, n\right)$.*

3

GEODESIC NETS WITH THREE BOUNDARY VERTICES

In this chapter, we will consider geodesic nets with three unbalanced vertices. Note that for three unbalanced vertices, the expressions *unbalanced vertices* and *boundary vertices* are indeed interchangeable (this will be formalized in Lemma 3.10).

Two of the most intuitive examples of geodesic nets on the flat plane with three unbalanced vertices are described as follows:

- A triangle with its three vertices and three edges is a geodesic net with three unbalanced and no balanced vertices.
- On the other hand, we can consider three points arranged in a triangle with all interior angles less than 120°. We can position a point inside the triangle so that, if connected to the three corners, this point is balanced (see Figure 3.1). That such a *Fermat point* exists is a result of classic Euclidean geometry.

Obviously, one can combine these two examples, but in any case one gets a geodesic net with three unbalanced vertices and at most one balanced vertex. This raises the question: Is there a geodesic net with three unbalanced vertices but more than one balanced vertex? More generally:

Question 3.1. Given the number of unbalanced vertices of a geodesic net, what is the maximal number of balanced vertices that the net can have?

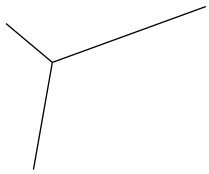

Figure 3.1: A geodesic net with 3 unbalanced vertices and 1 balanced vertex (the *Fermat Point*). We will show that this is in fact the maximal number of balanced vertices when only given 3 unbalanced vertices on the plane with a metric of nonpositive curvature.

This question is quite general in the following sense: We are assuming no a priori information on the distance/relative position of the unbalanced vertices. That is the bound should only depend on the number of unbalanced vertices. We also allow the unbalanced vertices to have arbitrary degree and therefore arbitrary imbalance.

We will show that, if the surface is $\mathbb{R}^2$ with a metric of nonpositive curvature (including flat and hyperbolic space as two special cases), then the configuration with the Fermat Point in Figure 3.1 is in fact maximal. Here is the main theorem of this chapter:

Theorem 3.2 (Main Theorem)**.** *Each geodesic net with 3 unbalanced vertices (of arbitrary degree) on the plane endowed with a Riemannian metric of non-positive curvature has at most one balanced vertex.*

In fact, the theorem is new even in the case when dealing with geodesic nets in the Euclidean plane (and the proof is almost as difficult as in the general case). On the other hand, the result is false for metrics of positive curvature on the plane. In Section 4.3, we exhibit and example of a geodesic net with 3 unbalanced and 3 balanced vertices on the round hemisphere (of course this Riemannian metric could be extended to a positively curved metric on the whole plane).

This result for three unbalanced vertices is somewhat surprising in the context of the examples in Section 4.1 and Section 4.2 which are showing that with four unbalanced vertices in the plane, there are nets with at least 28 balanced vertices as well as irreducible nets including cycles. Note that we do not claim that those examples are maximal. In fact, we think that, unlike for three unbalanced vertices, there is no maximal example for four unbalanced vertices, see Conjecture 2.11.

Conventions

Recall our conventions from Section 1.3. We require balanced vertices to have degree 3 or more. In fact allowing degree 2 balanced vertices would render the question meaningless: Obviously, one could add an arbitrary number of degree 2 balanced vertices to the edges of any geodesic net.

Also note that we do not put any bound on the degree of the unbalanced vertices. In other words, we allow a single unbalanced vertex to be adjacent to an arbitrary number of balanced vertices.

Previous results

In [Mem15], Memarian considered the question on the Euclidean plane with one restriction: each unbalanced vertex has degree 1. He studied

two special cases: If all balanced vertices have degree 3, he finds a sharp upper bound for what he calls *3-boundary regular critical graphs*. The bound is achieved by what resembles a tiling of the plane by hexagons. If all balanced vertices have degree 4, he notes the (presumably not sharp) upper bound given by the maximal number of intersections between straight line segments.

As Memarian points out, though, these two cases depend highly on the geometric restrictions that can be presumed for balanced vertices of degree 3 or degree 4: Indeed we observed in Section 2.1 that for degree 3, the edges must be arranged equiangularly around the vertex with angles of 120° between them. For degree 4, the vertex and its incident edges are given as the intersection of two straight lines (or, more generally, two geodesic segments). The examples in Figure 2.1 shows that for higher degrees, on the other hand, balanced vertices can be quite irregular.

This leaves the problem open for the case that we do not put a limit on the degree of the balanced vertices, and for the case of nonzero curvature. In fact, even the case of a planar geodesic net that has a mix of nothing but degree 3 and degree 4 balanced vertices is left open. Furthermore, as stated before, we will not require the unbalanced vertices to have degree 1 but instead allow arbitrary degree.

3.1 STRUCTURE OF THE PROOF

From now on, unless specified otherwise, any graph discussed will be a geodesic net $G = (V, E)$ with boundary vertex set $S \subset V$ as given by Definition 1.2.

We will prove the following reformulation of the main theorem.

Theorem 3.3. *Define $f : \mathbb{N}_0 \to \mathbb{N}_0 \cup \{\infty\}$ as follows: $f(n)$ is the smallest number such that $|V \setminus S| \leq f(|S|)$ is true for all geodesic nets on $\mathbb{R}^2$ with a metric of nonpositive curvature. Then*

(a) $f(0) = f(1) = f(2) = 0$
(b) $f(3) = 1$

Note that the bound for $n = 0, 1$ is obvious and the bound for $n = 2$ is nearly trivial as will be seen in Lemma 3.10. The case for $n = 3$ is the actually interesting result that we will prove.

To prove the theorem, we proceed as follows: We will first study the properties of a single balanced vertex in Section 3.2. In particular, we will prove restrictions on the angles between the edges. We will use these properties in Section 3.3 when we turn to global properties on the flat plane and study how the angles between edges not incident to the same

vertex are related by introducing the *turn angle* along a path. We will then prove the result regarding three vertices on the plane in Section 3.4. The results of Section 3.3 and Section 3.4 will then be generalized to the case of nonpositive curvature in Section 3.5.

This theorem obviously asks for an extension to larger n or positive curvature. We will construct an example for a gedesic net with $n = 4$ in Section 4.1. Furthermore, in Section 4.3, we will construct a geodesic net on a surface of positive curvature with just three unbalanced vertices but more than one balanced vertex. This example shows that Theorem 3.2 can't be true for metrics of positive curvature on $\mathbb{R}^2$, even when no closed geodesics exist.

3.2 LOCAL PROPERTIES

In the following, we prove helpful lemmas that describe local properties in the sense that they "zoom in" on a single vertex without considering properties of any other vertices of the geodesic net. It is important to point out that these local properties apply to the vertices of a geodesic net on any surface, no matter the curvature since we only consider the tangent space at a single vertex.

General Local Properties

Definition 3.4. Generally, if we consider several edges incident to the same vertex, we enumerate them in counterclockwise order, e.g. when we say "b directly follows a".

Note the following two facts:

Lemma 3.5. *If we draw a geodesic through any balanced vertex, there must always be an edge on each side of that line.*

Proof. Recall that a balanced vertex has at least degree 3 which means even after discounting for the possibility that two edges lie on the geodesic, there must be another edge lying on one side of it. To balance the unit vector parallel to that edge, one needs an edge on the other side of that geodesic, too. □

Lemma 3.6. *The angle between an edge at a balanced vertex and its immediately following edge must be less than* $180°$.

Proof. Otherwise there would be a geodesic through the vertex such that there are no edges on one side of it, contradicting Lemma 3.5. □

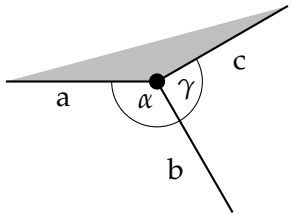

Figure 3.2: The combined angle of b at this vertex is $\alpha + \gamma$. Note that all other edges incident to the vertex are in the grey area.

Combined Angles

Definition 3.7. Consider a balanced vertex v and three incident edges a, b, c following in that counterclockwise order without any edges in between. Then the *combined angle of b at v* is the total angle from a to b to c (see Figure 3.2).

Lemma 3.8 (General Combined Angle Lemma)**.** *The combined angle of any edge at a balanced vertex is...*

(a) ... equal to 240° *if the vertex has degree* 3.

(b) ... equal to 180° *if the vertex has degree* 4.

(c) ... strictly smaller than $180^\circ + 2\arcsin\frac{1}{n-1}$ *if the vertex has degree* $n \geq 5$.

In particular, the combined angle is always less or equal than 240° *and strictly so if the vertex has degree larger than three.*

Proof. (a) is obvious.

(b) is obvious.

(c) consider a vertex of degree $n \geq 5$. Assume that the combined angle at an edge b is $180^\circ + 2\arcsin 1/(n-1)$ or more. Call the two edges realizing that angle a and c. Take v to be the unit vector that bisects the smaller of the two angles between a and c. Let $\{e_i\}$ be the edges other than a, b, c. There are at least two such edges since the degree is 5 or more. Note that the e_i lie on the side of the angle formed by a and c that does not contain b. By a slight abuse of notation we use the same names for the edges and the corresponding unit vectors (Compare Figure 3.3). Since the combined angle is $180^\circ + 2\arcsin 1/(n-1)$ or more, basic trigonometry yields:

$$\begin{aligned}\langle e_i, v\rangle > \langle a, v\rangle &\geq \sin((180^\circ + 2\arcsin\frac{1}{n-1} - 180^\circ)/2)\\ &= 1/(n-1)\end{aligned}$$

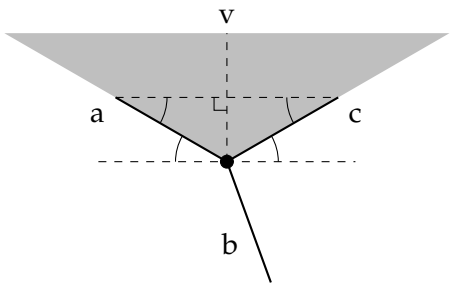

Figure 3.3: Proof of Lemma 3.8. Note that if we denote the combined angle of b by δ, then the marked angles are equal to $(\delta - 180^\circ)/2$ which leads to the stated formula for the projection of the vectors onto v. All other edges/vectors must lie in the grey area.

We deduce:

$$\begin{aligned} 0 &= \langle b + a + c + \sum e_i, v \rangle \\ &= \underbrace{\langle b, v \rangle}_{\geq -1} + \underbrace{\langle a, v \rangle}_{\geq 1/(n-1)} + \underbrace{\langle c, v \rangle}_{\geq 1/(n-1)} + \underbrace{\sum \langle e_i, v \rangle}_{> (n-3)/(n-1)} \\ &> -1 + \frac{1}{n-1} + \frac{1}{n-1} + \frac{n-3}{n-1} = 0 \end{aligned}$$

This is a contradiction.

□

In the next lemma we will show that for vertices of degree $n \neq 4$, only at a vertex of odd degree can we have a combined angle of 180° or more, and even then particular restrictions to the angles apply.

Lemma 3.9 (Special Combined Angle Lemma)**.** *Let a, b, c be three directly following edges of a balanced vertex of degree $n \geq 5$ with a combined angle of b that is 180° or more. Then the vertex must have odd degree.*

Furthermore, denote by α the angle between a and b and by γ the angle between b and c (i.e. $\alpha + \gamma$ is the combined angle of b) then:

(a) $60^\circ < \alpha < 120^\circ$

(b) $60^\circ < \gamma < 120^\circ$

Note that the result of n being odd will not be used when we apply this lemma later. But we get it as a "gratuitous result" which is worth noting.

Proof. We will prove the inequalities regarding α. The case for γ then follows by reflection and relabeling.

We arrange and label the edges as follows: Choose a coordinate system in the tangent space at the vertex such that the unit vector corresponding

to a lies on the negative x-axis. Since the combined angle at b is 180° or more, this implies that only the unit vector of b could lie in the lower half plane. And in fact by Lemma 3.6, it must lie in the lower half plane (see Figure 3.2).

From now on, we denote by b the unit vector corresponding to that edge and by $e_1 := a, e_2 := c, e_3, \ldots, e_j$ ($j := n-1 \geq 4$) the unit vectors corresponding to all other edges, including a and c as the first two. By the above setup, all e_i have a nonnegative y-component and only $e_1 = a$, $e_2 = c$ can have a zero y-component.

Note that if we define $s := \sum e_i$, then $s = -b$ by the balancing condition and therefore s is a unit vector. This means the lemma follows if we prove the following two claims:

(a′) $j = n-1$ must be even.

(b′) If $j = n-1$ is even, then the angle between s and the positive y-axis lies within $\pm 30^\circ$ (Then, the angle α is between 60° and 120°).

We will now prove (a′) and (b′).

Claim: None of the e_i can lie on the positive y-axis.
If that were not the case, note that there is at least four e_i in total, one of them lying on the y-axis. Even if another two lie on the x-axis (and therefore have zero y-component), there is a fourth one that has a positive y-component. Therefore the sum $s = \sum e_i$ would have a y-component of more than 1 which contradicts the fact that s must be a unit vector.

Due to the above claim, we can group the e_i according to the following rules:

- In one group, we have all e_i pointing to the left (negative x-coordinate). Call it the *left group*.
- Accordingly, the other vectors e_i form the *right group*.

Note that by our setup, a is in the left group. Also note that by the General Combined Angle Lemma 3.8 we have $\alpha + \gamma \leq 240^\circ$ and therefore c must be in the right group.

We denote the number of left and right vectors by L and R respectively. Note that $R + L = j$.

In the following, we will use the notation $\langle x, y \rangle$ to mean a vector in $\mathbb{R}^2$ with coordinates x and y.

Let $e : \{-1, 1\} \times [0^\circ, 90^\circ) \to \mathbb{R}^2$ be given by

$$e(C, \theta) := \langle C \cos\theta, \sin\theta \rangle$$

We can rewrite each of the right vectors as $e_i = e(1, \theta_i)$ where θ_i is the angle between the positive x-axis and e_i, and each of the left vectors as

$e_i = e(-1, \theta_i)$ where θ_i is the angle between the negative x-axis and e_i. Note that in either case, $0^\circ \leq \theta_i < 90^\circ$. Using this notation, we can write

$$s = e_1 + e_2 + \cdots + e_j = e(C_1, \theta_1) + e(C_2, \theta_2) + \cdots + e(C_j, \theta_j)$$

In the proof below, we will start at $\langle R - L, 0 \rangle$ and arrive at the actual vector sum s by iteration as follows:

$$\begin{aligned}
s_0 &= e(C_1, 0^\circ) + e(C_2, 0^\circ) + e(C_3, 0^\circ) + \cdots + e(C_j, 0^\circ) = \langle R - L, 0 \rangle \\
s_1 &= e(C_1, \theta_1) + e(C_2, 0^\circ) + e(C_3, 0^\circ) + \cdots + e(C_j, 0^\circ) \\
s_2 &= e(C_1, \theta_1) + e(C_2, \theta_2) + e(C_3, 0^\circ) + \cdots + e(C_j, 0^\circ) \\
&\vdots \\
s_j &= e(C_1, \theta_1) + e(C_2, \theta_2) + e(C_3, \theta_3) + \cdots + e(C_j, \theta_j) = s
\end{aligned}$$

We will use this iterative process to prove that s will lie in a "staircase region", defined as follows (see also Figure 3.4):

Definition: We define the *leftwards staircase of unit circles* starting at $\langle R - L, 0 \rangle$ as the union of the counterclockwise quarter arcs of unit circles starting at $\langle R - L - \ell, \ell \rangle$ and ending at $\langle R - L - (\ell + 1), \ell + 1 \rangle$ for $\ell = 0, 1, 2, \ldots$. We define the *rightwards staircase of unit circles* starting at $\langle R - L, 0 \rangle$ as the union of the clockwise quarter arcs of unit circles starting at $\langle R - L + \ell, \ell \rangle$ and ending at $\langle R - L + \ell + 1, \ell + 1 \rangle$ for $\ell = 0, 1, 2, \ldots$. The region between these two staircases, including the boundary, is called the *staircase region*.

Returning to our definition of the map $e(C, \theta)$ and of the sequence s_k above, we can describe the step from s_k to s_{k+1} as follows:

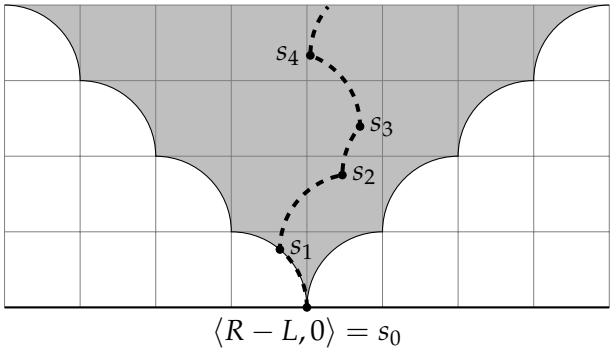

Figure 3.4: The staircase region at $\langle R - L, 0 \rangle$, with an integer lattice added for scale. Using the Arc Fact iteratively to go from s_k to s_{k+1}, we know that a concatenation of arcs on a unit circle of less than 90° that starts at $\langle R - L, 0 \rangle$ as depicted by the dashed line can never leave the grey area.

- If $e_{k+1} = e(1, \theta_{k+1})$ is a right vector, we start at s_k and go along a counterclockwise arc on a unit circle, with initial tangent vector pointing in the positive y-direction, to s_{k+1}.
- If $e_{k+1} = e(-1, \theta_{k+1})$ is a left vector, we start at s_k and go along a clockwise arc on a unit circle, with initial tangent vector pointing in the positive y-direction, to s_{k+1}.

In either case, the arc is less than a quarter circle since $0 \leq \theta_i < 90^\circ$.

We will for now suppose that the following fact is true and prove it later.

Arc Fact: A circular arc $\gamma(\theta) = \langle x, y \rangle + e(C, \theta)$ for $0^\circ \leq \theta < 90^\circ$ has the following properties for $C = \pm 1$ provided that $\gamma(0^\circ)$ is in the staircase region:

(i) $\gamma(\theta)$ is in the staircase region for any $0^\circ \leq \theta < 90^\circ$.

(ii) $\gamma(0^\circ)$ is the only point on the arc that can lie in a corner of the staircase region.

(iii) If $\gamma(0^\circ)$ is not in one of the corners of the staircase region, then $\gamma(\theta)$ lies in the *interior* of the staircase region for $0^\circ < \theta < 90^\circ$.

The iterative application of this Arc Fact can be restated in a more intuitive way using Figure 3.4 as follows: Take a pen and start at $\langle R - L, 0 \rangle$. If now, one is only allowed to draw arcs along a (clockwise or counterclockwise) unit circle of less than 90° (like the dashed line in the figure), one can never leave the grey area. Furthermore, once one is in the interior of the grey area (and therefore away from the corners), one is "stuck" in the interior and won't reach the boundary anymore.

Using these facts, we will now prove that $s_j = s$ must lie in the interior of the staircase region by studying the sequence s_k as described above. First, we will prove the following claim by induction:

Claim: s_k lies in the staircase region at $\langle R - L, 0 \rangle$ for $k = 0, 1, \ldots, j$ (so for now, it could be on the boundary).

The claim is obvious for $k = 0$ since $s_0 = \langle R - L, 0 \rangle$. Assume it is true for given k and s_k is lying in the staircase region. We can define a path as follows:

$$\gamma(\theta) = \underbrace{\sum_{i \leq k} e(C_i, \theta_i) + \sum_{i \geq k+2} e(C_i, 0)}_{=: \langle x, y \rangle} + e(C_{k+1}, \theta) \qquad 0^\circ \leq \theta \leq \theta_{k+1} < 90^\circ$$

Observe that the we can apply (i) of the Arc Fact to this path:

- $\gamma(0^\circ) = s_k$ is in the staircase region by hypothesis.
- $0^\circ \leq \theta < 90^\circ$ is given.
- Therefore, $s_{k+1} = \gamma(\theta_{k+1})$ is in the staircase region by the Arc Fact.

The claim follows for all $k = 0, 1, \ldots, j$. In particular $s = s_j$ is lying in the staircase region. We will now argue that it is in fact in the *interior* of that region.

Recall that $j \geq 4$, so besides $e_1 = a$ and $e_2 = c$ (that are left and right vectors respectively), there are at least two more vectors $e_3, \ldots, e_j$. These $j-2$ vectors can be written as $e_i = e(C_i, \theta_i)$ for $\theta_i > 0^\circ$ (a is horizontal, c can be horizontal, but all other $j-2$ vectors must have positive y component and therefore a positive angle).

We conclude that there is at least two vectors with positive angle θ_i. In that context, reconsider the Arc Fact and our sequence s_k and note:

- s_2 (which represents the sum after including a and c) is in the staircase region but could be in a corner (in fact, it could be at $\langle R - L, 0\rangle$ because both a and c could be horizontal vectors, so including their angles didn't actually change the sum).
- s_3 lies on an arc that starts at s_2 but reaches an angle $0 < \theta_i < 90^\circ$. Therefore, s_3 will not lie in a corner by (ii) of the Arc Fact.
- Applying (iii) of the Arc Fact to the arc from s_3 to s_4, note that s_3 does not lie in a corner. Therefore, s_4 lies in the interior of the staircase region.
- From now on, (iii) of the Arc Fact applies inductively: s_k lies in the interior, i.e. not in a corner. Therefore, s_{k+1} lies in the interior of the staircase region.

It follows that $s = s_j$ is in fact lying in the *interior* of the staircase region.

Assume for the sake of contradiction that $\langle R - L, 0\rangle \neq \langle 0, 0\rangle$. This means s is lying in the interior of the staircase region starting at a point $\langle R - L, 0\rangle \neq \langle 0, 0\rangle$ on the integer lattice. At the same time, s is a unit vector. However the unit circle centred at the origin does not intersect the interior of the staircase region at $\langle R - L, 0\rangle \neq \langle 0, 0\rangle$. This is a contradiction. It follows that $R - L = 0$.

We can now prove our initial claims (a') and (b')

(a') $R - L = 0$, therefore $j = R + L = 2R$ is even, proving the first claim.

(b') $R - L = 0$ implies that s lies on the intersection of the unit circle at the origin with the interior of the staircase region also starting at the origin. It follows that the angle between s and the positive y-axis lies strictly within $\pm 30^\circ$.

We finish by proving the Arc Fact for $C = 1$ (the case for $C = -1$ is just the mirror image). Let $\gamma(\theta) = \langle x, y\rangle + e(1, \theta) = \langle x, y\rangle + \langle \cos\theta, \sin\theta\rangle$ for $0^\circ \leq \theta < 90^\circ$. Note that we rotate "towards the left" as θ goes from 0° to 90°. Also, the staircase region only grows wider as we go up. So even if $\gamma(0^\circ)$ is on the right staircase, no other point on γ will be on or beyond the right staircase. We can therefore concentrate on the left staircase. Also,

if we don't start on the left staircase but in the interior of the staircase region, this situation is just a right shift of an arc that starts on the staircase (compare the left and right of Figure 3.5). So it is enough to prove that an arc starting *on* the staircase doesn't reach particular points.

We will now prove the three parts of the Arc Fact for a path starting on the left staircase.

(i) Note that it is enough to consider two subsequent "steps" of the left staircase, namely the one at $\gamma(0^\circ)$ and the next higher one that γ could possibly cross. It is obvious that γ will not cross any steps on the left staircase that are further above or below. Shift the picture so that the corner between the two relevant steps is at $\langle 0, 0\rangle$. This means we can write:

$$\gamma(0^\circ) = \langle 0, -1\rangle + \langle \cos\varphi, \sin\varphi\rangle \qquad \text{for some } \varphi \in [0, 90^\circ]$$

And therefore

$$\begin{aligned}\gamma(\theta) &= \langle x, y\rangle + \langle \cos\theta, \sin\theta\rangle \\ &= \gamma(0^\circ) - \langle 1, 0\rangle + \langle \cos\theta, \sin\theta\rangle \\ &= \langle \cos\varphi + \cos\theta - 1, \sin\varphi + \sin\theta - 1\rangle\end{aligned}$$

To prove that $\gamma(\theta)$ lies on or to the right of the two steps, we need to show

$$\operatorname{dist}(\langle -1, 0\rangle, \gamma(\theta)) \geq 1 \quad \operatorname{dist}(\langle 0, -1\rangle, \gamma(\theta)) \geq 1$$

Note that

$$\operatorname{dist}(\langle -1, 0\rangle, \gamma(\theta))^2 = (\cos\varphi + \cos\theta)^2 + (\sin\varphi + \sin\theta - 1)^2$$

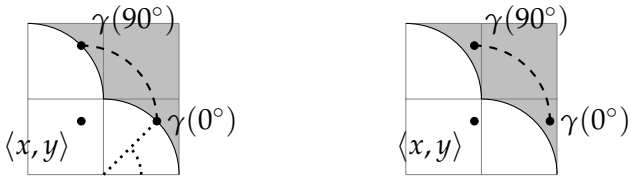

Figure 3.5: Proof of the Arc Fact. On the left is the case where the arc $\gamma(\theta)$ (dashed) starts on the boundary of the staircase region, on the right is the case where the arc starts in the interior of the staircase region. Note that the latter is just a right shift of the situation where we start on the arc. The point in the centre of both pictures is chosen to be $\langle 0, 0\rangle$. The dotted angle is φ.

Basic two-variable calculus yields that the minimum of this function for $(\varphi, \theta) \in [0°, 90°] \times [0°, 90°]$ is in fact 1. The same argument works for the second inequality.

(ii) Note that, in the notation of (i), the only corners that $\gamma(\theta)$ can reach are at $\langle 1, -1\rangle$, $\langle 0, 0\rangle$ and $\langle -1, 1\rangle$. Reconsidering $\gamma(\theta) = \langle \cos\varphi + \cos\theta - 1, \sin\varphi + \sin\theta - 1\rangle$ and $(\varphi, \theta) \in [0°, 90°] \times [0°, 90°]$ and using calculus, these three points can only be reached if (φ, θ) is one of $(0°, 0°)$, $(0°, 90°)$, $(90°, 0°)$ or $(90°, 90°)$. Since $\theta < 90°$ by assumption, corners can therefore only be reached at $\theta = 0°$.

(iii) Again we can consider $\gamma(\theta) = [\cos\varphi + \cos\theta - 1, \sin\varphi + \sin\theta - 1]$. If $\gamma(0°)$ is not in a corner of the left staircase, we have $\varphi \neq 0°, 90°$. Applying calculus one more time, $\operatorname{dist}(\langle -1, 0\rangle, \gamma(\theta))^2 > 1$ and $\operatorname{dist}(\langle 0, -1\rangle, \gamma(\theta))^2 > 1$ for any $0° < \theta < 90°$ and (iii) follows.

This finishes the proof of the Arc Fact and therefore also concludes the proof of the Special Combined Angle Lemma. □

3.3 GLOBAL PROPERTIES ON THE FLAT PLANE

Using the local properties derived in the previous section, we now turn towards global properties of geodesic nets. For now, let G be a geodesic net on the flat (zero curvature) plane. We will see later in Section 3.5 that these results readily extend to nonpositive curvature.

The Convex Hull Property

Lemma 3.10. *Let K denote the convex hull of all the unbalanced vertices in G. All balanced vertices lie in $K \setminus \partial K$.*

Proof. Assume there is a balanced vertex v lying on or outside ∂K. This implies that we can draw a straight line through v such that one side of that line is free of unbalanced vertices. Assume the line is vertical and all unbalanced vertices lie to the right of it. According to Lemma 3.5, there must be an edge to the left of the line, leading to a vertex to the left of the line. It can't be unbalanced. Therefore, we can again draw a vertical line through that new vertex and get another vertex to the left of it. This process would continue ad infinitum, contradicting the finiteness of the geodesic net. □

Lemma 3.11. *A geodesic net that has at least one balanced vertex must have at least three unbalanced vertices.*

Proof. Otherwise the convex hull of the unbalanced vertices has empty interior. Apply Lemma 3.10. □

Note that the last Lemma rephrases the trivial cases of Theorem 3.3 for $n = 0, 1, 2$.

Paths and the Turn Angle

From now on, we will frequently consider oriented paths using the following conventions:

- All paths that we consider are oriented, piecewise geodesic paths.
- A point on such a path that lies between two of its geodesic segments is called a *vertex*.
- We will often refer to the geodesic segments of a path as *edges*.
- For a path γ that goes through a vertex x, we write $\gamma(\to x)$ for the restriction of γ up to the point until it reaches x for the first time and $\gamma(x \to)$ for the restriction of γ starting at the point where it reached x for the last time.
- For two paths or edges, we use $*$ as the symbol for concatenation.
- The notation $-\gamma$ refers to γ with the opposite orientation.
- Given a closed path γ, we call the union of bounded components of $\mathbb{R}^2 \setminus \gamma$ the *inside* of γ and the unbounded component the *outside*.

Definition 3.12. Consider two consecutive edges e, f on a path. The *turn angle from e to f along the path* is defined as follows: If $e \neq -f$, the turn angle is the angle between the extension of e to the other side of the vertex and the edge f (By convention, a left turn is measured in positive angles and a right turn is measured in negative angles, see Figure 3.6). If $e = -f$, the turn angle is $+180°$ (so if we backtrack, this is considered a left turn).

For further clarification, note that if e and f lie on a path that circumscribes a polygon in counterclockwise direction (this means that no backtracking is happening), the turn angle is exactly what is known as the exterior angle at the vertex of a polygon.

Definition 3.13. Consider a path starting on an edge e and ending on an edge f. We define the *turn angle from e to f along the path* as the sum of all turn angles at the vertices between e and f.

Figure 3.6: A positive turn angle (left) and a negative turn angle (right). If $e = -f$, the turn angle is $+180°$ by convention.

Recall that all paths that we consider are piecewise geodesic. So the following well-known version of Gauß-Bonnet applies:

Lemma 3.14 (Gauß-Bonnet, simple closed paths in the flat plane)**.** *If e is an edge on a simple closed counterclockwise path, the turn angle from e to e along γ is $360°$.*

As it turns out, we will need to use this fact in a context where γ is not simple. We will carefully allow some exceptions to the requirement of simplicity, ensuring that Gauß-Bonnet still applies. To do so, we will define what it means for a path to be *essentially simple*, using the notions of *admissible backtracks* and *non-transversal crossings*.

Definition 3.15 (Admissible Backtrack)**.** Consider a path γ doing a backtrack along an edge as follows:

$$e * a * (-a) * f$$

Then this backtrack is *admissible* if $f \neq -e$ and a lies to the right of the path $e * f$. Otherwise it is *inadmissible*. See Figure 3.7.

When using the results of this section in the proofs of Lemma 3.25, Lemma 3.31, Lemma 3.32 and Lemma 3.33, we will see that the only backtracks that are happening are admissible backtracks. That means neither will we have backtracks that lie to the left of the path, nor will we have "double backtracks" of the form $e * a * b * (-b) * (-a) * f$.

Based on this definition, the following lemma is apparent from Figure 3.7 and the fact that a backtrack is considered a turn of $+180°$.

Lemma 3.16. *Consider an admissible backtrack $e * a * (-a) * f$. Then the turn angle along $e * f$ is the same as the turn angle along $e * a * (-a) * f$.*

We will now specify what kind of crossing of paths we allow.

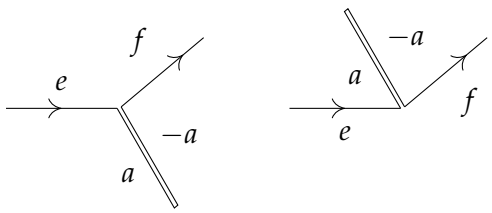

admissible inadmissible

Figure 3.7: Two examples of backtracks

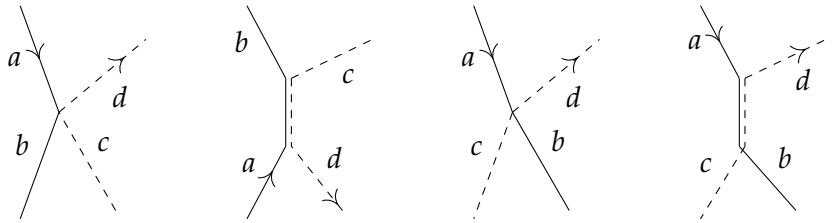

Figure 3.8: Examples of crossings. We will only allow non-transversal crossings. Note that our definition of non-transversal is quite strict. For example, the counterclockwise order *abdc* (not depicted) is not called non-transversal according to our definition (it will, however, never occur below).

Definition 3.17 (Non-Transversal Crossing)**.** Consider a non-closed, simple path $e_1 * \cdots * e_n$ ($n \geq 0$) and two paths $\alpha = a * e_1 * \cdots * e_n * b$ and $\gamma = c * (-e_n) * \cdots * (-e_1) * d$ with $a \neq -d$ and $b \neq -c$ (if $n = 0$, this means that $\alpha = a * b$ and $\gamma = c * d$ go through a common vertex). It follows that a, b, c, d are arranged around the path $e_1 * \cdots * e_n$ (or their common vertex in the case $n = 0$). We say that α and γ cross non-transversally if the edges are arranged counterclockwise in the order *abcd* or *dcba*. If $n = 0$ and either or both of the paths are backtracks (i.e. $a = -b$ or $c = -d$), it is still considered a non-transversal crossing.

We can now define what it means for a path to be essentially simple:

Definition 3.18 (essentially simple path)**.** We say that a path is *essentially simple* if it is simple apart from the following two exceptions:

- It may contain admissible backtracks as defined above.
- It can revisit edges or vertices as long as this is a non-transversal crossing as defined above.

Definition 3.19. If an essentially simple closed path γ has the property that the outside (the unbounded component of $\mathbb{R}^2 \setminus \gamma$) always lies to the right of γ, we call it a *counterclockwise* path.

Note that due to the presence of admissible backtracks and non-transversal intersections, there might be edges of an essentially simple path along which the outside lies simultaneously to the right *and* the left of the path. The above definition allows for this to happen. If, on the other had, the outside were lying *only* to the left (or on neither side) of at least one edge, the path would not be considered counterclockwise.

Based on this, we can rewrite Gauß-Bonnet from above:

Lemma 3.20 (Gauß-Bonnet, essentially simple closed paths in the flat plane)**.** *If e is an edge on an essentially simple closed counterclockwise path, the turn angle from e to e along γ is $360°$.*

Proof. If the path contains an admissible backtrack, due to Lemma 3.16, we can simply remove each such backtrack (even if it contains e) without changing the total turn angle.

If the path has a non-transversal crossing, consider Figure 3.8 showing examples of the only two allowed arrangements of edges: The arrangement *dcba* can't happen here since the path is counterclockwise (so the outside can't lie exclusively to the left at any edge). On the other hand, the arrangement *abcd* (around a common vertex or common edges) can be realized as the local limit of a sequence of simple paths for which the outside still lies to the right of the path.

We arrive at a sequence of simple closed counterclockwise paths $\gamma_i \to \gamma$. Gauß-Bonnet as in Lemma 3.14 applies to each γ_i and therefore by continuity also to the limit γ. □

This lemma in turn allows us to prove the following:

Lemma 3.21 (Conditional Path Independence)**.** *Consider two paths γ and δ with the same initial vertex u and the same terminal vertex v (i.e. $\gamma * (-\delta)$ is a closed path) as well as an edge e incident to u and an edge f incident to v. If the following conditions are met, then the turn angle from e to f will be the same along $e * \gamma * f$ and $e * \delta * f$:*

(a) Both e and f lie outside $\gamma * (-\delta)$ and they have no endpoints in common.

(b) Both γ and δ are simple, except for admissible backtracks.

(c) If γ and $-\delta$ meet anywhere except at their endpoints, it is a non-transversal crossing.

We call this the conditional path-independence *of the turn angle (see Figure 3.9).*

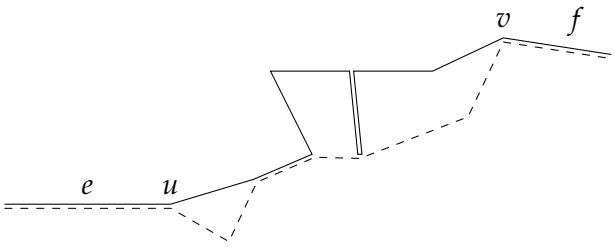

Figure 3.9: Conditional path-independence: The turn angle from e to f is the same along either path. Note that both paths are going in a left-right direction in this picture.

Before we get to the proof, it is worth pointing out that without the conditions, the respective turn angles would only agree modulo 360°.

Proof. First note that due to Lemma 3.16, we can remove all admissible backtracks from γ and δ. Furthermore, in case γ and δ agree on the first i edges, we can write $\gamma = \epsilon * \gamma'$ and $\delta = \epsilon * \delta'$ for some path ϵ such that γ' and δ' do not agree on their first edge. This reduces the proof to the question if γ' and δ' produce the same turn angle. We therefore assume that γ and δ do not agree on their first edge. For a similar reason, we assume that they don't agree on their last edge.

γ and δ are now both simple (since we removed all backtracks). That means that $-\gamma$ and $-\delta$ are also simple. Since γ and δ don't agree on their first or last edge, the closed path $\gamma * (-\delta)$ also has no backtracks. Combining γ and $-\delta$ can also not have produced transversal crossings by condition (c). It follows that $\gamma * (-\delta)$ is essentially simple. By the same arguments, $\delta * (-\gamma)$ is essentially simple.

We can assume that $\gamma * (-\delta)$ is counterclockwise according to Definition 3.19. This can be seen as follows: There must be some edge e so that the outside is to the left or right of it (since the boundary of the unbounded component consists of edges of the path). If the outside is *not* to the right of e, replace $\gamma * (-\delta)$ with $\delta * (-\gamma)$ and e with $-e$. Therefore, after relabeling if necessary, we can assume that the outside is to the right of e. Starting at e, we follow the path $\gamma * (-\delta)$. Each of γ and $-\delta$ is simple, therefore $\gamma * (-\delta)$ is simple except where γ and $-\delta$ cross non-transversally. Refer to Figure 3.8 which demonstrates that if γ and δ meet non-transversally and we arrive at the crossing with the outside to the right, we will also leave the crossing with the outside to the right (the outside would *also* be to the left of the path during the crossing, which we allow). So the outside is always to the right of $\gamma * (-\delta)$ and therefore this is an essentially simple counterclockwise path.

Now consider the closed path $\alpha = e * \gamma * f * (-f) * (-\delta) * (-e)$. Recall that e and f lie *outside* $\gamma * (-\delta)$ and have no endpoints in common. This implies two things: (1) α is still a counterclockwise path. (2) e and f both lie to the right of the remainder of the path. The latter means that the two backtracks of α along e and f are admissible. Note that since γ and δ don't agree on their first or last edges and have no backtracks themselves, there are no further backtracks. Therefore α is still essentially simple and Gauß-Bonnet as specified in Lemma 3.20 applies. Recalling that we consider backtracking to be a turn by $+180°$ and setting the turn angle along $e * \gamma * f$ to be x and the turn angle along $e * \delta * f$ to be y, we get

$$x + 180° - y + 180° = 360°$$

Note that δ is free of backtracks, so the turn angle along $-\delta$ is in fact $-y$ since a turn where we run into issues with $\pm 180^\circ$ doesn't happen. It follows that $x = y$. □

Another way of thinking of the turn angle along an essentially simple path that further illustrates the conditional path independence is: translate the initial edge e of the path to an edge e' that ends at the point where the terminal edge f starts. The turn angle from e' to f at that point is now the same as the turn angle from e to f along the path.

We are now considering paths on a geodesic net, which are of course also piecewise geodesic paths.

Definition 3.22 (First and Second Right Turn)**.** Consider a path through a balanced vertex.

(a) If the outgoing edge of the path immediately follows the incoming edge in counterclockwise order, we say that the path *takes the first right turn*.

(b) If the outgoing edge of the path is the second edge following the incoming edge in counterclockweise order, we say that the path *takes the second right turn*.

An example can be seen in Figure 3.10. Note that whenever a path takes the first or second right turn at a balanced vertex (which always has at least degree 3), it is not backtracking.

In the context of these definitions, we will revisit the Special Combined Angle Lemma (Lemma 3.9) and arrive at the following three lemmas:

Lemma 3.23 (First Turn Lemma)**.** *If a path takes the first right turn at a balanced vertex, the turn angle is negative.*

This Lemma is a direct consequence of Lemma 3.6.

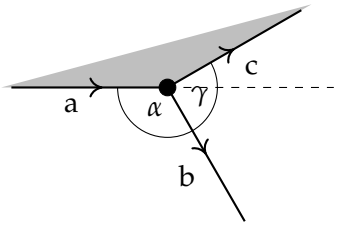

Figure 3.10: Note that the turn angle from a to b (first right turn) and from a to c (second right turn) is measured in reference to the dashed line and compare with Figure 3.2.

Lemma 3.24 (Second Turn Lemma)**.** *Consider a balanced vertex with incident edges a, b, c following counterclockwise directly in that order. If the path from a to c (i.e. a path that takes the second right turn) has a positive turn angle as depicted in Figure 3.10, then:*

- *the turn angle from a to c lies in $(0°, 60°]$,*
- *the turn angle from a to b lies in $(-120°, -60°]$, and*
- *the turn angle from $-b$ to c lies in $(-120°, -60°]$.*

Compare Figure 3.10 with Figure 3.2 and it is immediate that this lemma is a reformulation of Lemma 3.8 (for vertices of degree 3 and 4) and Lemma 3.9 (for vertices of degree 5 or more). More specifically, for a vertex of degree 3, the turn angles reach the extremal cases of $60°$, $-60°$, $-60°$ respectively. For a vertex of degree 4, the lemma is vacuously true since the turn angle along the second right turn can never be positive (it will, in fact, always be zero). For a vertex of degree 5 or more, the turn angles lie in the interior of the three given intervals which follows from Lemma 3.9.

The situation in the following lemma is visualized in Figure 3.11.

Lemma 3.25 ($60°$ Lemma, flat version)**.** *Consider a path going through four edges a, b, c, d of a geodesic net on the Euclidean plane and three vertices u, v, w in the order a, u, b, v, c, w, d. Assume that*

(a) $a \neq -b$, $c \neq -d$
(b) u and w are balanced (v can be balanced or not).
(c) b immediately follows a at u (i.e. $a * b$ takes the first right turn).
(d) d immediately follows c at w (i.e. $c * d$ takes the first right turn).
(e) The convex hull of u, v, w contains no unbalanced vertices (except, possibly, v itself).

Then the turn angle from a to d along that path is at most $60°$.

Note that by definition, v is different from both u and w. However, we allow $b = -c$ which then implies $u = w$. Note that we can't have both

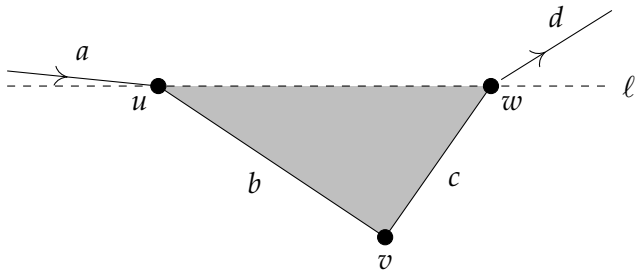

Figure 3.11: Setup of the $60°$ Lemma (Lemma 3.25). There are no unbalanced vertices in the grey area. The line ℓ is used for Case 2 of the proof.

$b = -c$ and $a = -d$ because then $u = w$ would be a degree 2 vertex which, for balanced vertices, is not possible.

The result of the lemma can be reformulated in the following way: If a is translated to an edge a' ending at w, the turn angle from a' to d is at most 60°, i.e. the clockwise angle from a' to d is at least 120°.

Proof. First note the following two trivial cases:

- If $u = w$, then the combined angle of $b = -c$ at $u = w$ is at most 240° according to Lemma 3.8. The turn angle from a to d is the combined angle minus 180°. The claim follows.
- If the turn angle from b to c at the vertex v is nonpositive, note that the turn angles from a to b and from c to d are negative. Therefore the sum of all three is negative and the claim follows.

We can therefore assume that $u \neq w$ and that the turn angle from b to c is positive. This means that the line ℓ through u and w is well-defined and unique and that we can rotate the picture such that ℓ is horizontal, u is to the left of w and v is below ℓ. So Figure 3.11 does in fact describe the only interesting situation (however a or d could also be below ℓ unlike in the figure).

We define a path γ starting at u as follows:

- Counting from a, we take the second right turn at u (see Definition 3.22) and leave u along that edge. This is the first edge of γ.
- From now on, always take the first right turn, unless that edge would lead to v. In that case, take the second right turn.
- Terminate as soon as the path either reaches w or as soon as it left the convex hull of u, v, w (this might mean that γ only consists of a single edge starting at u).

We first need to argue that this path is well-defined. In fact, there are no unbalanced vertices in the convex hull of u, v, w, so as long as we don't leave it (at which point the path terminates), we only reach balanced vertices and therefore a third edge in case we need it (to avoid v) always exists. Note that the same argument also implies that γ doesn't backtrack.

To show that the path terminates, assume that γ never leaves the convex hull of u, v, w but also never reaches w. Due to the finiteness of the geodesic net, it must eventually return to a vertex it has visited before. Note that γ cannot have visited an unbalanced vertex since it never left the convex hull of u, v, w and by definition never reaches v (the only possibly unbalanced vertex in the convex hull). γ therefore includes a closed polygon of balanced vertices which is contained inside the convex hull of u, v, w in its entirety. Assume that this polygon is travelled counterclockwise by γ (the clockwise case follows a very similar argument). Consider the rays

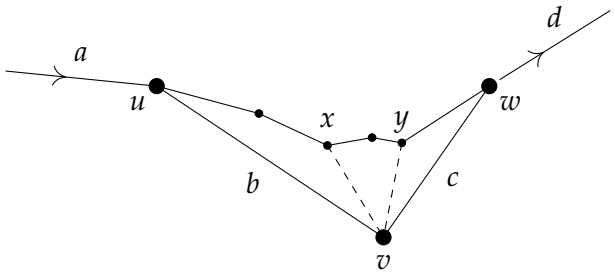

Figure 3.12: An example for the situation of Case 1. The upper path is γ. Note that the turn angle from a to d will be the same, no matter which of the paths we take. The dashed lines are e_v and f_v respectively.

from v through each of the vertices of that polygon. One of these rays is the furthest to the right. Denote the vertex on the polygon that the ray reaches by x (if there is more than one such vertex, pick the first one the ray reaches). The incoming edge of the path γ is reaching x from the left of the ray. Because x is balanced, there must be an edge leaving x to the right of the ray (Lemma 3.5) and that edge cannot reach v. Instead of travelling counterclockwise along the polygon, γ must therefore have taken one of the edges to the right of the ray, contradicting that x is on the rightmost ray as described above. Therefore, the path indeed terminates at w or leaves the convex hull of u, v, w and is therefore well-defined.

We now work on a case-by-case basis.

Case 1 γ reaches w.

An example of γ is given in Figure 3.12. Note that the path $a * \gamma * d$ and the path $a * b * c * d$ fulfil the requirements of conditional path independence as specified in Lemma 3.21. In fact:

(a) Due to $a * b$ taking the first right turn, a lies outside the convex hull and so does d. The path $b * c * (-\gamma)$ on the other hand lies in the convex hull. Also, since we consider $u \neq w$, the edges a and d could only share the other endpoint which would contradict the first right turn conditions.

(b) We excluded the trivial case where $b = -c$, so $b * c$ is simple. We argued above that γ can never return to a vertex. It follows that γ is simple.

(c) γ can't use b or c (it avoids any edges incident to v by definition). Therefore, $b * c$ and $-\gamma$ never meet except at the endpoints.

So conditional path independence applies and the claim follows if the turn angle along $a * \gamma * d$ is at most $60°$.

If this angle is nonpositive, there is nothing to show. If it is positive, then at some point the turn angle at a vertex on $a * \gamma * d$ must be positive.

Denote by x the first vertex with a positive turn angle and by y the last vertex with a positive turn angle. Note that the following argument still works in case any (or several) of u, w, x, y coincide.

At x: By the First Turn Lemma (Lemma 3.23), $a * \gamma * d$ must have taken the second right turn at x. Therefore, x is adjacent to v. Denote the incoming edge to x along the path by e_{in} and the edge from x to v by e_v. Now, by the Second Turn Lemma (Lemma 3.24), the turn angle from e_{in} to e_v is in $(-120°, -60°]$.

At y: By the First Turn Lemma (Lemma 3.23), $a * \gamma * d$ must have taken the second right turn at y. Therefore, y is adjacent to v. Denote the outgoing edge from y along the path by f_{out} and the edge from v to y by f_v. Now, by the Second Turn Lemma (Lemma 3.24), the turn angle from f_v to f_{out} is in $(-120°, -60°]$.

Consider the path $\gamma' := \gamma(\to x) * e_v * f_v * \gamma(y \to)$. Again, conditional path independence applies to $a * \gamma' * d$ and $a * b * c * d$. Let's check the three conditions:

(a) a and d still lie outside the convex hull and don't share any endpoints.

(b) $b * c$ is still simple. As long as it follows γ, the path γ' must be simple. It could only fail to be simple at $e_v * f_v$ in the case that these two edges coincide. In that case it would be an admissible backtrack, since by definition (first right turns), e_v and f_v lie to the right of the remainder of γ'.

(c) Note that $b * c$ is on the boundary of the convex hull whereas $-\gamma'$ is in the convex hull. So $b * c$ and $-\gamma'$ could meet at edges (for example, if $x = u$, then $e_v = b$) but for $-\gamma'$ to cross $b * c$ transversally to the other side (to produce anything but the the non-transversal counterclockwise orders as given in Definition 3.17), it would have to leave the convex hull which it doesn't.

It follows that it is enough to show that the turn angle along $a * \gamma' * d$ is $60°$ or less. And in fact note:

- At x, the turn angle is in $(-120°, -60°]$.
- At v, the turn angle is at most $180°$.
- At y, the turn angle is in $(-120°, -60°]$.
- All other turn angles are (by the choice of x and y) negative.

Since the turn angle along $a * \gamma' * d$ is the sum of these angles, the claim follows.

Case 2 γ leaves the convex hull of u, v, w and terminates.

We now need to consider three subcases depending on the position of a, d relative to the line ℓ. Recall that ℓ is the horizontal line through u and w. Denote by $\overline{\ell}$ the segment of ℓ between u and w.

Case 2a both a and d lie above ℓ. Because γ left the convex hull of u, v, w and a lies above ℓ, at some vertex the turn angle along $a * \gamma$ must be positive. Pick the first vertex for which that is the case and call it x (possibly this is u). Define e_{in} and e_v as above.

We define a path ϵ. Note that the following is the mirror image of the way we found γ: At w, counting from d, take the second left turn. Now always take the first left turn unless the edge leads to v in which case we take the second left turn. The path terminates when reaching u or when leaving the convex hull of u, v, w. The same arguments regarding the well-definedness still apply. But note that the resulting path can't actually reach u or otherwise $\epsilon = -\gamma$ and γ would have reached w, a case we already dealt with.

If we consider $-(d * \epsilon)$ (i.e. $d * \epsilon$ with the opposite orientation), because $d * \epsilon$ left the convex hull of u, v, w and d lies above ℓ, at some vertex the turn angle along $-(d * \epsilon)$ must be positive. Pick the last vertex for which that is the case and call it y (possibly this is w). Define f_v and f_{out} as above.

We now have the exact same angle setup as in Case 1 and the claim follows.

Case 2b d lies on or below ℓ. This is a rather pathological case that needs particular consideration.

Assume that the turn angle along the path $a * b * c * d$ is more than 60°. This means that the turn angle along $a * \overline{\ell} * d$ is more than 60° (In this case, it is obvious that conditional path independence applies to these two paths). However, since d lies on or below ℓ, the turn angle from $\overline{\ell}$ to d must be nonpositive. It follows that the turn angle from a to $\overline{\ell}$ must be more than 60°. In particular, the first edge of γ must lie inside the convex hull, otherwise $a * \gamma$ would take a turn of more than 60° at u, which contradicts the Second Turn Lemma (Lemma 3.24).

Consider the following path which we call γ_+: Truncate the path γ so that it terminates at the point where it intersects $\overline{\ell}$ for the last time. This means it most likely won't terminate on a vertex but in the middle of an edge. Now continue along $\overline{\ell}$ to w.

Note that the last edge of γ is either on $\overline{\ell}$ or it starts below $\overline{\ell}$ and ends above it. So the last turn of γ_+ onto $\overline{\ell}$ must have been a right turn or no turn at all (nonpositive turn angle).

The three conditions for conditional path independence are again met by $a * b * c * d$ and $a * \gamma_+ * d$ (see the arguments in case 1). So the turn angles must be the same and therefore $a * \gamma_+ * d$ also has a turn angle of more than 60°. But the last turn of $\gamma+$ had a nonpositive angle and the turn onto d is also negative as argued above, so it follows that the turn angle along the path γ must be more than 60°. So there must be at least

one vertex along γ with a positive turn angle. Call the first such vertex x and the last such vertex y. As usual, we allow x and y to coincide.

Using the same construction as before, we get a path $\gamma' = \gamma(\to x) * e_v * f_v * \gamma(y \to)$. Since γ' and γ agree on all edges apart from the middle section where γ' lies to the right of γ and has at most a single admissible backtrack (if $e_v = -f_v$), conditional path independence applies. But note that the turn angle along γ is more than $60°$, whereas, by the same arguments as in case 1, the turn angle along γ' is at most $60°$. This contradiction implies that our initial assumption that the turn angle along $a * b * c * d$ was more than $60°$ must have been wrong.

Case 2c *a* **lies on or below** ℓ. This case is simply the mirror image of Case 2b. □

Circumference

Recall that we are considering a geodesic net G on the plane, which is a connected graph embedded in $\mathbb{R}^2$. In this context, note the following definition, which is quoted from [GY06], page 312.

Definition 3.26. Consider a face F of an embedded graph G. The *boundary walk* of F is a closed walk in G that corresponds to a complete transversal of the perimeter of the polygonal region within the face. Note that vertices and edges can reoccur in a boundary walk. In particular, if both sides of an edge lie on a single region, the edge is retraced on the boundary walk.

Using the concept of boundary walks, we can define the following:

Definition 3.27. Since G is a connected graph embedded in $\mathbb{R}^2$, it has exactly one outer face, which is the unbounded component of $\mathbb{R}^2 \setminus G$. We call the boundary walk of this outer face the *circumference* of G. By convention, we orient it counterclockwise, i.e. such that the outer face lies to the right of the curve. For an example, see Figure 3.13.

Note that it is possible that the circumference, being a boundary walk, travels the same edge or vertex several times (as in the figure). It does not, however, cross itself transversally. Otherwise it would enclose other faces.

Lemma 3.28. *The circumference must always take the first right turn when going through a balanced vertex (see Definition 3.22).*

Proof. If the circumference took any other edge but the immediately following edge e in counterclockwise order at a vertex, note that e would lie to the right of the circumference. However, by definition, the circumference is a boundary walk and can therefore never cut off any edges from the graph. □

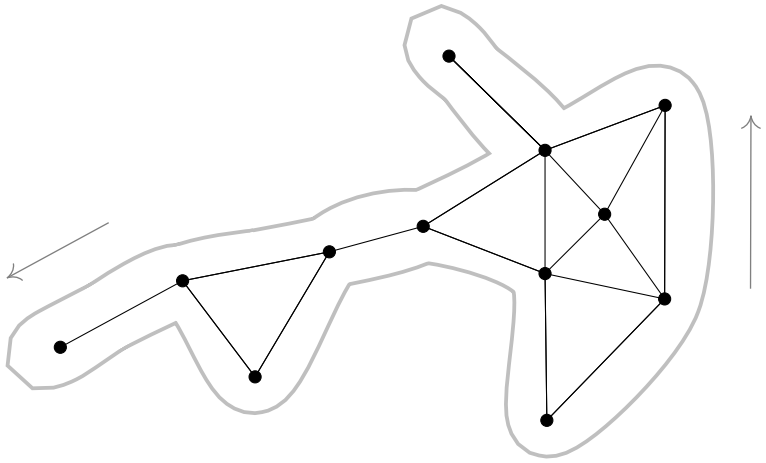

Figure 3.13: Example for the circumference of a graph which is the path resulting from "shrinking" the grey curve onto the graph.

An immediate consequence of the previous lemma and Lemma 3.23 is:

Lemma 3.29. *The turn angle at each balanced vertex on the circumference must be negative.*

We can now conclude:

Lemma 3.30. *The circumference includes unbalanced vertices.*

Proof. Otherwise the circumference would only visit balanced vertices. By the previous lemma, the turn angle at each vertex would therefore be negative. This implies that the turn angle along the whole circumference is negative. We now have a closed clockwise path such that the unbounded component of $\mathbb{R} \setminus G$ lies to the right of it and therefore inside a curve. This is a contradiction. □

3.4 MAIN PROOF ON THE FLAT PLANE

We can now prove the main result of Theorem 3.3 for the case of a geodesic net on the Euclidean plane. We will cover the case of nonpositive curvature in Section 3.5.

Lemma 3.31. *A geodesic net on the Euclidean plane with three unbalanced vertices has at most one balanced vertex.*

Proof. First, if the geodesic net G includes any edges that start *and* end at an unbalanced vertex, we remove them. This leads to two cases:

(a) We get a geodesic net G' with fewer unbalanced vertices (since removing an incident edge might balance a previously unbalanced vertex). So G' has one or two unbalanced vertices and therefore no balanced vertices as demonstrated previously. It follows that G also has no balanced vertices and we are done.

(b) We get a geodesic net G' with the same number of unbalanced and balanced vertices as G. In this case, it suffices to study G'.

We can therefore assume that no such "irrelevant edges" exist [1].

We can assume that the three unbalanced vertices x, y, z are not collinear (otherwise the interior of their convex hull is empty and by Lemma 3.10, there are no balanced vertices). This implies that x, y, z are arranged on a triangle.

All balanced vertices must lie inside the triangle formed by these three points.

Claim: We can assume that removing any one of x, y, z must not disconnect G.

If, say, removing x would disconnect the geodesic net, consider the following process: Remove x, splitting G into at least two connected components and add a copy of x to each of them. Each of the resulting components must contain at least two unbalanced vertices (otherwise the component would have no vertices besides x which isn't possible). But there are only three unbalanced vertices in total and at least two components. Therefore, each component has at most two unbalanced vertices and therefore no balanced vertices. We deduce that there is a total of zero balanced vertices.

Denote the circumference of the geodesic net by the path γ.

Claim: γ travels through each of x, y, z exactly once.

First note that the circumference must reach each of the three at least once, since the geodesic net is connected and x, y, z are on the boundary of the geodesic net. If it travelled through, say, x twice, removing x would split up G, a case we just excluded.

This implies that γ either visits the three unbalanced vertices in the order x, y, z or in the order x, z, y. After relabeling if necessary, we assume the order is x, y, z.

Therefore, the circumference travels along vertices in the order

$$x, u_1, \ldots, u_r, y, v_1, \ldots, v_s, z, w_1, \ldots, w_t, x$$

where all the u_i, v_j, w_k are balanced vertices.

First note that on the circumference, two unbalanced vertices never follow directly because we would have an "irrelevant edge". This implies $r, s, t \geq 1$. We will argue that $r = s = t = 1$.

1 This is in accordance with our conventions in Section 1.3.

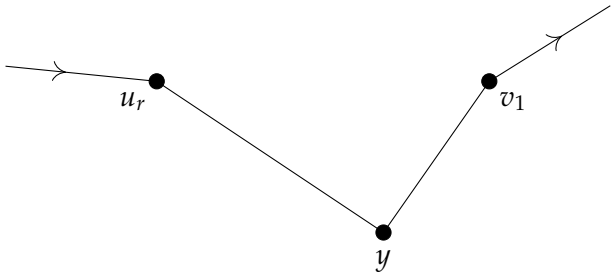

Figure 3.14: The circumference around the vertex y. Compare with Figure 3.11

Consider the neighbourhood of the vertex y in the following sense (compare Figure 3.14 to Figure 3.11):

- The edge entering u_r is called a.
- u_r is called u
- The edge from u_r to y is called b.
- y is called v.
- The edge from y to v_1 is called c.
- v_1 is called w.
- The edge leaving v_1 is called d.

Since there are only three unbalanced vertices, no unbalanced vertices are inside the convex hull of u, v, w.

We now have the setup of the 60° Lemma (Lemma 3.25) and can conclude that the turn angle from a to d is at most 60°. In other words: The sum of the turn angles at u_r, y and v_1 is at most 60°. We will abuse notation and use the names for the vertices also for the turn angles of the circumference at these vertices. So we can write:

$$u_r + y + v_1 \leq 60^\circ \tag{3.1}$$

By analogous arguments around x and z we get

$$w_t + x + u_1 \leq 60^\circ \tag{3.2}$$
$$v_s + z + w_1 \leq 60^\circ \tag{3.3}$$

Note that the circumference is essentially simple as specified by Definition 3.18:

- Backtracking could only happen while visiting one of the unbalanced vertices, since at balanced vertices, the circumference always takes the first right turn (see Lemma 3.28). If backtracking happened at, say, x, note that then w_t and u_1 would be the same balanced vertex. γ takes the first right turn both before and after visiting x, so

double backtracking would imply that $u_1 = w_t$ has degree 2 which is impossible for a balanced vertex. Also, since we do right turns right before and after x, the edge to/from x must lie to the right of the remainder of the circumference. We conclude that if backtracking happens, it is admissible.

- Since the circumference is a boundary walk, it can never cut off any edges, but this would be necessary for a transversal crossing.

Since the circumference is also closed and the outside always lies to the right of it by definition, it is counterclockwise according to Definition 3.19 and Gauß-Bonnet as described in Lemma 3.20 applies:

$$x + y + z + \sum u_i + \sum v_j + \sum w_k = 360^\circ \tag{3.4}$$

Now assume that $r > 1$ and therefore u_1 and u_r are indeed separate angles. Note that the turn angle at balanced vertices on the circumference must be negative and rewrite equation (3.4) to:

$$\underbrace{w_t + x + u_1}_{\leq 60^\circ} + \underbrace{u_r + y + v_1}_{\leq 60^\circ} + \underbrace{z}_{\leq 180^\circ} + \underbrace{\sum_{i \neq 1, r} u_i + \sum_{j \neq 1} v_j + \sum_{k \neq t} w_k}_{\leq 0} = 360^\circ$$

This is a contradiction. It follows that $r = 1$. By analogous arguments $s = t = 1$ and we have in fact the situation shown in Figure 3.15 . This means that the three inequalities (3.1), (3.2), (3.3) can be rewritten as:

$$u_1 + y + v_1 \leq 60^\circ \qquad w_1 + x + u_1 \leq 60^\circ \qquad v_1 + z + w_1 \leq 60^\circ$$

Adding up and rearranging, we get

$$x + y + z + u_1 + v_1 + w_1 \leq 180^\circ - (u_1 + v_1 + w_1)$$

But because of (3.4), we get

$$360^\circ = x + y + z + u_1 + v_1 + w_1 \leq 180^\circ - (u_1 + v_1 + w_1)$$

We see that $u_1 + v_1 + w_1 \leq -180^\circ$. But then also $x + y + z \geq 540^\circ$. Since each of x, y, z can be at most 180°, it follows that

$$x = y = z = 180^\circ$$

That implies $u_1 = v_1 = w_1$ and therefore G is just a tree with three unbalanced vertices and one degree three balanced vertex in the centre. So in fact, this tree is the only possible geodesic net with three unbalanced vertices that includes any balanced vertices. □

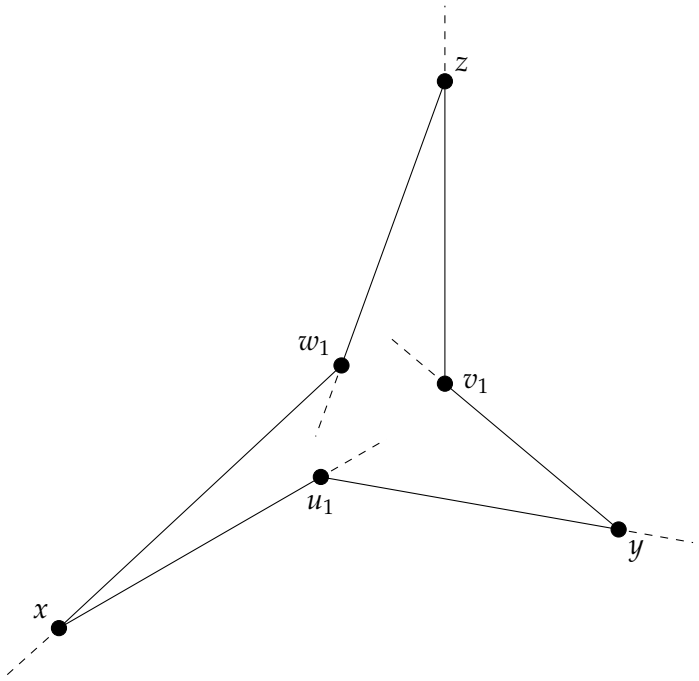

Figure 3.15: The circumference of the geodesic net after we have established that $r = s = t = 1$. The dashed lines are the lines of reference for the turn angles.

3.5 THE CASE OF NONPOSITIVE CURVATURE

In this section, we will establish that Theorem 3.3 holds true for nonpositive curvature on $\mathbb{R}^2$ as well:

First note that all local results of Section 3.2, in particular the Special Combined Angle Lemma (Lemma 3.9), apply without alteration on surfaces of any curvature. The global results of Section 3.3 on the other hand necessitate a closer look.

Note that the convex hull of a finite number of points in a plane of nonpositive curvature is still the geodesic polygon with vertices at some of these points. This can be shown using the fact that in a simply connected Riemannian manifold of nonpositive curvature, the exponential map at any point is a diffeomorphism (see theorem 2.6.6 in [Kli82]). Therefore Lemma 3.10 and Lemma 3.11 still apply (where, in the proofs, one replaces straight lines with geodesics). Also, the definition and results regarding the circumference still work without alteration. It is worth noting how we use that we are dealing with a metric on $\mathbb{R}^2$ and not an arbitrary surface: We used that the surface is simply connected and the definition of the circumference relies on the notion of an outer face, which uses that $\mathbb{R}^2 \setminus G$

has exactly one unbounded component. Either of these arguments would fail on, say, the flat torus.

Our version of Gauß-Bonnet for essentially simple curves as given by Lemma 3.20 still applies with the following adjustment: Since we have nonpositive curvature, the turn angle along such a counterclockwise closed path now is 360° *or more*. Unlike in flat geometry, we won't have conditional path independence as described by Lemma 3.21. We will see below that we can do without that fact. Note that the First and Second Turn Lemma (Lemma 3.23/Lemma 3.24) again describe local properties and therefore still apply.

We will now prove a generalized version of the flat 60°-Lemma (Lemma 3.25) before we prove the main result for nonpositive curvature. The proofs will closely follow the ideas of the flat case.

Lemma 3.32 (60° Lemma, nonpositive curvature)**.** *Consider a path going through four edges a, b, c, d of a geodesic net on $\mathbb{R}^2$ with a metric of nonpositive curvature and three vertices u, v, w in the order a, u, b, v, c, w, d. Assume that*

(a) $a \neq -b$, $c \neq -d$
(b) *u and w are balanced (v can be balanced or not).*
(c) *b immediately follows a at u (i.e. $a * b$ takes the first right turn).*
(d) *d immediately follows c at w (i.e. $c * d$ takes the first right turn).*
(e) *The convex hull of u, v, w contains no unbalanced vertices (except, possibly, v itself).*

Then there exists a piecewise geodesic path γ contained in the convex hull of u, v, w with the following properties:

- *γ starts at u and ends at w.*
- *The turn angle along $a * \gamma * d$ is 60° or less.*
- *γ is simple apart from possible admissible backtracks.*

Note that we do not require the path to be on the geodesic net. The important difference between the flat version and the version for nonpositive curvature is that we are merely looking for *some* path along which the turn angle is 60° or less. This is how we deal with the absence of conditional path independence.

Proof. We can again exclude the two trivial cases where $u = w$ or where the turn angle from b to c is nonpositive. In those cases, the path $\gamma = b * c$ fulfils the required properties.

We arrive at a picture similar to the one in Figure 3.11 with a geodesic triangle bounded by b, c where ℓ is the unique geodesic going through u and w. As before, a or d could also be below ℓ (for a consideration of what "below" means in this case, see Case 2).

We define a path γ as before: start at u. The first edge of γ is given by the second right turn at u, counting from a. Then γ always takes the first right turn (unless it leads to v, in which case it takes the second right turn) and terminates at w or once we leave the convex hull. The argument that γ is well-defined still applies. For clarification, in the argument that the path terminates, the "rays" from v would now be the geodesic rays starting at v and sweeping out the convex hull/geodesic triangle of u, v and w.

We again work on the following cases:

Case 1 γ reaches w. Note that by the same arguments as in the flat case, γ fulfills all properties required of a path according to the lemma, except possibly the turn angle. If the turn angle along $a * \gamma * d$ is nonpositive, we are therefore done.

Otherwise, at some point the turn angle at a vertex on $a * \gamma * d$ must be positive. Denote by x the first vertex with a positive turn angle and by y the last vertex with a positive turn angle. Follow the same construction as in the flat case and arrive at a path $a * \gamma(\to x) * e_v * f_v * \gamma(y \to) * d$. Note that now $\gamma' := \gamma(\to x) * e_v * f_v * \gamma(y \to)$ fulfills all requirements of the lemma, including the turn angle along $a * \gamma' * d$ which is, as argued before, at most $-60° + 180° - 60° = 60°$. The argument that γ' is simple apart from one possible backtrack is the same as in the flat case.

Case 2 γ leaves the convex hull of u, v, w and terminates.

Note that the terms of a or d lying "below ℓ" or "above ℓ" that we use in the following are to be understood in the sense that their tangent vectors at the vertex lie below or above the tangent vector of ℓ in the tangent space at the respective vertex, which is divided into two half planes by ℓ where the lower half plane u is the one including the tangent vector of b and the lower half plane at w is the one including the tangent vector of c. Denote by $\overline{\ell}$ the segment of ℓ between u and w.

Case 2a both a and d lie above ℓ. We find our vertex x on the path γ as follows: If the turn angle from a to the first edge of γ is positive (i.e. the turn angle at u is positive), then we choose $x := u$. Otherwise we must enter the interior of the convex hull of u, v and w and can consider the following path: Start at u, follow γ until it would leave the convex hull (at which point it crosses $\overline{\ell}$) and then return to u along $\overline{\ell}$. This is a simple, closed, counterclockwise path. The total turn angle along this path must be 360° or more (since it encloses a region of nonpositive curvature) and has three or more vertices. In particular, one of the vertices not incident to $\overline{\ell}$ must have a positive turn angle. Starting at u going counterclockwise, the first such vertex will be denoted by x. The vertex y can be found on a path starting with the second left turn at d and then always taking the first left turn, except if it leads to v (as before, this is the mirror image of the

process of finding γ an x) and we arrive at the familiar situation where we can define a path $u \to x \to v \to y \to w$ fulfilling the required properties.

Case 2b d lies on or below ℓ. As before, this case is rather pathological.

Consider the following path which we call γ_+: Truncate the path γ so that it terminates at the point where it intersects $\overline{\ell}$ for the last time. This means it most likely won't terminate on a vertex but in the middle of an edge. Now continue along $\overline{\ell}$ to w.

If the turn angle along $a * \gamma_+ * d$ is 60° or less, we are done (the argument for γ_+ being essentially simple is the same as previously). Otherwise note: The total turn angle along $a * \gamma_+ * d$ must be more than 60°, the last turn of $\gamma+$ onto $\overline{\ell}$ must be nonpositive (since the last edge of γ is on or below $\overline{\ell}$) and the turn from γ_+ onto d is nonpositive (since d lies on or below ℓ). So there must be at least one vertex along $a * \gamma_+$ with a positive turn angle and this is in fact a turn between two edges of the geodesic net. Call the first such vertex x and the last such vertex y. As usual, we allow x and y to coincide. Define e_v and f_v as before and we get a path $\gamma' := \gamma_+(\to x) * e_v * f_v * \gamma_+(y \to)$ such that the turn angle along $a * \gamma' * d$ can be at most 60°. Again the argument that γ' is simple apart from one possible admissible backtrack remains the same. We now have the path we were looking for.

Case 2c a lies on or below ℓ. This case is still the mirror image of Case 2c. □

We can now prove the general version of Theorem 3.3, i.e. the case of three boundary vertices and nonpositive curvature.

Again, we will closely follow the proof for the flat case, i.e. the proof of Lemma 3.31.

Lemma 3.33. *A geodesic net on $\mathbb{R}^2$ with a metric of nonpositive curvature with three unbalanced vertices has at most one balanced vertex.*

Proof. Call the three unbalanced vertices x, y and z. The initial observations regarding the circumference still apply to the nonpositive curvature case, so we can reduce to the case where the circumference travels along vertices in the order

$$x, u_1, \dots, u_r, y, v_1, \dots, v_s, z, w_1, \dots, w_t, x$$

Where all the u_i, v_j, w_k are balanced vertices with $r, s, t \geq 1$. We will argue that $r = s = t = 1$.

Looking back at Figure 3.14, we have the setup of the 60°-Lemma around the vertex y. We are using the non-flat version of the lemma this time and get a piecewise geodesic path inside the convex hull of u_r, y, v_1 starting at u_r and ending at v_1 that is simple apart from admissible backtracks and

such that the turn angle from the edge entering u_r along this path to the edge leaving v_1 is at most $60°$. Call this path α_y. In a similar fashion, we get paths α_z and α_x. Recall that the circumference is denoted by γ.

Assume that $r > 1$ which means we can define the following closed counterclockwise path:

$$\cdots \xrightarrow{\gamma} \underbrace{u_r \xrightarrow{\alpha_y} v_1}_{\leq 60°} \xrightarrow{\gamma} v_s \xrightarrow{\gamma} \underbrace{z}_{\leq 180°} \xrightarrow{\gamma} w_1 \xrightarrow{\gamma} \underbrace{w_t \xrightarrow{\alpha_x} u_1}_{\leq 60°} \xrightarrow{\gamma} \cdots$$

The angles given above are the turn angles along the respective parts of this path. It is important to point out that we assume $u_1 \neq u_r$ which justifies that the two segments of $\leq 60°$ don't overlap.

All other turn angles along this path are negative. Note that Gauß-Bonnet for essentially simple curves as stated in Lemma 3.20 applies: The argument that the circumference γ is essentially simple was provided in the flat case. Both α_x and α_y are simple apart from admissible backtracks as given by Lemma 3.32. Also, we are not using the parts of γ visiting x and y, therefore α_x and α_y can not meet γ except at their endpoints. Therefore, the resulting path is still essentially simple. So the turn angle along this path should be $360°$ or more. However, we can see above that this path has a total turn angle of $300°$ or less, a contradiction.

$r = 1$ follows. By analogous arguments $s = t = 1$ and we arrive at the situation shown in Figure 3.16.

We now consider the following closed path (for further reference, consider Figure 3.16) which we call β:

$$\cdots \xrightarrow{\gamma} \underbrace{u_1 \xrightarrow{\alpha_y} v_1}_{\leq 60°} \xrightarrow{\gamma} \underbrace{z}_{\leq 180°} \xrightarrow{\gamma} \underbrace{w_1 \xrightarrow{\alpha_x} u_1}_{\leq 60°} \xrightarrow{\gamma} \underbrace{y}_{\leq 180°} \xrightarrow{\gamma} \underbrace{v_1 \xrightarrow{\alpha_z} w_1}_{\leq 60°} \xrightarrow{\gamma} \underbrace{x}_{\leq 180°} \xrightarrow{\gamma} \cdots$$

Note that all angles that are not specified are negative and therefore the sum of all turn angles along this path β is $720°$ or less. We will use the notation $\mathrm{Turn}(\beta) \leq 720°$.

Claim: $\mathrm{Turn}(\beta) = 720°$.

β crosses itself transversally by design which means it is not essentially simple and we can't apply Gauß-Bonnet directly. We proceed as follows:

Consider the circumference γ (given by the solid lines in Figure 3.16) and the path $\alpha := \alpha_x * \alpha_y * \alpha_z$ (given by the dashed lines in Figure 3.16). γ is essentially simple as established before. Each of α_x, α_y and α_z is simple apart from admissible backtracks and they lie in separate convex hulls.

Therefore, their concatenation α is also essentially simple. So Gauß-Bonnet applies to each of γ and α and

$$\left.\begin{array}{l}\text{Turn}(\gamma) \geq 360^\circ \\ \text{Turn}(\alpha) \geq 360^\circ\end{array}\right\} \Rightarrow \text{Turn}(\gamma) + \text{Turn}(\alpha) \geq 720^\circ$$

If we show $\text{Turn}(\beta) = \text{Turn}(\gamma) + \text{Turn}(\alpha)$, the claim follows.

In fact, note that β follows α and γ, only switching between them at u_1, v_1 and w_1. So we need to show that the total turn angle of β at u_1 (which it visits twice) is the same as the sum of the turn angles of γ and α at u_1. The observation for v_1 and w_1 will then be the same.

Consider the situation at u_1 as depicted in Figure 3.17 and observe:

- The turn angle of α is d (dashed-dashed).
- The turn angle of γ is a (solid-solid).
- The turn angle of β for each of the two visits is b (solid-dashed) and c (dashed-solid) respectively.

We use a negative sign if we go backwards along one of these angles and can see in the figure that $a - c + d - b = 0$ and therefore $b + c = a + d$. So

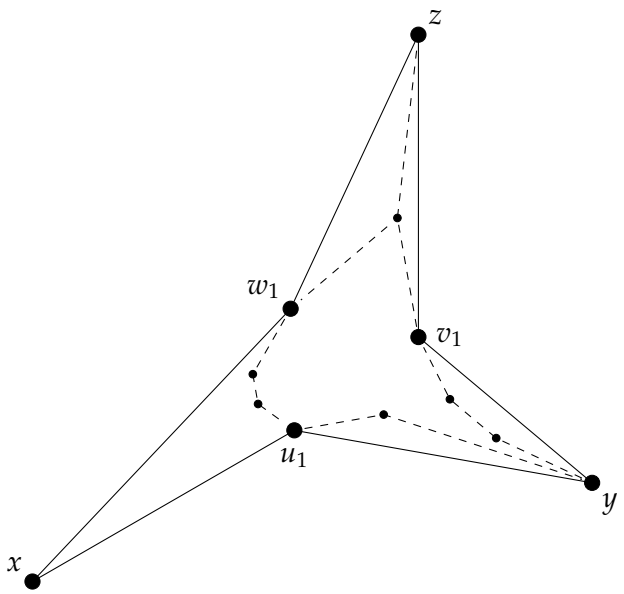

Figure 3.16: The situation described in the final steps of the proof for nonpositive curvature. The solid path is the circumference γ, the three dashed paths are α_x, α_y and α_z respectively. These paths could reach x, y or z as depicted. Note that since the situation where u_1, v_1 and w_1 don't coincide is shown to be inadmissible later in the proof, the angles in this picture can't be true to the angles as stated in the proof.

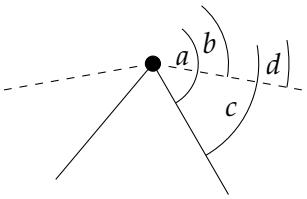

Figure 3.17: The situation at u_1. To simplify the picture, this sample situation is chosen so that all considered turn angles are negative.

indeed, the sum of the turn angles of α and γ at u_1 is the same as the sum of the turn angles of β at u_1.

Following the same argument at v_1 and w_1, we can conclude that in fact $\mathrm{Turn}(\beta) = \mathrm{Turn}(\gamma) + \mathrm{Turn}(\alpha)$.

This finishes the proof of the claim. Note that $\mathrm{Turn}(\beta) = 720^\circ$ can only be achieved if all turn angles as specified in the definition of β above are extremal. In particular, the angles at x, y and z must be equal to 180°. Therefore $u_1 = v_1 = w_1$ is the single balanced vertex of this geodesic net. □

4

CONSTRUCTION OF EXAMPLES

In Chapter 3, we proved the following theorem:

Theorem 3.2. *Each geodesic net with 3 unbalanced vertices (of arbitrary degree) on the plane endowed with a Riemannian metric of non-positive curvature has at most one balanced vertex.*

This raises the obvious question if this theorem can be generalized to a statement about positive curvature or to geodesic nets with more than three vertices. The examples constructed in this section show that such an immediate generalization is not possible:

- In Section 4.1, we will construct a geodesic net on the flat plane with four unbalanced vertices and 28 balanced vertices, illustrating how remarkable the small bound in the case of just three unbalanced vertices is. Recall that we expect no bound for four vertices to exist as stated in Conjecture 2.11.
- As it turns out, the above example will consist of an overlay of several trees. So, while it has a larger number of balanced vertices, it is not *irreducible*, as we will define in Section 4.2. We proceed with the construction of an irreducible geodesic net with four unbalanced vertices that is not a tree, showing that even for just four unbalanced vertices, quite complex geodesic nets can exist.
- Finally, we will consider positive curvature in Section 4.3, where we construct an example of a geodesic net with just three unbalanced vertices that has a cycle of three balanced vertices, showing that the bound of the above theorem does not apply in the case of positive curvature.

In this chapter, we will frequently use the notation ABC for the the angle at B from A to C.

4.1 FOUR VERTICES IN THE PLANE

In the following, we will give a detailed construction of the example geodesic net in flat $\mathbb{R}^2$ with four unbalanced vertices and 28 balanced vertices given in Figure 4.2.

We will use the following classical theorem of Euclidean Geometry:

Theorem 4.1. *Consider a circle with centre O and three points A, B, C on this circle, in clockwise order. Then the angle AOC is twice as large as the angle ABC.*

Using this theorem, we can construct the geodesic net. For a visualization, refer to Figure 4.1.

When describing circular arcs below we use the canonical angle on a circle where 0° describes the rightmost point and we go counterclockwise. The choice of the units 1, 2 and 5 during the construction will be justified below.

- Fix two points P and Q with distance 5 units on a vertical axis. The line through P and Q will from now on be called *the axis*.
- Draw a circular segment of radius 2 centred at P starting at angle 210° and ending at angle 330° (so that the outer angle of the circular segment will be 240°).
- Draw a circular segment of radius 1 centred at Q starting at angle 30° and ending at angle 150° (so that the outer angle of the circular segment will be 240°).
- The endpoints of these arcs are denoted by A, C and X, Z respectively. They will be the four unbalanced vertices of the geodesic net.
- Note that now, by Theorem 4.1, any point B_i on the circular arc centred at P will have the following property: $CB_iA = 120^\circ$.
- By the same argument, any point Y_i on the circular arc centred at Q will give an angle $XY_iZ = 120^\circ$.
- The vertices B_2 and Y_2 will be positioned at the intersection of the two circular arcs with the axis.
- Add the edges AB_2, CB_2, B_2Y_2, XY_2 and ZY_2. We now have two balanced degree 3 vertices B_2 and Y_2.
- Find B_1 as follows: We want to add B_1 to the circular arc between A and B_2. We will find the exact position as follows: Note that if $B_1 = B_2$, then

  $$XB_1C = XB_2C > Y_2B_2C = 120^\circ$$

  and if $B_1 = A$, then

  $$XB_1C = XAC \leq 90^\circ$$

  Note that $XAC \leq 90^\circ$ is due to the fact that the distance from X to the axis is smaller than the distance from A to the axis. By continuity, there now must be some choice for B_1 on the circular arc between A and B_2 such that $XB_1C = 120^\circ$.

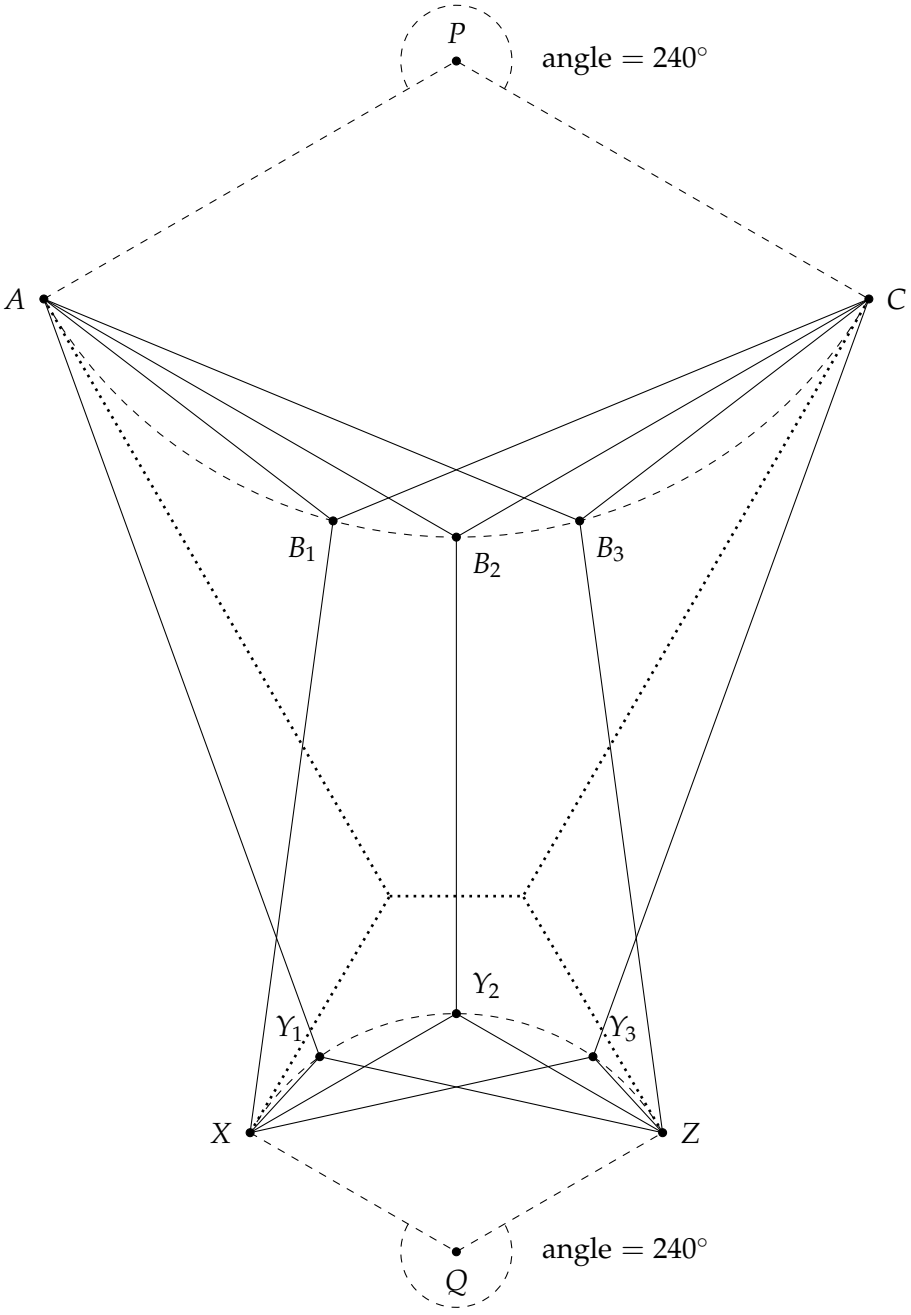

Figure 4.1: Construction of the geodesic net in Figure 4.2. For better overview, the segments XC and ZA are not displayed. Using Theorem 4.1, we know that if the angle at P is 240°, then the angle CB_iA will be 120°. The same is true for the angles XY_iZ. The subgraph G' is given in dotted lines.

- Now add the edges AB_1, CB_1 and XB_1 making B_1 a balanced degree 3 vertex.
- Y_1 can be found in a very similar fashion: As above, we have to find the position of Y_1 on the arc between X and Y_2. Note that if $Y_1 = Y_2$, we would have

$$ZY_1A = ZY_2A > ZY_2B_2 = 120^\circ$$

  and if $Y_1 = X$, then

$$ZY_1A = ZXA < 120^\circ$$

  The inequality $ZXA < 120^\circ$ will be justified below. Again by continuity there is a choice for Y_1 such that $ZY_1A = 120^\circ$. Add the appropriate edges to make Y_1 a balanced degree 3 vertex.
- B_3 and Y_3 are simply the reflection of B_1 and Y_1 along the axis. We add the appropriate edges to make them balanced degree 3 vertices.
- Now add a subgraph G' with two degree 3 balanced vertices (shown with dotted lines in Figure 4.1). That adding G' is possible should be clear from the figure but will be justified further below.
- Finally, add the two segments AZ, and CX (not depicted in Figure 4.1) which will intersect at a vertex M on the axis. This is the single degree 6 vertex of the geodesic net.

We now have a geodesic net with the unbalanced vertices A, C, X and Z, with eight balanced degree 3 vertices (B_i, Y_i and the two vertices of G'), nineteen balanced degree 4 vertices (these are all the intersections between straight line segments) and one balanced degree 6 vertex (M).

During the construction, we made three seemingly liberal choices regarding length: The radii of the two arcs are given as $R = 2$ and $r = 1$ and the distance between P and Q was chosen to be $d = 5$. While these are not the only possible choices, there are still some restrictions on these numbers:

- If $r = R$, the subgraph G' added in the last step would intersect the axis in the point M. This would produce a geodesic net where M is a vertex of degree 8, however the total number of balanced vertices is larger if M does not lie on G'. Therefore, $r \neq R$ gives more balanced vertices.
- Clearly, $d > R + r$ because otherwise the two arcs would intersect.
- We have to choose R, r, d such that the angle $ZXA < 120^\circ$, a fact we used above. It is an exercise in trigonometry that $R = 2$, $r = 1$ and $d = 5$ is one such choice but of course not the only one. For the given numbers, we have $ZXA \approx 104^\circ$.

- Finally, we have to ensure that the subgraph G' "fits" in the picture, i.e. that it is possible to position the two degree 3 vertices in a way that allows all three angles at each vertex to be 120°. The choices we made for R, r, d are one possibility for which, by basic arguments involving the angle sum in triangles and quadrilaterals, adding such a subgraph is possible.

In fact, the restrictions on R, r and d allow for enough freedom that, with any two fixed, the third one can be slightly pertubed still allowing the same construction. In other words, the set of admissible (R, r, d) is an open set in $\mathbb{R}^3$.

The geodesic net constructed in this section shows that in the context of Theorem 3.3, we have $f(4) \geq 28$. This example only makes use of degree 3, 4 and 6 balanced vertices and is also highly symmetric, suggesting that it is not the maximal example. In fact, we can observe that once we go beyond three unbalanced vertices, we gain much more "freedom" as to how the balanced vertices can be distributed. In particular, for very large degree we should be able to construct with very small restrictions. In the context of the proof in Chapter 3, the 60° Lemma (Lemma 3.25) "looses its teeth". These observations support the conjectures stated in Chapter 2. In fact, for four unbalanced vertices, other constructions are possible, as the next section shows.

4.2 AN IRREDUCIBLE GEODESIC NET THAT IS NOT A TREE

First, consider again the geodesic net in Figure 4.2 that we constructed in the previous section. At first sight, it seems rather complicated. However, as the figure and the details of the above construction highlight, it is essentially an "overlay" of several geodesic nets, each of them being a tree: four geodesic nets with 3 unbalanced vertices and the Fermat point in the middle, and three well-known tree-shaped geodesic nets with 4 unbalanced vertices and 1 or 2 balanced vertices (plus the balanced vertices that appear as points of the intersections of edges of these elementary geodesic nets). With this example in mind, it is of interest to define *irreducible* geodesic nets as geodesic nets without proper geodesic subnets which are defined as follows

Definition 4.2. G' is a *proper gedesic subnet* of G if

(i) The set of balanced (resp. unbalanced) vertices of G' is a subset of the balanced (resp. unbalanced) vertices of G.

(ii) The set of edges of G' is a non-empty, proper subset of the set E of edges of G.

To our knowledge, the only known examples of irreducible geodesic nets with four unbalanced vertices were the trees with 1 or 2 balanced vertices that can be seen at the right side of Figure 4.2.

This brings us to the questions that we are answering below:

Question 4.3. Do there exist irreducible geodesic nets with 4 unbalanced vertices in the Euclidean plane with at least 3 balanced vertices? Can they contain cycles of balanced points?

This section will show that the answer for these questions is yes:

Theorem 4.4. *There exists an irreducible geodesic net in the Euclidean plane that has* 16 *balanced vertices and* 4 *unbalanced vertices and that is not a tree.*

It is tempting to conjecture that our example is one of a series of similar examples with arbitrary large number of balanced vertices, but at the moment this is the only new example of an irreducible geodesic net with four unbalanced vertices that we were able to construct.

The Construction

Before we start, it is worth noting that the geodesic net G we are constructing here will be symmetric under a rotation by $90°$.

$\mathcal{O} = (0, 0)$ will denote the origin. The end result of the construction is given in Figure 4.4.

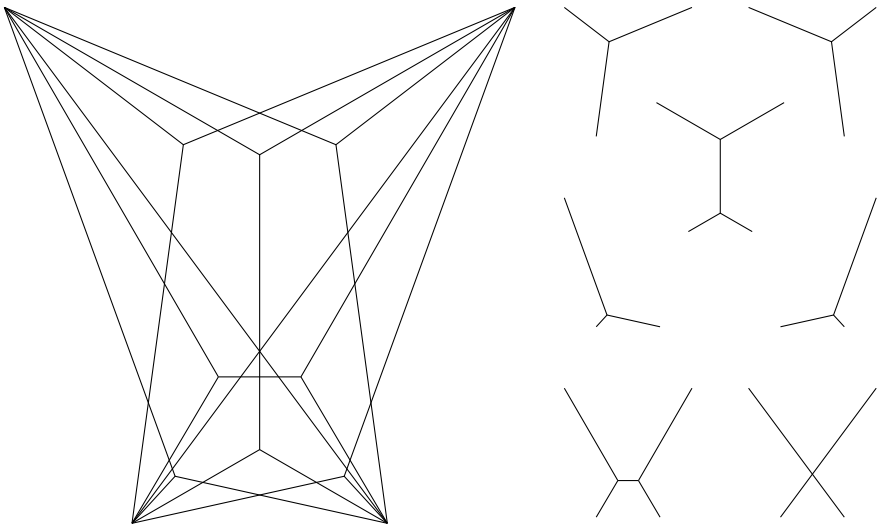

Figure 4.2: A geodesic net in the plane with four unbalanced vertices. While this net has a notable amount of balanced vertices, it is just a union of seven trees as depicted. In other words, in is an "overlay" of more elementary nets and therefore not *irreducible* as defined in Section 4.2.

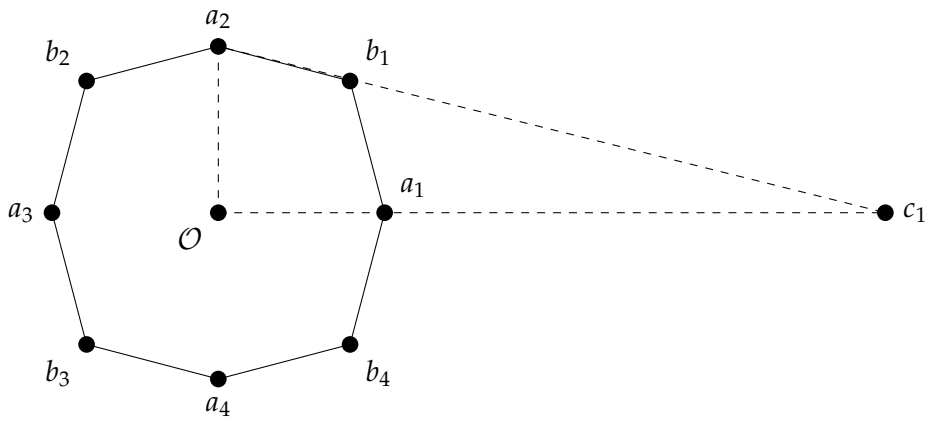

Figure 4.3: The octagon in the first step with alternating interior angles of 150° and 120°. The dashed triangle is used to define the position of c_1. Note that the side a_2c_1 does *not* go through b_1. In fact, the angle $\mathcal{O}a_2b_1$ is 75° whereas the angle $\mathcal{O}a_2c_1$ is just over 76°.

The Octagon of a_i and b_i

Fix four vertices at $a_1 = (1,0)$, $a_2 = (0,1)$, $a_3 = (-1,0)$ and $a_4 = (0,-1)$. Now add another four vertices b_1, b_2, b_3, b_4 so that we arrive at an octagon $a_1b_2a_2b_2a_3b_3a_4b_4$ where the interior angle at each a_i is 150° and the interior angle at each b_i is 120°.

The Four Unbalanced Vertices c_i

There is a uniquely defined triangle as follows, see Figure 4.3:

- The left side is $a_2\mathcal{O}$.
- The angle at $\mathcal{O}$ is 90°.
- The angle at a_2 is $\arccos\left(\frac{1}{2} - \cos 75^\circ\right) \approx 76.04^\circ$.

The resulting third vertex of this triangle is denoted by c_1. By rotation around $\mathcal{O}$ we get vertices c_2, c_3 and c_4, see Figure 4.4.

The Fermat Points d_i

We define d_1 as follows (again, d_2, d_3 and d_4 will be defined by rotational symmetry): It is the Fermat point of the triangle $b_1c_1c_2$. Recall that the Fermat point is the unique point x in a triangle such that the angle at x between any two corners of the triangle is 120°. It exists as long as all interior angles of the triangle are less than 120°. So we are left to show:

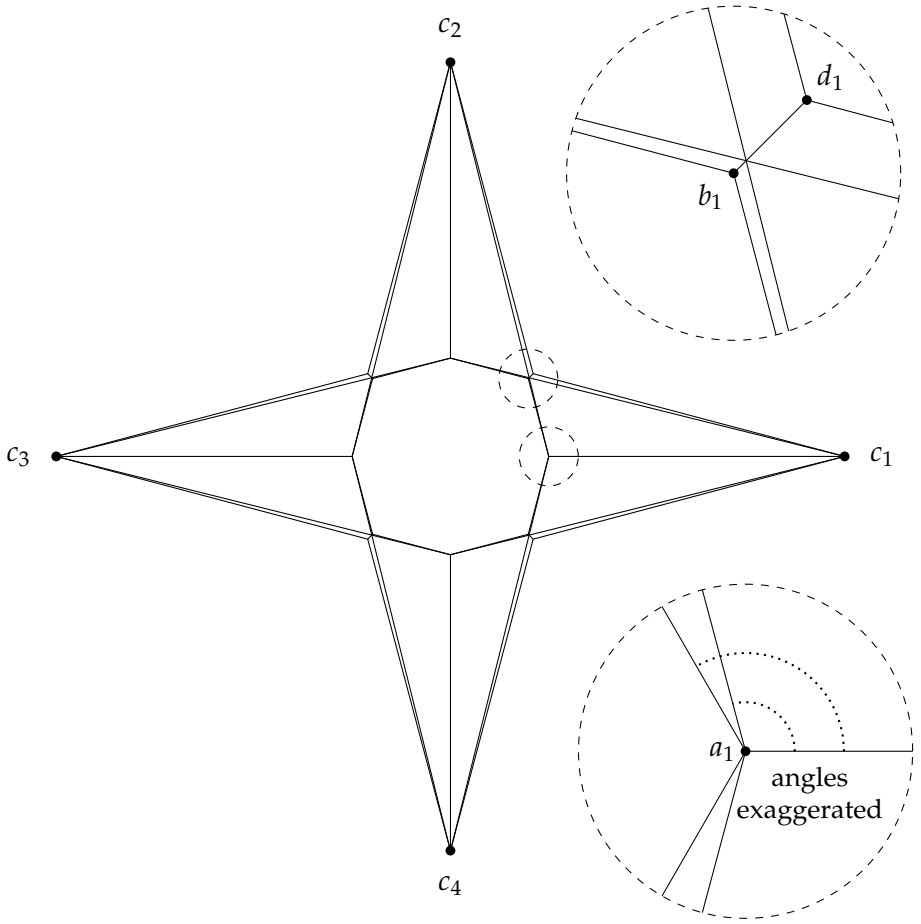

Figure 4.4: The complete geodesic net with the unbalanced vertices c_1, c_2, c_3, c_4. The zoom-ins are provided for overview of the balanced vertices. The two dotted angles at a_1 are $180^\circ - 75^\circ = 105^\circ$ and $180^\circ - \arccos\left(\frac{1}{2} - \cos 75^\circ\right) \approx 103.96^\circ$ respectively. In the zoom-in, they are exaggerated for clarity.

Lemma 4.5. *All three interior angles of the triangle $b_1c_1c_2$ are less than* $120°$.

Proof. It is obvious that the interior angles at c_1 and c_2 are less than $120°$ (in fact they are both significantly smaller than $90°$). So it remains to show that the angle at b_1 is less than $120°$. This can be shown as follows:

- $c_1\mathcal{O}b_1 = 45°$ follows from the symmetries of the octagon.
- The segment a_2c_1 is above the segment b_1c_1 (see Figure 4.3). It follows that

$$b_1c_1\mathcal{O} < a_1c_1\mathcal{O} \approx 180° - 90° - 76.04° = 13.96°$$

- We now have estimates for two of the angles of the triangle with corners $\mathcal{O}$, c_1, b_1 and get

$$\begin{aligned}\mathcal{O}b_1c_1 &= 180° - c_1\mathcal{O}b_1 - b_1c_1\mathcal{O} > 180° - c_1\mathcal{O}b_1 - a_1c_1\mathcal{O}\\ &\approx 180° - 45° - 13.96° = 121.04°\end{aligned}$$

- We can use the symmetry of the picture and conclude:

$$\begin{aligned}c_1b_1c_2 &= 360° - \mathcal{O}b_1c_1 - c_2b_1\mathcal{O}\\ &= 360° - 2\cdot\mathcal{O}b_1c_1 \approx 117.92 < 120°\end{aligned}$$

□

The Edges

Finally, we add the edges of the geodesic net. We recommend referring again to Figure 4.4 for better understanding.

The following definitions have to be read circular, e.g. a_5 is the same as a_1. With that in mind, the edges of the geodesic net for $i = 1, 2, 3, 4$ are:

- The edges of the octagon, given by a_ib_i and $a_{i+1}b_i$.
- The radial edges given by a_ic_i.
- The edges given by a_ic_{i+1} and $a_{i+1}c_i$.
- Finally, the edges for each Fermat point, given by d_ib_i, d_ic_i and d_ic_{i+1}.

The Additional Vertices x_i

Note that we are getting four additional vertices of degree 6 which are situated on the edge connecting b_i and d_i (again, see Figure 4.4). We call these vertices x_1, x_2, x_3 and x_4.

Checking the Edges and the Balance

Lemma 4.6. *The net constructed above is a valid geodesic net with four unbalanced vertices, more specifically:*

- *Different edges can intersect only at their common endpoints (in other words: there never is an "overlay" of edges, so all edges have weight one).*
- *Each a_i, b_i, d_i, x_i is balanced.*

Proof. Note again that the picture is rotationally symmetric by design. So we can concentrate on the corner c_1Oc_2 (the upper right quadrant).

As long as we prove that none of the edges are parallel, the result follows. We will go through the edges as defined above, adding them step by step.

- It is apparent that none of a_1b_1, a_2b_1 and a_1c_1 are parallel.
- Adding a_1c_2, note that the angle between a_1b_2 and a_1c_2 is approximately $1.04°$, so these two edges are not parallel. It is apparent that a_1c_2 is never parallel to any other edge. By symmetry, adding a_2c_1 doesn't create issues either.
- The line segment d_1b_1 (which consists of the two edges d_1x_1 and x_1b_1) is radial at the angle $45°$. No other edge is. This finally brings us to the only two interesting edges: adding d_1c_1 and d_1c_2. We will consider the former. Symmetry will then deal with the latter. The only problem could arise if d_1c_1 coincides with the previously added a_2c_1 (which would then also imply that $d_1 = x_1$). Elementary calculations involving the angle sum in triangles, however, show that $d_1c_1\mathcal{O} = 15°$ whereas $a_2c_1\mathcal{O} \approx 13.96°$. It follows that the two edges in question are not parallel.

We finish with showing that all vertices except the c_i are balanced. By symmetry, it is again enough to consider $i = 1$:

- a_1 is a degree 5 balanced vertex. Putting the origin of the coordinate system at a_1, the sum of the unit vectors parallel to the five edges can be written as follows (refer to the zoom-in in Figure 4.4):

$$\begin{aligned}
&\langle 1, 0\rangle \\
&+\langle \cos(180° - \arccos(1/2 - \cos(75°))), \sin(180° - \arccos(1/2 - \cos(75°)))\rangle \\
&+\langle \cos(180° - 75°), \sin(180° - 75°)\rangle \\
&+\langle \cos(180° + \arccos(1/2 - \cos(75°))), \sin(180° + \arccos(1/2 - \cos(75°)))\rangle \\
&+\langle \cos(180° + 75°), \sin(180° + 75°)\rangle = \langle 0, 0\rangle
\end{aligned}$$

  In fact, the very reason for choosing the "odd angle" $\arccos(1/2 - \cos(75°))$ early in the construction was to ensure that the a_i are balanced.

- b_1 is a degree three balanced vertex. This follows from the fact that two of the incident edges belong to the octagon, so the angle between them at b_1 is 120°. The third edge at b_1 is the bisector of the larger angle between the other two edges by symmetry. The balancedness of b_1 follows.
- d_1 is balanced by the definition of a Fermat point.
- Finally x_1 is just the point of intersection of several straight line segments and is trivially balanced.

□

Proof that G is Irreducible

While it is obvious that G is not a tree, we need to show that:

Lemma 4.7. *G is irreducible.*

Proof. We are going to give a proof by contradiction. Assume that G' is a proper geodesic subnet of G as defined in Definition 4.2. First, assume that the set of (balanced) vertices of G' does not contain any a_i. Then G' does not contain any edges incident to a_i. Now it is easy to see that G' does not contain any vertices b_i as well as edges incident to b_i. From here, it is easy to see that the edge set of G' is empty - a contradiction.

So, we can assume without any loss of generality that a_1 is a (balanced) vertex of G'.

A simple check of the 2^5 subsets of edges incident to a_1 (there are many symmetric cases) show that the only way that a_1 can be balanced is if *all* incident edges are used. It follows that G' includes all vertices adjacent to a_1.

We therefore know that $a_1, b_1, b_4, c_1, c_2, c_4$ are in the vertex set of G'.

Consider b_1 which is a degree three vertex. Obviously one can't take a proper subset of the set of incident edges to balance b_1 (and the same will be true for all degree 3 vertices). It follows that G_1 includes all vertices adjacent to b_1.

We therefore know that $a_1, a_2, b_1, b_4, c_1, c_2, c_4, d_1$ are in the vertex set of G_1.

Now that a_2 is in the net, we can reuse the argument based on a_1 above, adding b_2 and c_3 to the picture. Again, reuse previous arguments for b_2 and it follows that d_2 and a_3 are part of G'. It should now be apparent how to conclude that c_4, b_3, d_3, a_4 and d_4 are in G'.

So G_1 includes all balanced vertices of G, except possibly the x_i. However, as previously argued, since all the b_i and d_i are of degree 3, all their incident edges are in G'. Also since the a_i can only be balanced with all incident

edges included, all edges of G are in G_1. Since the x_i are just points of intersection of edges, they are also in G.

We can conclude that $G' = G$. So, G' is not proper, and we obtain the desired contradiction. Hence, G is irreducible. □

4.3 THREE VERTICES ON A SURFACE OF POSITIVE CURVATURE

Based on the result for nonpositive curvature in Theorem 3.2, one should consider if similar statements can be made for geodesic nets on surfaces of positive curvature.

There is an example of a geodesic net on the round hemisphere with 3 unbalanced and 3 balanced vertices. The example is given in Figure 4.5 and can be constructed as follows:

- Parametrize the upper hemisphere by latitude (0° is the north pole, 90° is the equator) and longitude (from 0° to 360°).
- Position three vertices A, B and C as follows: they have longitude 0°, 120° and 240° respectively and all three have the same latitude L which will be chosen below.
- Note that for each $0^\circ \leq L \leq 90^\circ$, the three vertices A, B and C form an equilateral geodesic triangle.
- At $L = 0^\circ$, the triangle is empty, at $L = 90^\circ$ the triangle has area 2π. Therefore, for some $0^\circ < L < 90^\circ$, the area is π. This is the latitude we choose for the three vertices.
- The result is a geodesic triangle where the interior angle at each of A, B and C is 120°. This follows directly from Gauß-Bonnet.
- Finally, position three vertices X, Y and Z at the equator at longitude 0°, 120° and 240° respectively.
- Add the edges XA, YB and ZC.

The result is a geodesic net with three unbalanced vertices X, Y, Z and three balanced vertices A, B, C, each of degree three.

Note that we can avoid the equator altogether by moving up X, Y and Z to a latitude of less than 90°. This implies that the example can be constructed on a surface of positive curvature with no closed (nontrivial) geodesics.

It is obvious that we can extend this example to one on $\mathbb{R}^2$ with positive curvature.

Actually, all that is needed for this example is an equiangular geodesic triangle with total curvature equal to π. Any surface with such a triangle allows this geodesic net to be embedded.

This observation raises the following question:

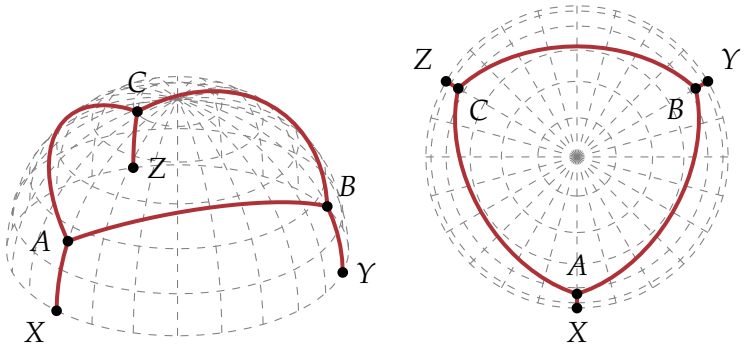

Figure 4.5: A geodesic net on the unit hemisphere with three unbalanced vertices and three balanced vertices.

Question 4.8. Is there an example of a geodesic net with three unbalanced vertices on $\mathbb{R}^2$ endowed with a metric of positive curvature such that the interior of the geodesic net has total curvature less than π but still there is more than one balanced vertex?

While we conjecture the answer to this question to be "No", note that the proofs for the flat and negatively curved cases in Chapter 3 make extensive use of the fact that the turn angle along any counterclockwise path is at least 360°, a fact that isn't true even for small amounts of positive curvature. This conjecture therefore necessitates a different proof.

5

THE STAR

The sequence of "stars" $G_n(\varphi)$ constructed in this section is a possible example of how a geodesic net can be constructed that fulfills the following requirements:

- The net has 14 unbalanced vertices (of arbitrary degree)
- The net has an arbitrarily large (finite) number of balanced vertices for large enough n
- All edges have weight one (as is required by our definition of geodesic nets)

In fact, the third condition is what makes the present construction both interesting but also quite sophisticated. If we allowed integer weights on our edges, there would be much simpler constructions of geodesic multinets with just three unbalanced vertices and an arbitrary number of balanced vertices, see Example 2.5. Assuming the third condition to be true, this star would solve the first part of Conjecture 2.13 with $N_0 = 14$.

Our construction will work as follows: First, we will construct a highly symmetric geodesic multinet $G_n(0)$, layer by layer, that provides for an arbitrarily large number of balanced vertices. To arrive at a result as depicted in Figure 5.3, we first need to build a toolbox to be used during the construction.

This highly symmetric net has edges of integer weights and is therefore a geodesic multinet. That is why we will make sure that our construction works for a small deviation from the symmetric case as well, arriving at a geodesic net $G_n(\varphi)$. This deviation is intended to split any edges with integer weights into edges with weight one.

As it turns out, showing that for some nonzero deviation $\varphi \in (-\epsilon, \epsilon)$, none of the edges of $G_n(\varphi)$ "overlap" necessitates a close look at a quite complicated finite recursive sequence. More precisely, we need to ensure that this sequence never repeats. We will present explicit formulas for this sequence as well as numerical evidence strongly suggesting that this sequence does in fact never repeat.

Assuming that this sequence never repeats, the "stars" constructed in this section would therefore be an example for a sequence of geodesic nets with a fixed number of unbalanced vertices but an arbitrarily large number of balanced vertices.

5.1 CONSTRUCTION TOOLBOX

We will first build our "toolbox" to facilitate the construction of the geodesic net below.

Suspending

Suspending is a process that adds an additional edge to a vertex v to change its imbalance.

Method 5.1 (Single-hook suspension)**.** Consider a vertex v and another vertex P, called the *hook*. We *suspend* v from P by adding the edge vP.

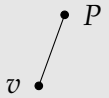

Method 5.2 (Two-hook suspension)**.** Consider a vertex v and two other vertices P, Q such that all three interior angles of the triangle ΔPvQ are less than 120°.

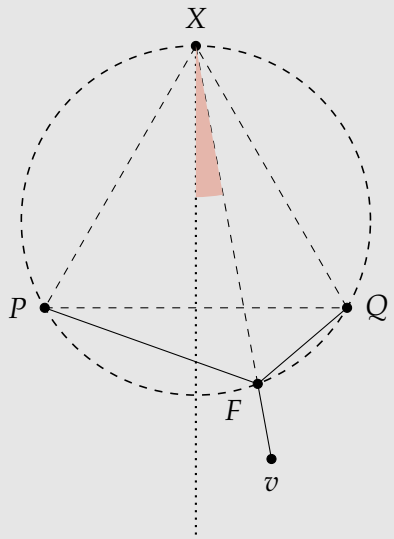

There is a unique point F – called the Fermat point – inside the triangle ΔPvQ such that the edges PF, QF and vF form angles of 120° at F. It can be constructed as follows:

- Let X be the third vertex of the unique equilateral triangle that has base PQ and that is lying outside the triangle ΔPvQ.
- Let c be the unique circle defined by the points P, Q and X.

- Note that c and the segment Xv intersect at two points: X itself and one other point. That other point is F.

That this construction does indeed yield the Fermat point is a result of classic Euclidean Geometry.

We *suspend* v from P and Q by adding F and the edges PF, QF and vF. Note that now F is a degree three balanced vertex.

The angle between Xv and the axis of symmetry of the equilateral triangle will be denoted by φ later. Note that if $\varphi = 0$, then the picture is symmetric under reflection along vX.

Winging

Winging is a process that turns an unbalanced vertex into a balanced vertex.

Method 5.3 (Winging a degree 2 vertex)**.** Consider an unbalanced vertex v of degree 2 with α_i being the larger angle between the two incident edges, i.e. with $180^\circ < \alpha_i < 360^\circ$. We can balance this vertex by "spreading wings" as follows: Extend the two incident edges to the other side of the vertex, resulting in a degree 4 balanced vertex.

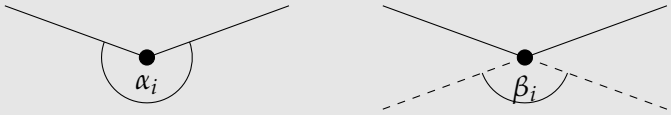

If β_i is the smaller of the two angles between the two new edges ("wings"), then $\beta_i = 360^\circ - \alpha_i$.

Method 5.4 (Winging a degree 3 vertex)**.** Consider an unbalanced vertex v of degree 3 such that the total imbalance (i.e. the sum of the unit vectors parallel to an edge) is less than 2.

We can balance this vertex by adding two edges in a unique way as follows: Since the imbalance is a vector of length less than 2, there is one (and only one) way of writing its inverse as the sum of two unit vectors. Add the two corresponding edges that balance the vertex in this way (these edges might coincide with existing edges). We arrive at a balanced vertex of degree 5.

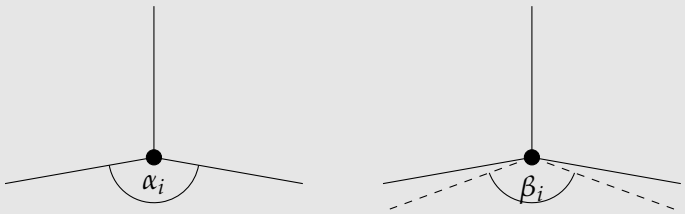

Note that this construction does *not* require the picture to be symmetric as in the sketch on the right. However, in the case that it is in fact symmetric, it is important to point out a special relationship: After winging, the picture will remain symmetric and we also get the following angle relation: If we denote the smaller of the two angles between the newly added wings by β_i, basic trigonometry yields $\beta_i = 2 \cdot \arccos(1/2 - \cos(\alpha_i/2))$. Also, as long as $\alpha_i \neq 2\arccos(1/4)$ the two dashed edges will *not* coincide with already present edges since then $\beta_i \neq \alpha_i$.

About Algebraic and Transcendental Cosines and Sines

Recall the following theorem based on Lindemann-Weierstraß:

Theorem 5.5. *If the angle α is algebraic (in radians), then* $\cos\alpha$ *and* $\sin\alpha$ *are transcendental.*

We will fix an angle $\alpha_0 > 240^\circ$ which will be close to 240°, but so that α_0 is in fact algebraic (and therefore its sine and cosine are transcendental, a property that we will need below). We will choose $\alpha_0 = 88/21$ (rad) $\approx 240.1^\circ$, but of course any other algebraic angle closer to 240° would also work.

Also note that the cosine and sine of rational multiples of π are algebraic (since they are the real an imaginary parts of roots of unity).

We will use these facts about algebraic numbers below.

The Parameters n and φ

The construction of the geodesic net $G_n(\varphi)$ relies on two parameters, the number of layers n and the deviation angle φ.

We will start with an *outer circle*, that is fixed and doesn't change under any of the parameters. We then proceed and construct an *inner circle* whose deviation from the symmetric case is measured by the angle φ. This inner circle is the "zeroth layer" of the construction. We will then add a total of

n layers, producing more and more balanced vertices while keeping the number of unbalanced vertices fixed.

Outer Circle

The *outer circle* is given by seven equiangularly distributed points on a circle. These seven vertices will be one half of the 14 unbalanced vertices of the resulting net.

Note that the whole construction will be scaling invariant, so we can choose an arbitrary radius for the outer circle. We will fix the scale of the picture further below.

Whenever we will use the process of *suspending* a vertex as defined above, the *hooks* will be two neighbouring vertices on the outer circle or a single vertex on the outer circle.

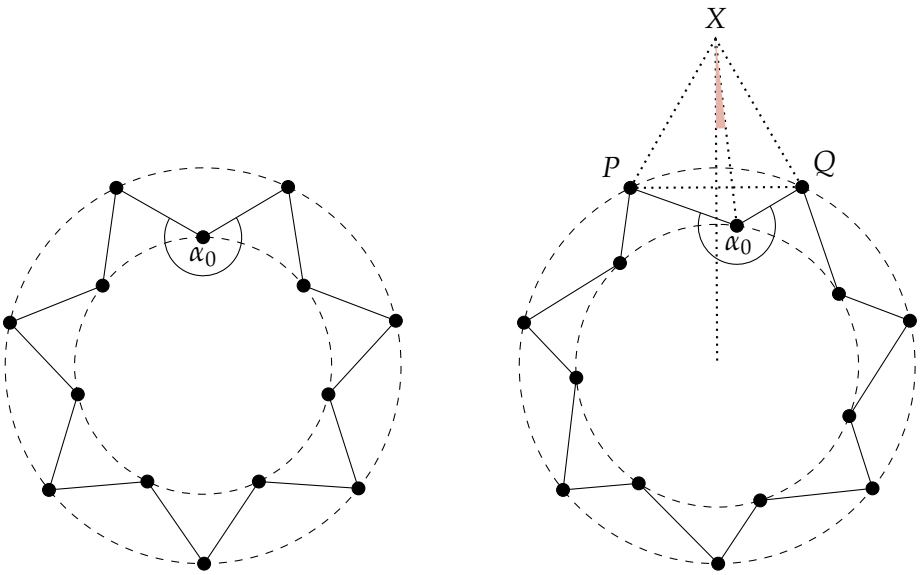

Figure 5.1: Outer circle and inner circle (= zero-th layer), symmetric case (left) and deviated case (right). Note that for fixed α_0, there is a unique way to construct the inner circle from the outer circle once the deviation $\varphi \in (-\epsilon, \epsilon)$ is given. The reference point for deviation is given by X, which is the third point of the equilateral triangle that has two adjacent points P and Q on the outer circle as base. Note that the seven points on the inner circle are always deviated by the same angle φ. In other words: with deviation, there is no reflectional symmetry anymore, but rotational symmetry is maintained.

Inner Circle

The *inner circle* is defined as follows: First, we fix α_0 as specified above. Note that this angle will not change under deviation later. Fix two neighbouring points P and Q on the outer circle and let X be the third vertex of the equilateral triangle with base PQ that lies outside the outer circle (see Figure 5.1). Recall that we are provided a deviation angle $\varphi \in (-\epsilon, \epsilon)$. Consider the segment OX (where O is the center of the outer circle) and rotate this segment around X by φ. There is a unique vertex v on the resulting segment such that $\angle PvQ = \alpha_0$. This is one vertex of the inner circle. The other six vertices of the inner circle are then provided by rotational symmetry (again, see Figure 5.1).

We then connect the outer and inner circles by edges as depicted. To later simplify calculations, we now scale the picture so that the radius of the inner circle is 1.

5.2 THE ITERATIVE CONSTRUCTION

The initial setup of *outer and inner circle* as described above is denoted as $G_0(\varphi)$. It is a geodesic net with 14 unbalanced and no balanced vertices.

We will now add *layers* to $G_0(\varphi)$ to arrive at geodesic multinets $G_0(\varphi), G_1(\varphi), \ldots, G_n(\varphi)$ with the following properties:

- Each $G_i(\varphi)$ has 14 unbalanced vertices.
- The number of balanced vertices goes to infinity as $n \to \infty$.

So by choosing n large enough, we get a geodesic multinet $G_n(\varphi)$ with 14 unbalanced vertices and N balanced vertices.

However, we want to construct a geodesic net, i.e. at net where all edges have weight one. As stated above: If we allowed for weighted edges, much simpler examples could be constructed.

In light of that requirement, we will observe the following:

- If we do *not* introduce deviation, i.e. if we fix $\varphi = 0$, we get a highly symmetric geodesic multinets $G_n(0)$, since many edges used in the construction will overlap. This means that some edges would need to be represented using integer weights.
- However, for small nonzero $\varphi \in (-\epsilon, \epsilon)$, we get a net $G_n(\varphi)$ with significantly less symmetry and for which numerical results strongly suggest that all edges intersect transversally (if at all). So this is in fact a geodesic net with edges of weight one.

About the Feasibility of the Process and Smooth Dependence

As we will see in the constructive process below, there are certain requirements on the behaviour of angles and lengths that are necessary to make this construction possible. We will proceed as follows:

- We will first describe the construction, which will be the same for the non-deviated and the deviated case. This construction will use several such requirements.
- We will then prove that all requirements are fulfilled for the non-deviated case $\varphi = 0$.
- We will observe that each iteration of the construction smoothly depends on the previous one.
- Since all our requirements turn out to be restrictions of angles and lengths to open intervals and since the construction smoothly (and therefore continuously) depends on the initial setup, the requirements will also be fulfilled for small $\varphi \in (-\epsilon, \epsilon)$.

Iterative Process

We denote the set of vertices on the outer circle by V_{-1} and on the inner circle by V_0 and proceed to construct V_i for $i \geq 1$.

The reader is encouraged to first consult Figure 5.2 that explains the process visually.

Consider the vertices of V_i, each of which is a degree 2 vertex that is adjacent to two vertices of V_{i-1}. Using the 14 connecting edges, we get a 14-gon whose vertices alternate between vertices of V_{i-1} and vertices of V_i. For the interior angle α_i at the vertices V_i (*not* at the vertices of V_{i-1}), one of the following two cases can occur: $\alpha_i > 180°$, called Case A; or $\alpha_i < 180°$, called Case B (We justify $\alpha_i \neq 180°$ for all i later).

Case A: $\alpha_i > 180°$**.** In this case, the vertices of V_i are unbalanced vertices of degree 2 such that we can *wing a degree* 2 *vertex* getting an angle $\beta_i = 360° - \alpha_i < 180°$ as described in Method 5.3. Each wing will end as soon as it intersects with another wing. At those seven points of intersection, we fix the seven vertices of V_{i+1}. Proceed to the next iteration.

Examples for Case A in Figure 5.2 are the first two steps, namely the grey and red vertices.

Case B: $\alpha_i < 180°$**.** In this case, we will first add an outwards edge to each vertex of V_i using suspension. We distinguish two cases by the parity of i.

Case B1, i **is even:**. In this case, by construction, each vertex v of V_i is close to a radial line through the origin and at the half-angle between

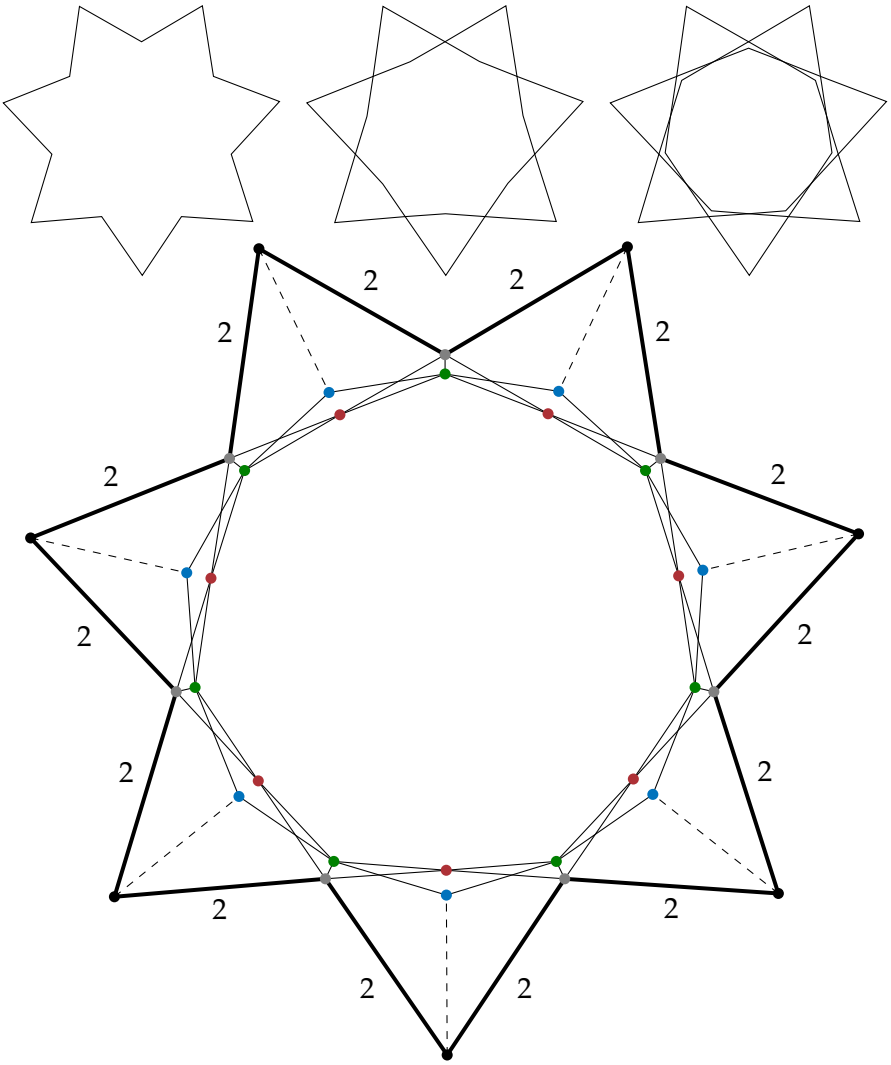

Figure 5.2: First steps of the construction for $\alpha_0 = 240^\circ$ and $\varphi = 0$.
Top left: Outer vertices (V_{-1}, black) and inner vertices (V_0, grey)
Top centre: The vertices of V_0 (grey) have been winged and the wings meet at the new vertices of V_1 (red)
Top right: The vertices of V_1 (red) have been winged and the wings meet at the new vertices of V_2 (green)
Bottom: The vertices of V_2 (green) first were suspended (note the edges from green to grey and the double weight on the outer edges) and then were winged. The wings meet at the new vertices of V_3 (blue)
After these first three steps, the seven vertices on the outer circle as well as the vertices of V_3 are unbalanced. There are 21 balanced vertices indicated. During the construction, we also get additional "accidental" degree four balanced vertices at points of intersection.
For the next step, the dashed edges would be added to *suspend* the vertices of V_3 (blue) and then each of them would be "winged" again.

two outer vertices P and Q (for deviation $\varphi = 0$, v is in fact *on* that radial line). Consider the triangle ΔPvQ. For the angles, it is clear that $vPQ, PQv \leq 90° < 120°$. Furthermore note that v is inside the *inner circle* (we will prove this in Lemma 5.9). Even if v were *on* the inner circle, we would have $QvP < 120°$ (by the choice of $\alpha_0 > 240°$). So since v is inside the inner circle, we still have $QvP < 120°$. Consequently, we can do a *two-hook suspension* of v from the hooks P and Q as described in Method 5.2.

An example for Case B1 in Figure 5.2 is the third step, namely the green vertices.

Case B2, i is odd:. In this case, by construction, each vertex v of V_i is close to a radial line through the origin and one of the vertices P on the outer circle (again, for deviation $\varphi = 0$, v is *on* that radial line). We will do a *one-hook suspension* of v from P by adding their connecting edge as described in Method 5.1.

An example for Case B2 in Figure 5.2 is the fourth step, namely the blue vertices.

After applying case B1 or B2, each vertex of V_i now is a degree 3 unbalanced vertex. We will prove below that it has imbalance of less than 2. Therefore, we can *wing* this vertex of degree 3 as described in Method 5.4. Each wing will end as soon as it intersects with another wing. At those seven points of intersection, we fix the seven vertices of V_{i+1}. Proceed to the next iteration.

This describes the whole construction. An example of the non-deviated case ($\varphi = 0$) can be found in Figure 5.3. We are left to show that the claims that make this construction possible are actually true.

Helpful Lemmata

The above construction implicitly uses several geometric facts which we will prove in this section. It is interesting to note that parts of the following lemma could be proven similarly for a construction starting with more than 7 outer vertices, but fail for 6 vertices. More specifically, we prove $\alpha_i > 120°$ below, which would not be true if we started with 3, 4, 5, 6 vertices. This is the reason for the seemingly arbitrary choice of seven as the "magic number" of the construction.

Note the following:

Lemma 5.6. *The positions of all vertices depend smoothly on the deviation φ.*

Proof. The outer circle never moves. The definition of the inner circle (which is the layer V_0) makes it clear that the position of the vertices of that layer depend smoothly on φ.

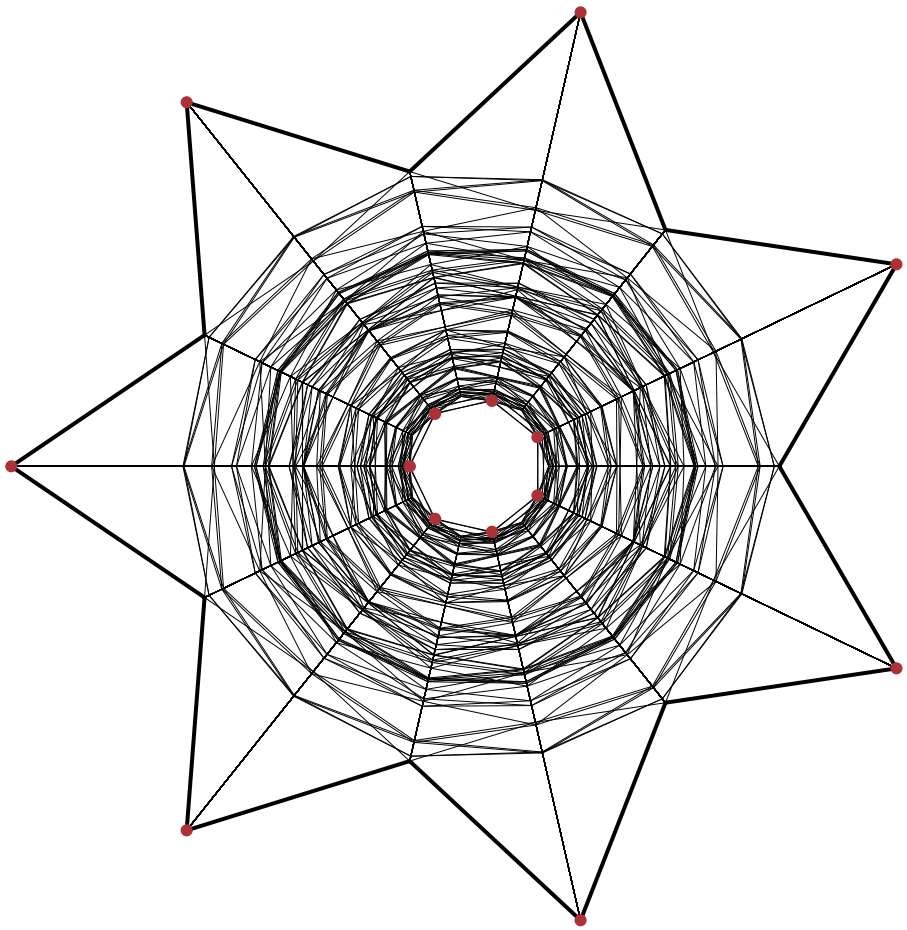

Figure 5.3: G_{100} of the non-deviated case. The 14 circled vertices are the only unbalanced vertices of this geodesic net. Note that some edges have integer weights of more than 1. Those are the radial edges, as well as the edges of the outermost 14-gon. After introducing deviation, these edges will split into weight-one-edges.

Since, to find all the other layers, we are using nothing but suspending and winging as defined previously, we only need to check those processes. Assume the position of the vertices up to V_i depend smoothly on φ.

- The angles of the incoming edges to V_i from V_{i-1} only depend on the positions of V_i and V_{i-1} which depend smoothly on φ by induction hypothesis.
- If *one-hook suspension* is necessary: P is on the outer circle, so it doesn't change under φ. Since the position of v depends smoothly on φ, so does the angle of the hooking edge. So the imbalance of v before winging will change smoothly.
- If *two-hook suspension* is necessary: P, Q and X don't change under φ. Since the position of v depends smoothly on φ, so does the angle of the hooking edge. So the imbalance of v before winging will change smoothly.

We now have established that the angles of all incoming edges to the vertices of V_i and therefore the imbalance at the vertices of V_i after possible suspension depend smoothly on φ. Checking the two possibilities for winging, it is apparent that the angles of the outgoing wings depend smoothly on the imbalance. Since the vertices of the next layer are defined to be the intersection of those wings, the positions of the next layer depend smoothly on φ. □

Note that all the following lemmas assert inequalities regarding angles and distances. In light of the previous lemma, it is therefore enough to prove them for $\varphi = 0$. By smooth dependence (and therefore continuous dependence), they are then still true for small $\varphi \in (-\epsilon, \epsilon)$.

We will first prove the following technical lemma, the usefulness of which will be apparent later.

Lemma 5.7. *Consider the angles α_i and β_i as the angle between the incoming edges and the angle between the outgoing edges during winging (see the figures describing the winging process). We have:*

(a) $\alpha_i \neq 180^\circ, 2\arccos(1/4)$ *for all* $i \geq 0$
(b) $120^\circ < \alpha_i < 190^\circ$ *for all* $i \geq 1$
(c) $120^\circ < \beta_i < 180^\circ$ *for all* $i \geq 1$

Proof. As established, it is enough to consider the symmetric case $\varphi = 0$.

Recall that $\alpha_0 = 88/21(\text{rad}) \approx 240.1^\circ$ and therefore $\beta_0 \approx 119.9^\circ$. The formulas for β_i depending on α_i were derived above when *winging* was defined:

$$\beta_i = \begin{cases} 360^\circ - \alpha_i & \alpha_i > 180^\circ \quad \text{(winging of degree 2 vertex)} \\ 2 \cdot \arccos\left(\frac{1}{2} - \cos\frac{\alpha_i}{2}\right) & \alpha_i < 180^\circ \quad \text{(winging of degree 3 vertex)} \end{cases}$$

Furthermore, since the vertices of V_i and the vertices of V_{i+1} form a 14-gon for which the interior angles at V_i are β_i (outgoing edges) and the interior angles at V_{i+1} are α_{i+1} (incoming edges), we have

$$7\beta_i + 7\alpha_{i+1} = 12 \cdot 180^\circ \Leftrightarrow \alpha_{i+1} = \frac{12 \cdot 180^\circ}{7} - \beta_i$$

For a visualization of the interdependence of these sequences see Figure 5.4.

Note that after proving (a), it is indeed clear that we do not need to consider the case $\alpha_i = 180^\circ$. We proceed by induction. Note that (a) starts at $i = 0$ whereas (b) and (c) start at $i = 1$:

(a) Recall that $\cos\alpha_0$ is not algebraic (by our initial choice of α_0, see above). We will prove the following fact which will imply the required result: $\cos\alpha_i$ is never algebraic for $i \geq 0$. The base case is given.

To proceed with induction, first consider the case where $\alpha_i > 180^\circ$ and therefore

$$\begin{aligned}
\alpha_{i+1} &= \frac{12 \cdot 180^\circ}{7} - 360^\circ + \alpha_i \\
\Rightarrow \cos\alpha_{i+1} &= \cos\left(\frac{12 \cdot 180^\circ}{7} - 360^\circ + \alpha_i\right) \\
\Rightarrow \cos\alpha_{i+1} &= \cos\left(\frac{12 \cdot 180^\circ}{7} + \alpha_i\right) \\
\Rightarrow \cos\alpha_{i+1} &= \cos\frac{12 \cdot 180^\circ}{7}\cos\alpha_i - \sin\frac{12 \cdot 180^\circ}{7}\sin\alpha_i \\
\Rightarrow \cos\alpha_{i+1} &= \cos\frac{12 \cdot 180^\circ}{7}\cos\alpha_i - \sin\frac{12 \cdot 180^\circ}{7}\sqrt{1-\cos^2\alpha_i}
\end{aligned}$$

It follows that $\cos\alpha_{i+1}$ is algebraic if and only if $\cos\alpha_i$ is algebraic.

Similarly, if $\alpha_i < 180^\circ$, then

$$\begin{aligned}
\alpha_{i+1} &= \frac{12 \cdot 180^\circ}{7} - 2 \cdot \arccos\left(\frac{1}{2} - \cos\frac{\alpha_i}{2}\right) \\
\Rightarrow \cos\left(\frac{\alpha_{i+1}}{2} - \frac{6 \cdot 180^\circ}{7}\right) &= \frac{1}{2} - \cos\frac{\alpha_i}{2} \\
\Rightarrow \cos\frac{\alpha_{i+1}}{2}\cos\frac{6 \cdot 180^\circ}{7} + \sin\frac{\alpha_{i+1}}{2}\sin\frac{6 \cdot 180^\circ}{7} &= \frac{1}{2} - \cos\frac{\alpha_i}{2} \\
\Rightarrow \cos\frac{\alpha_{i+1}}{2}\cos\frac{6 \cdot 180^\circ}{7} + \sqrt{1-\cos^2\frac{\alpha_{i+1}}{2}}\sin\frac{6 \cdot 180^\circ}{7} &= 1/2 - \cos\frac{\alpha_i}{2}
\end{aligned}$$

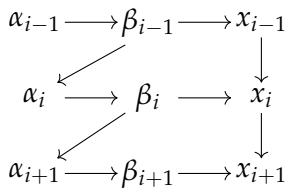

Figure 5.4: The interdependences of α_i, β_i and x_i

It follows that $\cos\frac{\alpha_{i+1}}{2}$ is algebraic if and only if $\cos\alpha_i$ is algebraic. But note that $\cos\alpha_{i+1} = \cos^2\frac{\alpha_{i+1}}{2} - \sin^2\frac{\alpha_{i+1}}{2}$. Therefore $\cos\alpha_{i+1}$ is algebraic if and only if $\cos\frac{\alpha_{i+1}}{2}$ is algebraic. The claim follows.

(b) The base case for α_1 can be verified by calculation. Now assume $120^\circ < \alpha_i < 190^\circ$ and consider α_{i+1}. We have two cases. If $\alpha_i > 180^\circ$, then

$$\alpha_{i+1} = \frac{2160^\circ}{7} - 360^\circ + \alpha_i$$

We can see that $120^\circ < \alpha_{i+1} < 190^\circ$ is true provided $180^\circ < \alpha_i < 190^\circ$. If, on the other hand, $\alpha_i < 180^\circ$, then

$$\alpha_{i+1} = \frac{2160^\circ}{7} - 2 \cdot \arccos\left(\frac{1}{2} - \cos\frac{\alpha_i}{2}\right)$$

It follows that α_{i+1} is an increasing function of α_i for $120^\circ < \alpha_i < 180^\circ$ and that for $\alpha_i = 120^\circ$ we get $\alpha_{i+1} \approx 129^\circ$ whereas for $\alpha_i = 180^\circ$ we get $\alpha_{i+1} \approx 188^\circ$. So $120^\circ < \alpha_{i+1} < 190^\circ$ is indeed the case.

(c) The bounds for β_i are immediate from the bounds on α_i and the formula for β_i above.

□

We can now proceed to prove facts that were relevant to our construction.

Lemma 5.8. *In the construction as defined above:*

(a) The incoming edges never meet at an angle of $\alpha_i = 180^\circ$, i.e. we always end up with Case A or Case B as described in the construction.

(b) The total imbalance before winging, even after possible suspension, is always less than 2, i.e. winging is always possible.

(c) The outgoing edges produced by winging a degree 3 vertex never coincide with the incoming edges.

(d) The incoming edges never meet at an angle of $\beta_i = 180^\circ$, i.e. their point of intersection (which defines the point in the next layer) is uniquely defined.

Proof. It is again enough to consider the symmetric case $\varphi = 0$ since each of the asserted properties can be expressed as an inequality, so they remain true for small $\varphi \in (-\epsilon, \epsilon)$.

(a) This is given explicitly in the previous lemma.

(b) α_i is the angle between incoming edges. Since $120^\circ < \alpha_i < 190^\circ$ (see previous lemma), the imbalance produced by the two incoming edges is always less than 1. Suspension adds an imbalance of at most 1. Therefore the total imbalance is less than 2.

(c) We are considering the symmetric case. As stated in the definition of winging, the edges would only coincide if $\alpha_i = \beta_i$ which requires $\alpha_i = 2\arccos(1/4)$, which is never the case by the previous lemma.

(d) This is again given explicitly in the previous lemma.

□

Finally, we asserted that adding a Fermat point for two-hook suspension is always possible if necessary. This assertion was based on the following fact:

Lemma 5.9. *All layers V_i lie strictly inside the inner circle for $i \geq 1$. Furthermore, the radius of the layers goes to zero as $i \to \infty$.*

Proof. We will again only consider the symmetric case. By smooth dependence on φ, the claim follows for the deviated case.

Recall that we scaled the construction so that the inner circle is at a radius of $x_0 = 1$. During the construction as defined above, if we denote by x_i the distance of the vertices of the i-th layer from the origin, the claim follows if we prove $x_i < 1$ for all $i \geq 1$ and that $x_i \to 0$ as $i \to \infty$. Note that in the symmetric case:

$$x_{i+1} = x_i f(\beta_i) \quad \text{where } f(\beta_i) = \frac{\sin \beta_i/2}{\sin(1080^\circ/7 - \beta_i/2)} \quad \text{(see Figure 5.5)}$$

where the formula for β_i, which in itself depends on α_i, can be found above.

By brute force calculation (for $\alpha_0 = 88/21$), we can verify the following:

- $x_i < 1$ for $1 \leq i \leq 8$
- $x_9 < 0.7$
- $180^\circ < \alpha_9 < 190^\circ$

We will now proceed to prove $x_i < 1$ for $i > 9$, using the fact that the values of x_i are going through loops, at the end of which x_i will have decreased. This can be formalized by the following claim:

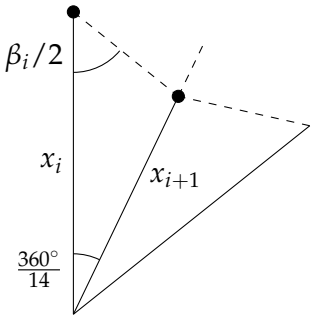

Law of sines:
$$\frac{x_{i+1}}{\sin \beta_i/2} = \frac{x_i}{\sin(180^\circ - 360^\circ/14 - \beta_i/2)}$$

Figure 5.5: Finding the relation between x_i and x_{i+1}.

Claim: Let $N \geq 9$ such that $180^\circ < \alpha_N < 190^\circ$. Then the following is true for either $\ell = 8$ or $\ell = 9$:

- $180^\circ < \alpha_{N+\ell} < 190^\circ$
- $x_{N+j} \leq 1.3 \cdot x_N$ for all $j = 1, 2, \ldots, \ell - 1$, and
- $x_{N+\ell} < 0.96 \cdot x_N$

Note that the lemma follows from inductive application of this claim using $N = 9$ as the base case since $1.3 \cdot 0.7 < 1$ and since the sequence is "generally geometrically decreasing".

We will now prove the claim. Observe the following facts:

- $180^\circ < \alpha_N < 190^\circ$
- Therefore, $\alpha_{N+1} = \frac{2160^\circ}{7} - 360^\circ + \alpha_N$, implying $120^\circ < \alpha_{N+1} < 180^\circ$.
- Furthermore, the larger α_N is, the larger α_{N+1} will be.
- As long as $\alpha_{N+j} < 180^\circ$, we can write

$$\alpha_{N+j+1} = \underbrace{\frac{2160^\circ}{7} - 2 \arccos\left(\frac{1}{2} - \cos\frac{\alpha_{N+j}}{2}\right)}_{=: g(\alpha_{N+j})}$$

  We can therefore rewrite the sequence $\alpha_{N+1}, \alpha_{N+2}, \alpha_{N+3} \ldots$ as

$$\alpha_{N+1}, g(\alpha_{N+1}), g(g(\alpha_{N+1})), \ldots$$

  This continues until, for some ℓ, $\alpha_{N+\ell} = g^{(\ell-1)}(\alpha_{N+1}) > 180^\circ$. In other words, the behaviour of $\alpha_N, \alpha_{N+1}, \alpha_{N+2}, \ldots$ can be summarized as follows: It starts at $\alpha_N > 180^\circ$, then α_{N+1} jumps below 180° and the sequence α_{N+i} climbs back up until $\alpha_{N+\ell} > 180^\circ$.
- We already established that the larger α_N is, the larger α_{N+1} will be. Also, $g(\alpha)$ is an increasing function for $120^\circ < \alpha < 180^\circ$. Therefore, the larger α_N is, the larger each α_{N+j} will be for $j = 1, \ldots, \ell$.

We observe the following two cases:

Case 1: $183^\circ \leq \alpha_N < 190^\circ$. Checking the extremal cases (183° and 190°), we can observe that either $\alpha_{N+8} > 180^\circ$ or $\alpha_{N+9} > 180^\circ$. We pick $\ell = 8, 9$ accordingly.

Case 2: $180^\circ < \alpha_N < 183^\circ$. Again checking the extremal cases (180° and 183°), we can observe that α_{N+9} will be the first angle above 180°. So we pick $\ell = 9$.

For both cases, note that $x_{N+j+1} = x_{N+j} f(\beta_{N+j})$. We can link the factor $f(\beta)$ to the angles α as follows

- β is a decreasing function of α (no matter if $\alpha > 180^\circ$ or $\alpha < 180^\circ$).
- $f(\beta) = \frac{\sin \beta/2}{\sin(1080^\circ/7 - \beta/2)}$ is an increasing function of β, since $120^\circ < \beta < 180^\circ$ as established in a previous lemma.
- Therefore, we can write $f(\beta(\alpha)) = h(\alpha)$ and *as long as we underestimate α, we overestimate $h(\alpha)$.*

We write

$$\begin{aligned} x_{N+j} &= x_N f(\beta_N) f(\beta_{N+1}) f(\beta_{N+2}) \cdots f(\beta_{N+j-1}) \\ &= x_N h(\alpha_N) h(\alpha_{N+1}) h(\alpha_{N+2}) \cdots h(\alpha_{N+j-1}) \\ &= x_N h(\alpha_N) h(\alpha_{N+1}) h(g(\alpha_{N+1})) \cdots h(g^{(j-2)}(\alpha_{N+1})) \end{aligned}$$

Recall that g is increasing and that h is decreasing, so *as long as we underestimate α_N (and therefore also α_{N+1}), we overestimate x_{N+j}.*

We can return to the two cases:

Case 1 $183^\circ \leq \alpha_N < 190^\circ$**.** In this case we need 8 or 9 steps and α_N is at least 183°. By the above considerations, we can simply study the case $\alpha_N = 183^\circ$. For larger starting values of α, the values of x can only be smaller. In that context, using the above equation:

$$x_{N+j} \leq x_N h(183^\circ) h(131^\circ) h(g(131^\circ)) \cdots h(g^{(j-2)}(131^\circ))$$

Now calculations yield that $h(183^\circ) h(131^\circ) h(g(131^\circ)) \cdots h(g^{(j-2)}(131^\circ))$ will be less than 1.3 for $j = 1, 2, \ldots, 8, 9$ and less than 0.96 for $j = 8, 9$. So $\ell = 8$ or $\ell = 9$ has the properties stated in the claim.

Case 2 $180^\circ < \alpha_N < 183^\circ$**.** In this case we need 9 steps and α_N is at least 180°. By the above considerations, we can simply study the case $\alpha_N = 180^\circ$ (as a limiting case, of course $\alpha = 180^\circ$ never happens). For larger starting values of α, the values of x can only be smaller. In that context, using the above equation:

$$x_{N+j} \leq x_N h(180^\circ) h(128^\circ) h(g(128^\circ)) \cdots h(g^{(j-2)}(128^\circ))$$

Now calculations yield that $h(180^\circ)h(128^\circ)h(g(128^\circ))\cdots h(g^{(j-2)}(128^\circ))$ will be less than 1.3 for $j = 1, 2, \ldots, 8, 9$ less than 0.96 for $j = 9$. So $\ell = 9$ has the properties stated in the claim.

It is noteworthy that a split like the one at 183° was necessary. In fact would we have a starting value of $\alpha_N = 180^\circ$ but only 8 steps, the factor would be greater than 1. Hence the casework to show that this case doesn't happen.

This finishes the proof of the claim and the lemma. □

This concludes the proof that the exact construction works, both in the symmetric case $\varphi = 0$ and for small deviation $\varphi \in (-\epsilon, \epsilon)$.

5.3 ANALYZING THE NON-DEVIATED CONSTRUCTION

Note that our goal was to construct a sequence of geodesic multinets $G_n(0)$ such that

(a) Each $G_n(0)$ has 14 unbalanced vertices
(b) The number of balanced vertices goes to infinity as $n \to \infty$.

The first observation is true as explained above: The only unbalanced vertices are the vertices on the outer ring as well as the seven vertices of the last layer that has been added.

Regarding the second observation, note that Lemma 5.9 demonstrates that the radius of the layers V_i approaches zero as $i \to \infty$. Therefore, increasing the number of layers increases the number of balanced vertices (otherwise, there would have to be a cyclical phenomenon in the construction, contradicting the fact that the radius goes to zero).

However, $G_n(0)$ is a geodesic multinet, whereas we want to construct a geodesic net, which is what makes the introduction of deviation necessary. Note that the edges of the geodesic net can be categorized as follows:

- Whenever a new layer is added through the process of *winging*, this adds 14 edges from V_{i-1} to V_i to the net. We call those the *layer-connecting edges*. This includes the very first 14 edges to set up the outer circle and inner circle as seen in Figure 5.1.
- Whenever we *suspend* a vertex from a single hook, a single edge is being added. We call it the suspension edge.
- Whenever we *suspend* a vertex from two hooks, three edges are being added: two edges from two vertices of the *outer circle* (the *hooks*) to the Fermat point, as well as one edge from the Fermat point to the vertex that is being suspended – we again call these *suspension edges*.

This now raises the question: Which edges can and will intersect non-transversally on $G_i(0)$ (i.e. if $\varphi = 0$), either partially or in their entirety? We can observe (see also Figure 5.3):

- Note that the Fermat point used in the process of suspension is the same for each layer in the symmetric case. Therefore, two of the three *suspension edges* involving the same two hooks are the same from the hooks to the Fermat point, every single time these hooks are being used. The third suspension edge then always starts at the same Fermat point and continues radially to the vertex that is being suspended. So those suspension edges are overlaying as well.
- Similarly, if we do a one-hook suspension, the suspension edge is always radial, so all the suspension edges going to the same hook have an overlay.
- Layer-connecting edges, on the other hand, can only intersect any other edge transversally: The Fermat points are outside the inner circle and therefore never meet the layer-connecting edges. Regarding the radial suspension edges, note that layer-connecting edges are never radial, so they are always transversal to radial edges. Besides that, note that layer-connecting edges always start and end on the boundary of a $260°/14$ disk sector of the construction. So they could only be completely identical to another layer-connecting edge or intersect them transversally (if at all). For the sake of contradiction, assume that any layer-connecting edge would coincide with another layer-connecting edge. This would imply that the layer produced by them must be the same, including the incoming edges. Therefore, layers would repeat. This would contradict the phenomenon described in Lemma 5.9, namely that the radius of the layers must converge to zero.

As established previously, everything depends smoothly on the deviation φ. Therefore, any small deviation will maintain transversality where it already is given. Deviation will, however, have to make sure that we split up suspension edges.

5.4 EDGES UNDER DEVIATION

As just established above, we only need to be concerned with the edges produced using the method of *suspension*. This section serves to support the following claim:

Whereas for $\varphi = 0$, the geodesic multinets $G_n(0)$ are highly symmetrical and many suspension edges overlap, for nonzero $\varphi \in (-\epsilon, \epsilon)$, all suspension edges of $G_n(\varphi)$ intersect transversally (if at all), i.e. we get geodesic nets $G_n(\varphi)$.

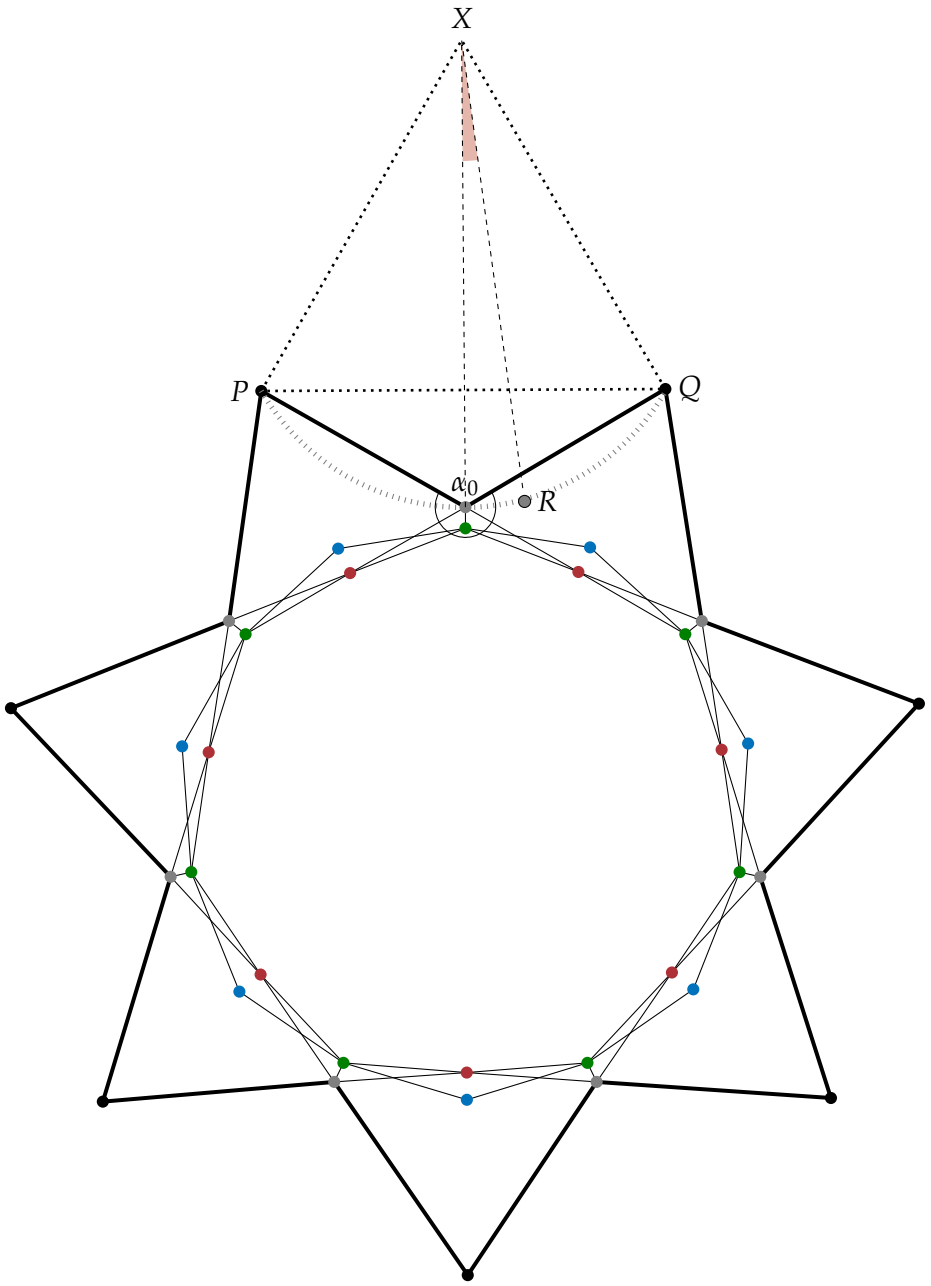

Figure 5.6: Note the dotted equilateral triangle XPQ as well as the unique circular arc given by P, R and Q. Denote by φ the angle OXR (where O is the origin/center). The symmetric case is given by $\varphi = 0$. *To introduce deviation*, we would slightly increase φ, and get a new position for R. This does not change the value of α_0 (since we go along the circular arc). The same deviation is done at *all* seven grey points. This means that the star remains rotationally symmetric under a rotation by $360°/7$, but loses its symmetry under reflections.

The Sequence of Suspension Angles φ_i

To demonstrate this, we will study the sequence of suspension angles, which is defined as follows, based on the two types of suspension that we employ:

Definition 5.10 (Suspension angle for one-hook suspensions, layers V_i for i odd)**.** Whenever we do a one-hook suspension for a layer V_i, we are connecting a vertex v to the closest vertex on the outer circle.

Denote the center of the outer circle by O and the hook by P. Then we define the suspension angle φ_i to be the angle OPv. For clarification, consider the following figure giving a positive suspension angle.

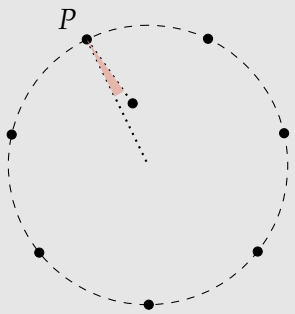

Note that φ_i depends only on the deviation φ (which is the only free parameter of our construction) and that $\varphi_i(0) = 0$ for all layers.

We can define this suspension angle for all odd layers, even though in some cases we don't need to suspend a vertex (if case A occurs).

Definition 5.11 (Suspension angle for two-hook suspensions, layers V_i for i even)**.** Whenever we do a two-hook suspension for a layer V_i, we are connecting a vertex v to the closest two vertices on the outer circle P and Q through the Fermat point of the triangle PvQ, see the figure when defining two-hook suspension above).

As before, we denote by X the third vertex of the equilateral triangle PQX used for the construction of the Fermat point. Let O be the center of the outer circle. Then we define the suspension angle φ_i to be the angle OXv. For clarification, consider the following figure showing a positive suspension angle.

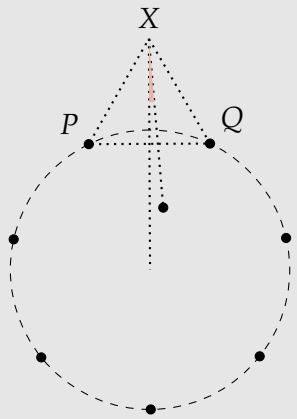

Note that φ_i depends only on the deviation φ (which is the only free parameter of our construction) and that $\varphi_i(0) = 0$ for all layers. Most importantly, for $i = 0$ (the initial layer, aka the inner circle) the suspension angle is $\varphi_0(\varphi) = \varphi$.

We can define this suspension angle for all even layers, even though in some cases we don't need to suspend a vertex.

With this definition, we can now make the following observations:

Fact 5.12. Consider $\varphi \in (-\epsilon, \epsilon)$ a geodesic net $G_n(\varphi)$ as constructed above with layers $V_0, \ldots, V_n$. Then

- As established before, only suspension edges could overlap/intersect non-transversally.
- For all one-hook suspensions (odd layers), only the edges going from vertices v_i, v_k of two different layers to the same hook P could overlap. But as long as $\varphi_i \neq \varphi_k$, they will not do so (this is apparent from the figure in the definition above).
- For all two-hook suspensions (even layers), only the edges suspending vertices v_i, v_k of two different layers from the same two hooks P and Q could overlap. But as long as $\varphi_i \neq \varphi_k$, they will not do so (see Figure 5.7).

Fact 5.13. $G_n(\varphi)$ consists of finitely many layers, therefore $\varphi_0, \varphi_1, \ldots, \varphi_n$ is a *finite* sequence.

Based on Definition 5.10, Definition 5.11 and Fact 5.12, we arrive at the following lemma:

Lemma 5.14. *If for any fixed $\varphi \in (-\epsilon, \epsilon)$, the finite sequence $\varphi_i(\varphi)$ never repeats itself, all edges of the resulting geodesic net $G_n(\varphi)$ intersect transversally (if at all). In other words, there are no edges with weight other than one.*

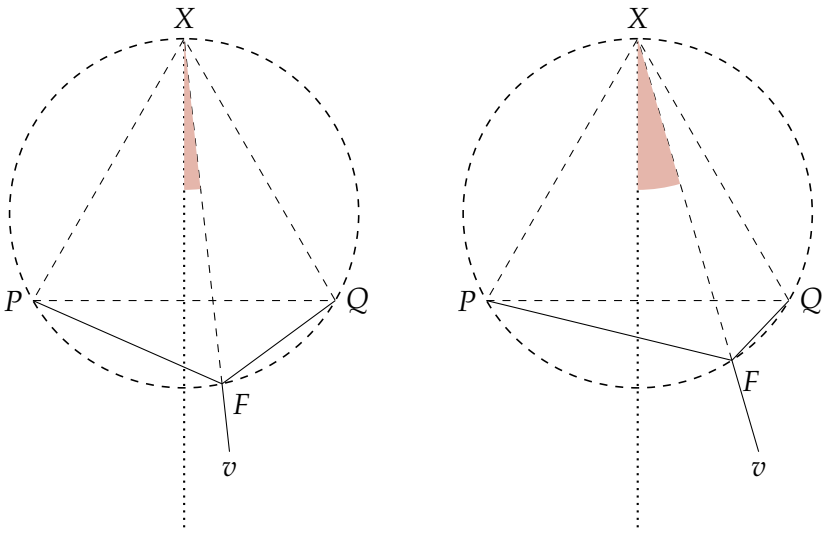

Figure 5.7: Construction of the Fermat point F to suspend $v_i \in V_i$ from P and Q. φ_i is the angle between the axis of symmetry of PQX and the segment vX. Observe: Whenever φ_i (the marked suspension angle) is different, the segment PF is at a different angle. The same is true for QF and vF. So we only need to establish that φ_i is different at every layer and this implies that none of the suspension edges overlap.

Note that, in fact it would be enough if the φ_i are different for the same parity (since even and odd layers never have suspension edges in common).

Based on symmetry (see also Figure 5.3), we can observe

Fact 5.15. $\varphi_i(0) = 0$ for all i.

Also, since we established smooth dependence of the construction on the deviation φ before and since this is in fact the only free parameter, we can consider the derivative of $\varphi_i(\varphi)$. We make the following conjecture:

Conjecture 5.16. *$\varphi_i'(0)$ is a sequence that never repeats itself.*

Keeping in mind that φ_i is a finite sequence, the previous fact and conjecture (i.e. same value at 0, but different derivatives) would then imply the following:

Conjecture 5.17. *For small nonzero $\varphi \in (-\epsilon, \epsilon)$, the sequence $\varphi_i(\varphi)$ never repeats itself. This implies that $G_n(\varphi)$ is a geodesic net for which all edges have weight one.*

So this $G_n(\varphi)$ would in fact fulfill all required conditions as specified at the beginning of the chapter.

5.5 STUDYING THE SEQUENCE $\varphi_i'(0)$

We are left with Conjecture 5.16. For the remainder, we will consider statements we can make about the sequence $\varphi_i'(0)$.

We will do the following:

- We will provide an explicit recursive formula for $\varphi_i'(0)$.
- We will present numerical results that strongly suggest that Conjecture 5.16 is true.

In the following, all derivatives will be with respect to φ. First note that $\varphi_0 = \varphi$ and therefore obviously $\varphi_0'(0) = 1$. We will now find a recursive formula for $\varphi_i'(0)$. The crucial question is how $\varphi_{i+1}'(0)$ depends on $\varphi_i'(0)$.

Figure 5.8 shows the two cases for i even and i odd. Note that if $\varphi = 0$, then the picture is symmetric along a horizontal reflection. In both cases, we get a hexagon made of two quadrilaterals.

In either case, by the angle sum in the lower quadrilateral:

$$\tau_i + \varphi_i + \gamma_i + \psi_{i+1} + (\mu_i - \varphi_{i+1}) = 360^\circ$$

Note that τ_i and μ_i are constants that don't change under φ. Therefore, differentiation by φ leads to:

$$\varphi_i' + \gamma_i' + \psi_{i+1}' - \varphi_{i+1}' = 0 \Rightarrow \varphi_{i+1}' = \varphi_i' + \gamma_i' + \psi_{i+1}'$$

In Section 5.6, we will establish the following relationships at $\varphi = 0$.

$$\varphi_0' = 1 \qquad \psi_0' = 1/2 - \sin(\pi/6 - \alpha_0)$$

$$\varphi_{i+1}' = \varphi_i' + \gamma_i' + \psi_{i+1}' \qquad \psi_{i+1}' = b_i\gamma_i' + a_i\varphi_i' \qquad \gamma_i' = c_i\psi_i'$$

The formulas for the coefficients make use of x_i and α_i, which were defined previously:

$$a_i = -\tan\frac{\alpha_{i+1}}{2}\left(\frac{\sin\left(\frac{\pi}{7}+\sigma_{i+1}\right)\sin\left(\frac{\pi}{7}+\sigma_{i+1}+\tau_i\right)}{\sin\tau_i} + \frac{\frac{1}{2} - \frac{\sin(\tau_i+2\pi/7+2\sigma_{i+1})}{2\sin\tau_i}}{\tan(\frac{\alpha_{i+1}}{2}-\sigma_{i+1})}\right)$$

$$b_i = -\frac{\tan\alpha_{i+1}/2}{\tan(\alpha_{i+1}/2-\sigma_{i+1})} \qquad c_i = \begin{cases} -1 & \alpha_i > 180^\circ \\ \dfrac{2\cos\alpha_i/2}{1-2\cos\alpha_i/2} & \alpha_i < 180^\circ \end{cases}$$

$$\tau_i = \begin{cases} \dfrac{\pi}{6} & i \text{ even} \\ \dfrac{29\pi}{42} & i \text{ odd} \end{cases} \qquad \sigma_{i+1} = \begin{cases} \arctan\dfrac{\sin\pi/7}{\frac{\sin\alpha_0/2}{x_i\sin(\frac{\pi}{7}+\alpha_0/2)} - \cos\frac{\pi}{7}} & i \text{ even} \\ \arctan\dfrac{\sin\frac{\pi}{7}}{\frac{\sin\alpha_0/2}{x_i\sin(\frac{\pi}{7}+\alpha_0/2)}\frac{\sin(\pi/7+\pi/6)}{\sin\pi/6} - \cos\frac{\pi}{7}} & i \text{ odd} \end{cases}$$

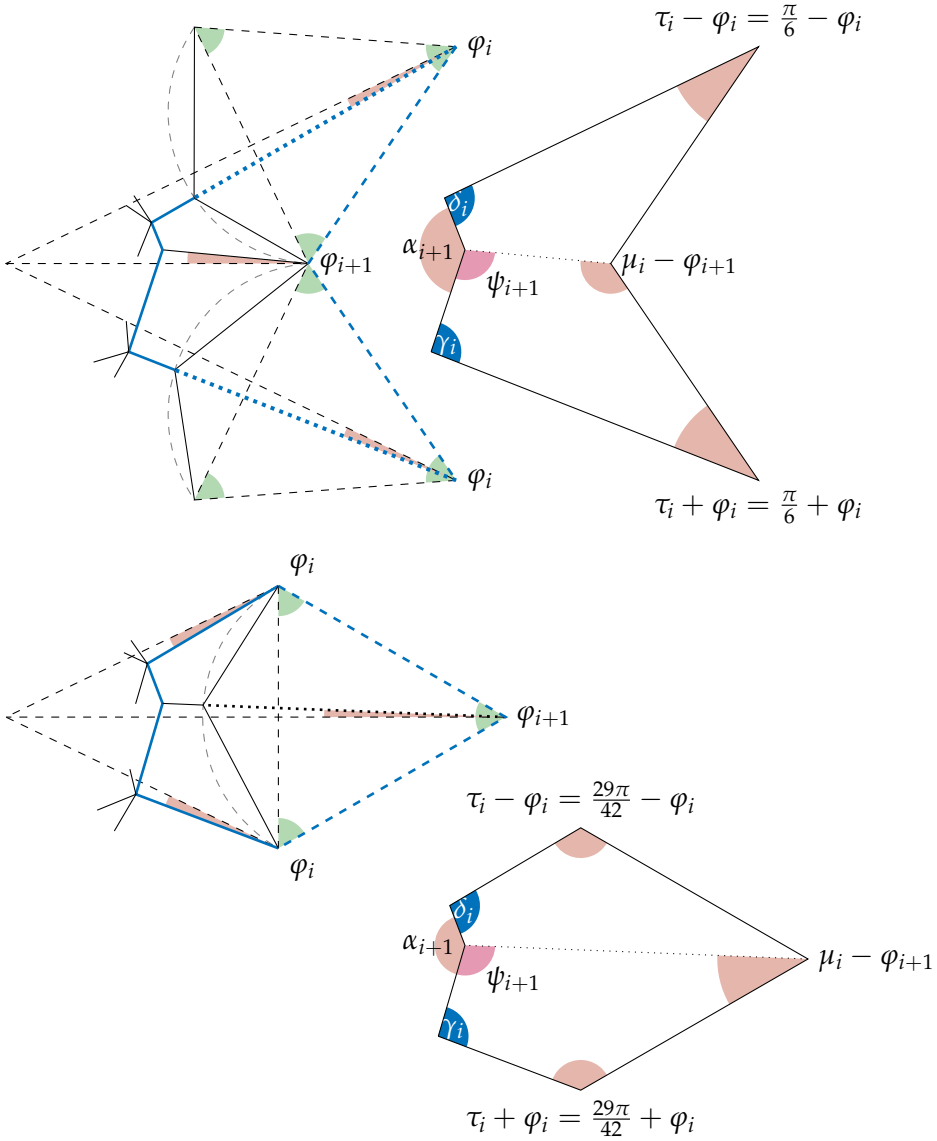

Figure 5.8: We want to relate φ_{i+1}' to φ_i'. The upper pictures are considering the case i even, the lower pictures are considering the case i odd. All green angles are $60°$. μ is a constant angle. All dashed lines are stationary, all dotted and solid lines vary over a change of the deviation φ. The picture on the right extracts the blue hexagon out of the left picture. Note that in this example, φ_i is positive whereas φ_{i+1} is negative

Numerical Consideration of the Sequence $\varphi_i'(0)$

While the formulas above are all explicit, they are arguably not very "handy" which makes understanding their behaviour a challenging task. Recall that all we need is that $\varphi_i'(0)$ never repeats. This would then imply that a small deviation from $G_n(0)$ to $G_n(\varphi)$ would in fact split up all edges as required.

For a better understanding, we used MATLAB to compute the first items of the sequence. Figure 5.9 shows the first 100 elements of the sequence $\varphi_i'(0)$, on a logarithmic scale. These calculations lead to the following observations, which in turn support Conjecture 5.16, saying that $\varphi_i'(0)$ doesn't repeat:

- The magnitude of the sequence grows exponentially.
- The sequence seems to be generally increasing (i.e. increasing with a small amount of variation)
- Since it is enough if the sequence differs for all even i and for all odd i, we get additional "leeway".

In fact, numerical evidence suggests that the first 100 elements of the sequence do not repeat. We computed the first 100 elements of $\varphi_i'(0)$ with MATLAB using variable precision arithmetic, using between 10 and 100 significant digits. The following result remained stable under variable precision:

$$\min_{i \neq j} |\varphi_i'(0) - \varphi_j'(0)| \approx 3.743673268$$

This minimum is realized by $\varphi_0'(0)$ and $\varphi_2'(0)$. This suggests that the result remains the same even for more than 100 steps.

5.6 FINDING THE FORMULAS FOR THE SEQUENCE $\varphi_i'(0)$

Consider Figure 5.8 and the following formula we derived previously:

$$\varphi_{i+1}' = \varphi_i' + \gamma_i' + \psi_{i+1}'$$

In this appendix, we intend to do the following:

- Find the starting values of $\varphi_0'(0)$ and $\psi_0'(0)$.
- Establish that $\alpha_i'(0) = 0$ for all i.
- Derive a formula for $\gamma_i'(0)$ in terms of $\psi_i'(0)$.
- Derive a formula for $\psi_{i+1}'(0)$ in terms of $\psi_i'(0)$ and $\varphi_i'(0)$.

Starting Values

Since φ is defined to be the *suspension angle* for the inner circle, which is the zeroth level (compare Definition 5.11 and compare with the initial definition of the inner circle), $\varphi_0 = \varphi$ and therefore

$$\varphi_0'(0) = 1$$

To find $\psi_0'(0)$, consider Figure 5.10, more specifically the isosceles triangle with two sides of length a. Using angle sums in triangles:

$$\psi_0 = (\pi - (\pi - \lambda - \theta))/2 - \lambda = \theta/2 - \lambda/2 \;\Rightarrow\; \psi_0' = \theta'/2 - \lambda'/2$$

Finding λ'. The law of sines, applied to the two triangles that share the common side of length b but have two different sides of length a gives us

$$\begin{aligned} \frac{\sin\lambda}{\sin\varphi} = \frac{b}{a} = \frac{\sin\mu}{\sin\pi/6} = 2\sin\mu \;&\Rightarrow\; \sin\lambda = 2\sin\mu\sin\varphi \\ &\Rightarrow\; \cos\lambda\;\lambda' = 2\sin\mu\cos\varphi \end{aligned}$$

At $\varphi = 0$, we also have $\lambda = 0$ and therefore $\lambda'(0) = 2\sin\mu = 2\sin(\pi - \pi/6 - (2\pi - \alpha_0)) = 2\sin(\pi/6 - \alpha_0)$.

Finding θ'. Using the angle sum in triangles, we get $\theta + \mu + \pi/6 - \varphi = \pi$ and therefore $\theta' = 1$.

Combining these we arrive at $\psi_0'(0) = \frac{1}{2} - \sin(\pi/6 - \alpha_0)$.

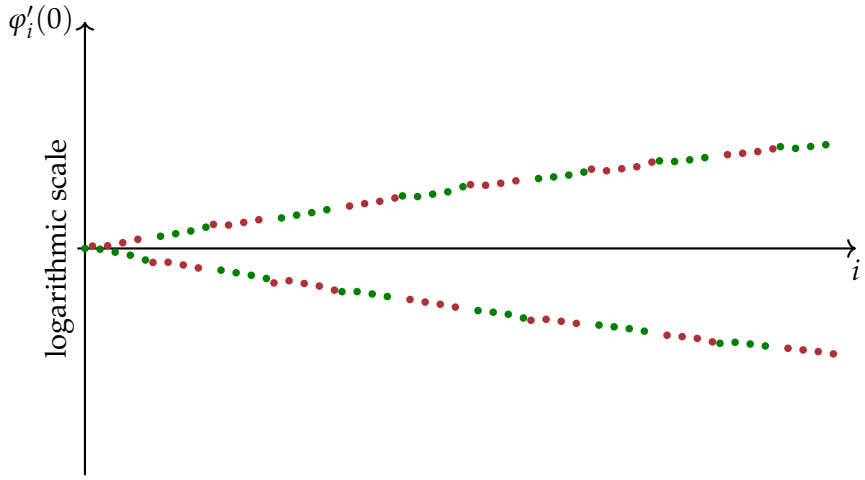

Figure 5.9: The first 100 values of $\varphi_i'(0)$ on a *logarithmic* scale, calculated with $\alpha_0 = 88/21$. All points for i even are marked in green. All points for i odd are marked in red.

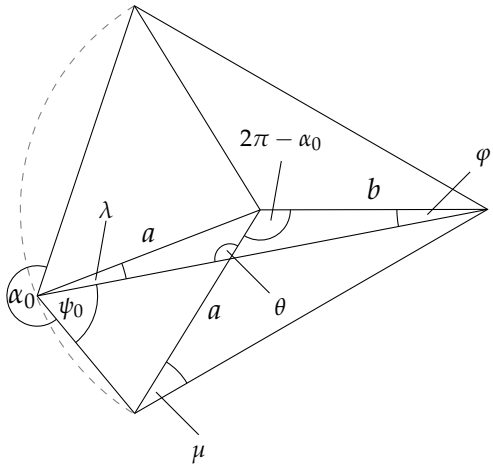

Figure 5.10: Dependence of ψ_0 on φ

Finding $\alpha_i'(0)$ and $\gamma_i'(0)$

Recall that α_i is the interior angle at the vertices V_i of the 14-gon formed by V_{i-1} and V_i. It is one of the two angles between the incoming edges at the vertex of a layer, before winging (see also Method 5.3 and Method 5.4 as well as the formulas in the proof of Lemma 5.7). Like all other angles, each $\alpha_i = \alpha_i(\varphi)$ is a smooth function of the deviation angle φ. Figure 5.8 and Figure 5.11 show how γ is one of the angles between an outgoing edge and the suspension edge, whereas ψ is one of the angles between an incoming edge and the suspension edge (even if we do not suspend, as is the case for a degree 4 vertex where $\alpha > 180°$, we can still consider the angle compared to a hypothetical suspension edge.

Lemma 5.18. *For all $i = 0, 1, 2, \ldots, n$, we have at $\varphi = 0$ that*

(a) $\alpha_i' = 0$

(b) $\gamma_i' = c_i \psi_i'$ *where* $c_i = \begin{cases} -1 & \alpha_i > 180° \\ \dfrac{2\cos \alpha_i/2}{1 - 2\cos \alpha_i/2} & \alpha_i < 180° \end{cases}$

It is important to emphasize that these relationships between derivatives only hold at $\varphi = 0$, which is, however, enough for us.

Proof. (a) For the base case, note that the inner circle is chosen precisely to ensure that $\alpha_0 = 88/21$ for any choice of φ. So $\alpha_0(\varphi)$ is constant and the base case follows.

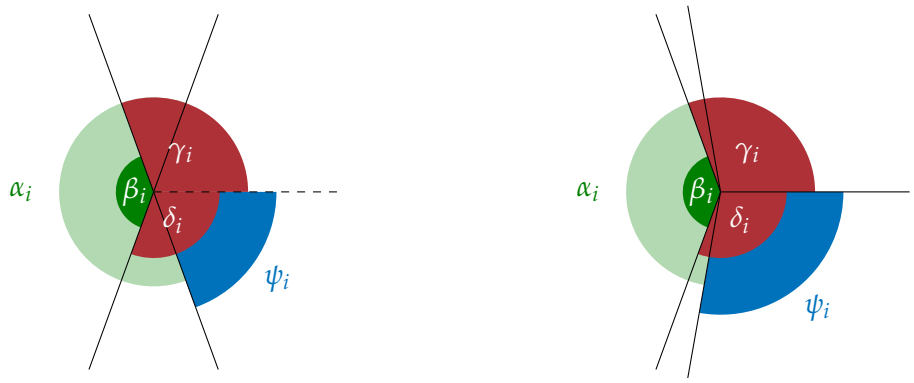

Figure 5.11: The angle relationships at a vertex of V_i in the case of $\alpha_i > 180°$ (left, winging a degree 2 vertex) and in the case of $\alpha_i < 180°$ (right, winging a degree 3 vertex)

For the induction step, recall the following formulas (see proof of Lemma 5.7) for the symmetric case $\varphi = 0$:

$$\alpha_{i+1} = \frac{12 \cdot 180°}{7} - \beta_i$$

$$\beta_i = \begin{cases} 360° - \alpha_i & \alpha_i > 180° \quad \text{(degree 2 vertex)} \\ 2 \cdot \arccos(1/2 - \cos(\alpha_i/2)) & \alpha_i < 180° \quad \text{(degree 3 vertex)} \end{cases}$$

It is worth checking which of these formulas still apply in the deviated case $\varphi \neq 0$.

- The relation $\alpha_{i+1} = \frac{12 \cdot 180°}{7} - \beta_i$ remains unchanged, since the formula is based on the angle sum in the 14-gons during construction. Therefore $\alpha_{i+1}'(0) = -\beta_i'(0)$.
- The formula for β_i in the case of $\alpha_i > 180°$ also applies to the non-symmetric case (see Method 5.3). It follows that $\beta_i'(0) = -\alpha_i'(0) = 0$ by induction hypothesis and we are done.
- The formula for β_i in the case of $\alpha_i < 180°$, however, cannot be used for the asymmetric situation (as explained in Method 5.4, it only works for the symmetric case).

So we are left to show that $\beta_i'(0) = 0$ assuming that $\alpha_i'(0) = 0$ and $\alpha_i < 180°$, but we can't use the given formula.

Instead, lets consider the right of Figure 5.11, depicting this case. Note that when $\varphi = 0$, the picture is symmetric under reflection along the horizontal axis. Generally, though, this is not the case.

However, the vertex is always balanced, so we have

$$\begin{aligned}&[1,0]+[\cos\gamma_i,\sin\gamma_i]+[\cos\delta_i,-\sin\delta_i]+[\cos\psi_i,-\sin\psi_i]\\&\quad+[\cos(\psi_i+\alpha_i),-\sin(\psi_i+\alpha_i)]=[0,0]\\\Leftrightarrow&\begin{cases}1+\cos\gamma_i+\cos\delta_i+\cos\psi_i+\cos(\psi_i+\alpha_i)=0\\\sin\gamma_i-\sin\delta_i-\sin\psi_i-\sin(\psi_i+\alpha_i)=0\end{cases}\end{aligned}$$

We can derive everything with respect to φ and arrive at

$$\begin{aligned}-\gamma_i'\sin\gamma_i-\delta_i'\sin\delta_i-\psi_i'\sin\psi_i-(\psi_i'+\alpha_i')\sin(\psi_i+\alpha_i)=0\\\gamma_i'\cos\gamma_i-\delta_i'\cos\delta_i-\psi_i'\cos\psi_i-(\psi_i'+\alpha_i')\cos(\psi_i+\alpha_i)=0\end{aligned}$$

We are concerned with the derivatives at $\varphi=0$. As pointed out, the picture is symmetric in that case and we get $\gamma_i=\delta_i$ as well as $\psi_i+\alpha_i=2\pi-\psi_i$. By induction hypothesis, we also have $\alpha_i'=0$. So we can simplify to

$$\begin{aligned}-\gamma_i'\sin\gamma_i-\delta_i'\sin\gamma_i-\psi_i'\sin\psi_i-\psi_i'\sin(2\pi-\psi_i)=0\\\gamma_i'\cos\gamma_i-\delta_i'\cos\gamma_i-\psi_i'\cos\psi_i-\psi_i'\cos(2\pi-\psi_i)=0\end{aligned}$$

We can simplify further to

$$\begin{aligned}-\gamma_i'\sin\gamma_i-\delta_i'\sin\gamma_i-\psi_i'\sin\psi_i+\psi_i'\sin\psi_i=0\\\gamma_i'\cos\gamma_i-\delta_i'\cos\gamma_i-\psi_i'\cos\psi_i-\psi_i'\cos\psi_i=0\end{aligned}$$

Note that γ_i can't be a multiple of π at $\varphi=0$ since that would imply $\beta_i=0$ or $\beta_i=2\pi$ which is never the case as established previously. So $\sin\gamma_i\neq0$ and the two equations do in fact simplify to

$$\begin{aligned}\gamma_i'+\delta_i'=0\\(\gamma_i'-\delta_i')\cos\gamma_i=2\psi_i'\cos\psi_i\end{aligned}$$

As is clear from Figure 5.11, $\beta_i=2\pi-(\gamma_i+\delta_i)$. Therefore $\beta_i'=-(\gamma_i'+\delta_i')=0$ as required.

(b) If $\alpha_i>180^\circ$ consider the left of Figure 5.11 from which it is clear that $\gamma_i=180^\circ-\psi_i$. It follows that $\gamma_i'=-\psi_i'$ as stated (this relationship, in fact, would be true for any $\varphi\in(-\epsilon,\epsilon)$, not just for $\varphi=0$).

If $\alpha_i<180^\circ$, we have just established the following at $\varphi=0$

$$\begin{aligned}&\gamma_i'+\delta_i'=0\text{ and }(\gamma_i'-\delta_i')\cos\gamma_i=2\psi_i'\cos\psi_i\\\Rightarrow\;&2\gamma_i'\cos\gamma_i=2\psi_i'\cos\psi_i\;\Rightarrow\;\gamma_i'=\frac{\cos\psi_i}{\cos\gamma_i}\psi_i'\end{aligned}$$

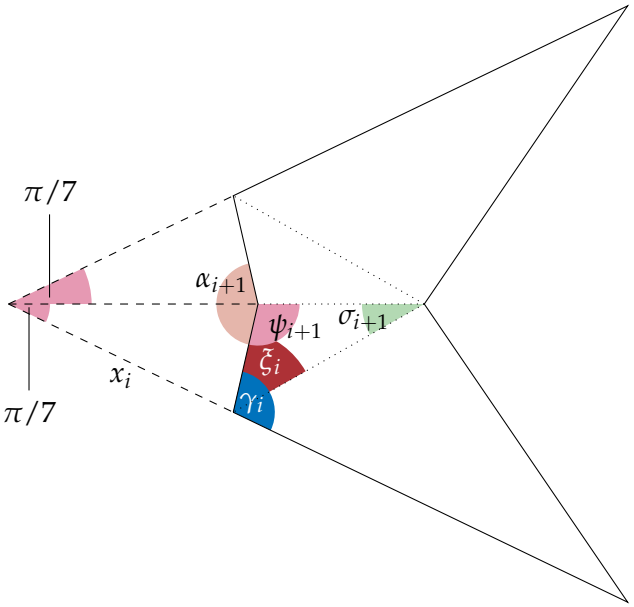

Figure 5.12: A figure showing the relationship between angles at $\varphi = 0$ for i even.

Furthermore, again due to symmetries at $\varphi = 0$

$$\begin{aligned}\cos\gamma_i &= \cos(\pi - \beta_i/2) = -\cos(\beta_i/2)\\ &= -\cos\left(\frac{2\arccos(1/2 - \cos(\alpha_i/2))}{2}\right)\\ &= -(1/2 - \cos\alpha_i/2)\\ \cos\psi_i &= \cos(\pi - \alpha_i/2) = -\cos\alpha_i/2\end{aligned}$$

Combining these equations, we arrive at $\gamma_i' = c_i\psi_i'$ with

$$c_i = \frac{2\cos\alpha_i/2}{1 - 2\cos\alpha_i/2}$$ □

τ_i and σ_i

τ_i is the "reference angle" from which the suspension angle φ_i is measured. Consider the 14-gon formed by the two outer sides of each of the seven equilateral triangles built on the outer circle. The interior angle at seven corners is $\pi/3$, the interior angle at the other seven corners is $29\pi/21$. These are the values for $2 \cdot \tau_i$ even and odd respectively.

The angle σ_{i+1} for i even, is depicted in two figures for different situations. Figure 5.12 shows the symmetric case at $\varphi = 0$ whereas Figure 5.13

shows the general case. σ_{i+1} changes under deviation, but at $\varphi = 0$, it can be directly calculated from the sequence of x_i. Note in Figure 5.12 that σ_{i+1} is one of the angles in a triangle with side x_i and angle $\pi/7$. Since σ_{i+1} is the angle at a vertex of the *outer circle*, we know one more side of the triangle. Recall that the inner circle is fixed at radius 1 and consider Figure 5.1, giving the other side as $\frac{\sin \alpha_0/2}{\sin(\pi/7+\alpha_0/2)}$. Using the law of sines, we get the following relation:

$$\sin \sigma_{i+1} = x_i \sin(\sigma_{i+1} + \pi/7) \frac{\sin(\pi/7 + \alpha_0/2)}{\sin \alpha_0/2}$$

If i is odd, a similar argument yields

$$\sin \sigma_{i+1} = x_i \sin(\sigma_{i+1} + \pi/7) \frac{\sin(\pi/7 + \alpha_0/2)}{\sin \alpha_0/2} \frac{\sin \pi/6}{\sin(\pi/7 + \pi/6)}$$

which is based on the fact that the additional vertex of σ_i is at radius

$$\frac{\sin \alpha_0/2}{\sin(\pi/7 + \alpha_0/2)} \frac{\sin(\pi/7 + \pi/6)}{\sin \pi/6}$$

Since $\sigma_{i+1} < 90°$, we can solve both of the above equations for σ_{i+1} and get

$$\sigma_{i+1} = \begin{cases} \arctan \dfrac{\sin \pi/7}{\frac{\sin \alpha_0/2}{x_i \sin(\pi/7+\alpha_0/2)} - \cos \pi/7} & i \text{ even} \\ \arctan \dfrac{\sin \pi/7}{\frac{\sin \alpha_0/2}{x_i \sin(\pi/7+\alpha_0/2)} \frac{\sin(\pi/7+\pi/6)}{\sin \pi/6} - \cos \pi/7} & i \text{ odd} \end{cases}$$

The Formula for $\psi_i'(0)$

Lemma 5.19. *For all $i = 0, 1, 2, \ldots, n$ at $\varphi = 0$, we have $\psi_{i+1}' = b_i \gamma_i' + a_i \varphi_i'$ where*

$$b_i = -\frac{\tan \frac{\alpha_{i+1}}{2}}{\tan(\frac{\alpha_{i+1}}{2} - \sigma_{i+1})}$$

$$a_i = -\tan \frac{\alpha_{i+1}}{2} \left(\frac{\sin\left(\frac{\pi}{7} + \sigma_{i+1}\right) \sin\left(\frac{\pi}{7} + \sigma_{i+1} + \tau_i\right)}{\sin \tau_i} + \frac{\frac{1}{2} - \frac{\sin(\tau_i + 2\pi/7 + 2\sigma_{i+1})}{2 \sin \tau_i}}{\tan(\frac{\alpha_{i+1}}{2} - \sigma_{i+1})} \right)$$

Proof. Consider the two cases in Figure 5.8. We will cover the first case in detail (i even). The other case, as given the lower of the two figures, can be deduced in the same way (the pictures only differ in the size of the angles, the underlying setup of polygons is the same). For this first case, Figure 5.13 gives a more detailed overview.

ψ_i is a particular angle in the given hexagon. The angles κ_i and τ_i don't change under φ and neither does K (it is the length of the sides of the equilateral triangles over the outer circle). Note the following: If we consider the length L_i and the angles φ_i, γ_i, δ_i, then there is a one-to-one correspondence (within an open set) between tuples $(L_i, \varphi_i, \gamma_i, \delta_i)$ and hexagons (as long as other angles and lengths remain unchanged as mentioned above).

Since these quantities uniquely define the hexagon and since ψ_{i+1} is an angle defined by the hexagon, we arrive at

$$\psi_{i+1}' = \frac{\partial \psi_{i+1}}{\partial L_i} L_i' + \frac{\partial \psi_{i+1}}{\partial \gamma_i} \gamma_i' + \frac{\partial \psi_{i+1}}{\partial \delta_i} \delta_i' + \frac{\partial \psi_{i+1}}{\partial \varphi_i} \varphi_i'$$

As usual, we consider these derivatives at $\varphi = 0$. The proof of the previous lemma established that in that case $\gamma_i' = -\delta_i'$. Also note that the picture is symmetric at $\varphi = 0$ and therefore a change in L_i will not affect ψ_i. It follows that $\frac{\partial \psi_{i+1}}{\partial L_i}$ at $\varphi = 0$. Combining all these, we arrive at

$$\psi_{i+1}' = \left(\frac{\partial \psi_{i+1}}{\partial \gamma_i} - \frac{\partial \psi_{i+1}}{\partial \delta_i} \right) \gamma_i' + \frac{\partial \psi_{i+1}}{\partial \varphi_i} \varphi_i'$$

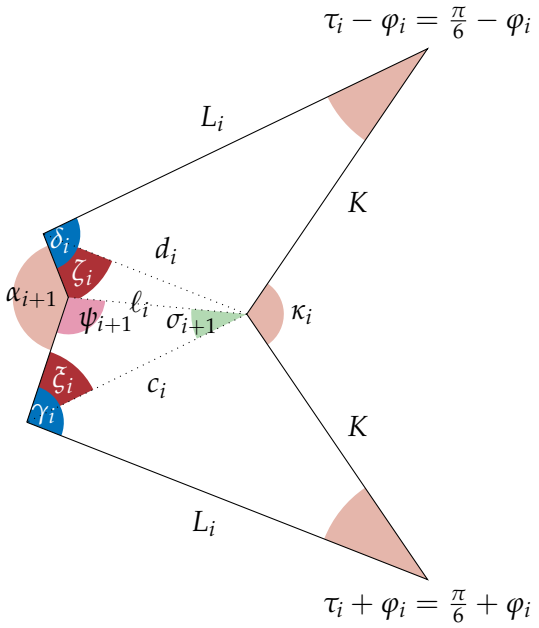

Figure 5.13: A detailed overview of a part of Figure 5.8

So we are left to show that

(a) $b_i = \left(\dfrac{\partial\psi_{i+1}}{\partial\gamma_i} - \dfrac{\partial\psi_{i+1}}{\partial\delta_i}\right) = -\dfrac{\tan\frac{\alpha_{i+1}}{2}}{\tan(\frac{\alpha_{i+1}}{2} - \sigma_{i+1})}$

(b) $a_i = \dfrac{\partial\psi_{i+1}}{\partial\varphi_i} = -\tan\dfrac{\alpha_{i+1}}{2}\left(\dfrac{\sin\left(\frac{\pi}{7}+\sigma_{i+1}\right)\sin\left(\frac{\pi}{7}+\sigma_{i+1}+\tau_i\right)}{\sin\tau_i} + \dfrac{\frac{1}{2} - \frac{\sin(\tau_i+2\pi/7+2\sigma_{i+1})}{2\sin\tau_i}}{\tan(\frac{\alpha_{i+1}}{2}-\sigma_{i+1})}\right)$

To do so, we will make extensive use of trigonometric identities and laws.

The law of sines provides

$$\ell_i = c_i\frac{\sin\xi_i}{\sin\psi_{i+1}}$$

$$\ell_i = d_i\frac{\sin\zeta_i}{\sin(4\pi-\gamma_i-\delta_i-(\tau_i+\varphi_i)-(\tau_i-\varphi_i)-(2\pi-\kappa_i)-\psi_{i+1})}$$

$$\Rightarrow c_i\sin\xi_i\sin(4\pi-\gamma-\delta-2\tau_i-(2\pi-\kappa_i)-\psi_{i+1}) = d_i\sin\zeta_i\sin\psi_{i+1}$$

(a) Deriving with respect to γ_i yields

$$\text{deriv. w.r.t. } \gamma_i \begin{cases} c_i\cos\xi_i\ \xi_i'\sin(4\pi-\gamma_i-\delta_i-2\tau_i-(2\pi-\kappa_i)-\psi_{i+1}) \\ +c_i\sin\xi_i\cos(4\pi-\gamma_i-\delta_i-2\tau_i-(2\pi-\kappa_i)-\psi_{i+1})\ (-1-\psi_{i+1}') \\ = d_i\sin\zeta_i\ \cos\psi_{i+1}\ \psi_{i+1}' \end{cases}$$

We are considering values at $\varphi = 0$. Due to symmetry

$$\xi_i = \zeta_i \quad c_i = d_i \quad \psi_{i+1} = 4\pi-\gamma-\delta-2\tau_i-(2\pi-\kappa_i)-\psi_{i+1} = \pi - \frac{\alpha_{i+1}}{2}$$

Also, $\xi_i = \gamma_i + \theta$ where θ is an angle that doesn't change under γ_i. Therefore (since we are currently considering derivatives with respect to γ_i) we have $\xi_i' = 1$. Combining all these, we arrive at:

$$\text{derivatives w.r.t. } \gamma_i \begin{cases} c_i\cos\xi_i\ \sin\frac{\alpha_{i+1}}{2} - c_i\sin\xi_i\ \cos\frac{\alpha_{i+1}}{2}\ (-1-\psi_{i+1}') \\ = -c_i\sin\xi_i\ \cos\frac{\alpha_{i+1}}{2}\ \psi_{i+1}' \\ \text{which can be simplified to} \\ \cot\xi_i\ \tan\frac{\alpha_{i+1}}{2} - (-1-\psi_{i+1}') = -\psi_{i+1}' \end{cases}$$

So we finally arrive at

$$\frac{\partial \psi_{i+1}}{\partial \gamma_i} = -\frac{1}{2}\left(\cot \xi_i \tan \frac{\alpha_{i+1}}{2} + 1\right)$$

Note that at $\varphi = 0$, we have $\pi = \xi_i + \sigma_{i+1} + \psi_{i+1} = \xi_i + \sigma_{i+1} + \pi - \frac{\alpha_{i+1}}{2}$ and therefore $\cot \xi_i = \cot(\frac{\alpha_{i+1}}{2} - \sigma_{i+1})$, so we can rewrite this as

$$\frac{\partial \psi_{i+1}}{\partial \gamma_i} = -\frac{1}{2}\left(\frac{\tan \frac{\alpha_{i+1}}{2}}{\tan(\frac{\alpha_{i+1}}{2} - \sigma_{i+1})} + 1\right)$$

Very similar deductions based on derivatives with respect to δ_i allow us to arrive at

$$\frac{\partial \psi_{i+1}}{\partial \delta_i} = \frac{1}{2}\left(\frac{\tan \frac{\alpha_{i+1}}{2}}{\tan(\frac{\alpha_{i+1}}{2} - \sigma_{i+1})} - 1\right)$$

The claim for b_i follows.

(b) We return to the identity based on the law of sines from above, but will now consider derivatives with respect to φ_i. Note that this time, c_i, d_i, ξ_i and ζ_i vary whereas γ_i and δ_i are constant.

$$\text{deriv. w.r.t. } \varphi_i \begin{cases} c_i' \sin \xi_i \sin(4\pi - \gamma_i - \delta_i - 2\tau_i - (2\pi - \kappa_i) - \psi_{i+1}) \\ +c_i \cos \xi_i \ \xi_i' \sin(4\pi - \gamma_i - \delta_i - 2\tau_i - (2\pi - \kappa_i) - \psi_{i+1}) \\ +c_i \sin \xi_i \cos(4\pi - \gamma_i - \delta_i - 2\tau_i - (2\pi - \kappa_i) - \psi_{i+1}) \ (-\psi_{i+1}') \\ = d_i' \sin \zeta_i \sin \psi_{i+1} + d_i \cos \zeta_i \ \zeta_i' \sin \psi_{i+1} + d_i \sin \zeta_i \cos \psi_{i+1} \ \psi_{i+1}' \end{cases}$$

We are considering values at $\varphi = 0$. Due to symmetry

$$\xi_i = \zeta_i \qquad c_i = d_i \qquad c_i' = -d_i' \qquad \xi_i' = -\zeta_i'$$
$$\psi_{i+1} = 4\pi - \gamma_i - \delta_i - 2\tau_i - (2\pi - \kappa_i) - \psi_{i+1} = \pi - \frac{\alpha_{i+1}}{2}$$

Combining all these, we arrive at

$$\text{deriv. w.r.t. } \varphi_i \begin{cases} c_i' \sin \xi_i \sin \frac{\alpha_{i+1}}{2} + c_i \cos \xi_i \ \xi_i' \sin \frac{\alpha_{i+1}}{2} + c_i \sin \xi_i \cos \frac{\alpha_{i+1}}{2} \ \psi_{i+1}' \\ = -c_i' \sin \xi_i \sin \frac{\alpha_{i+1}}{2} - c_i \cos \xi_i \ \xi_i' \sin \frac{\alpha_{i+1}}{2} - c_i \sin \xi_i \cos \frac{\alpha_{i+1}}{2} \ \psi_{i+1}' \\ \text{and therefore} \\ c_i' \sin \xi_i \sin \frac{\alpha_{i+1}}{2} + c_i \cos \xi_i \ \xi_i' \sin \frac{\alpha_{i+1}}{2} + c_i \sin \xi_i \cos \frac{\alpha_{i+1}}{2} \ \psi_{i+1}' = 0 \\ \text{which can be solved for} \\ \psi_{i+1}' = -\tan \frac{\alpha_{i+1}}{2}\left(\frac{c_i'}{c_i} + \cot \xi_i \ \xi_i'\right) \end{cases} \tag{5.1}$$

We now have to find c_i'/c_i and ξ_i'. We start with c_i'/c_i. Recall that we are still considering derivatives with respect to φ_i. The law of cosines gives us

$$\text{derivatives w.r.t. } \varphi_i \begin{cases} c_i^2 = K^2 + L_i^2 - 2KL_i\cos(\tau_i + \varphi_i) \\ \Rightarrow 2c_ic_i' = 2KL_i\sin(\tau_i + \varphi_i) \\ \Rightarrow \frac{c_i'}{c_i} = \frac{K}{c_i}\frac{L_i}{c_i}\sin(\tau_i + \varphi_i) \end{cases}$$

At $\varphi = 0$, we have $\varphi_i = 0$ as well as

$$\frac{K}{c_i} = \frac{\sin(\gamma_i - \xi_i)}{\sin\tau_i} \quad \frac{L_i}{c_i} = \frac{\sin(\pi - (\gamma_i - \xi_i) - \tau_i)}{\sin\tau_i} = \frac{\sin(\gamma_i - \xi_i + \tau_i)}{\sin\tau_i}$$

We finish with finding ξ_i' (still as a derivative with respect to φ_i). We invoke the law of tangents for the triangle with sides c_i, K, L_i.

$$\begin{aligned} \frac{L_i - K}{L_i + K} &= \frac{\tan(\frac{1}{2}(\pi - (\tau_i + \varphi_i) - (\gamma_i - \xi_i) - (\gamma_i - \xi_i))}{\tan(\frac{1}{2}(\pi - (\tau_i + \varphi_i) - (\gamma_i - \xi_i) + (\gamma_i - \xi_i))} \\ &= \frac{\tan(\frac{1}{2}(\pi - \tau_i - \varphi_i - 2(\gamma_i - \xi_i)))}{\tan(\frac{1}{2}(\pi - \tau_i - \varphi_i))} \end{aligned}$$

Note that the left-hand side doesn't change under a change of φ_i. So if we derive (and subsequently multiply by the denominator), we get

$$\text{deriv. w.r.t. } \varphi_i \begin{cases} 0 = \sec^2(\frac{1}{2}(\pi - \tau_i - \varphi_i - 2(\gamma_i - \xi_i)))(-1 + 2\xi_i')\tan(\frac{1}{2}(\pi - \tau_i - \varphi_i)) \\ \quad + \tan(\frac{1}{2}(\pi - \tau_i - \varphi_i - 2(\gamma_i - \xi_i)))\sec^2(\frac{1}{2}(\pi - \tau_i - \varphi_i)) \\ \\ \text{Elementary trigonometric identities lead us to} \\ \xi_i' = \frac{1}{2} - \frac{\sin(\pi - \tau_i - \varphi_i - 2(\gamma_i - \xi_i))}{2\sin(\pi - \tau_i - \varphi_i)} \end{cases}$$

At $\varphi = 0$, we have $\varphi_i = 0$. So we get

$$\text{derivatives w.r.t. } \varphi_i \begin{cases} \xi_i' = \dfrac{1}{2} - \dfrac{\sin(\tau_i + 2(\gamma_i - \xi_i))}{2\sin\tau_i} \end{cases}$$

We now have explicit formulas for c_i'/c_i as well as ξ_i'. We can substitute them into Equation 5.1 and also use the following two identities at $\varphi = 0$ (see Figure 5.12):

$$\begin{aligned} &\xi_i = \pi - \psi_{i+1} - \sigma_{i+1} = \frac{\alpha_{i+1}}{2} - \sigma_{i+1} \\ &\pi - (\gamma_i - \xi_i) + \pi/7 + \sigma_{i+1} = \pi \;\Rightarrow\; \gamma_i - \xi_i = \pi/7 + \sigma_{i+1} \end{aligned}$$

Doing so, we arrive at the desired formula for $a_i = \frac{\partial\psi_{i+1}}{\partial\varphi_i}$ □

BIBLIOGRAPHY

[AA76] W. K. Allard and F. J. Almgren, Jr., *The structure of stationary one dimensional varifolds with positive density*, Invent. Math. **34** (1976), no. 2, 83–97. MR 0425741

[BK] Spencer Becker-Kahn, unpublished.

[GL] Larry Guth and Yevgeny Liokumovich, in preparation.

[GY06] Jonathan L. Gross and Jay Yellen, *Graph theory and its applications*, second ed., Discrete Mathematics and its Applications (Boca Raton), Chapman & Hall/CRC, Boca Raton, FL, 2006. MR 2181153

[Hep64] Aladár Heppes, *Isogonale sphärische Netze*, Ann. Univ. Sci. Budapest Eötvös, Sect. Math. **7** (1964), 41–48. MR 0173193

[HM96] Joel Hass and Frank Morgan, *Geodesic nets on the* 2*-sphere*, Proc. Amer. Math. Soc. **124** (1996), no. 12, 3843–3850. MR 1343696

[IT94] Alexandr O. Ivanov and Alexei A. Tuzhilin, *Minimal networks*, CRC Press, Boca Raton, FL, 1994, The Steiner problem and its generalizations. MR 1271779

[IT16] Alexander O. Ivanov and Alexey A. Tuzhilin, *Minimal networks: a review*, Advances in dynamical systems and control, Stud. Syst. Decis. Control, vol. 69, Springer, [Cham], 2016, pp. 43–80. MR 3616371

[Kli82] Wilhelm Klingenberg, *Riemannian geometry*, de Gruyter Studies in Mathematics, vol. 1, Walter de Gruyter & Co., Berlin-New York, 1982. MR 666697

[Mem15] Yashar Memarian, *On the maximum number of vertices of critically embedded graphs*, International Electronic Journal of Geometry **8** (2015), 168 – 180. MR 3418465

[NP19] Alexander Nabutovsky and Fabian Parsch, *Geodesic nets: Some examples and open problems*, arXiv:1904.00483 (2019).

[NR07] Alexander Nabutovsky and Regina Rotman, *Shapes of geodesic nets*, Geom. Topol. **11** (2007), 1225–1254. MR 2326944

[Par19a] Fabian Parsch, *An example for a nontrivial irreducible geodesic net in the plane*, arXiv:1902.07872 (2019).

[Par19b] ———, *Geodesic nets with three boundary vertices*, Journal of Differential Geometry **to appear** (2019).

[Rot] Regina Rotman, *Short wide geodesic loops on closed riemannian manifolds*, in preparation.

[Rot11] ———, *Flowers on Riemannian manifolds*, Math. Z. **269** (2011), no. 1-2, 543–554. MR 2836083

COLOPHON

This thesis was typeset using the typographical look-and-feel `classicthesis` developed by André Miede and Ivo Pletikosić.

The style was inspired by Robert Bringhurst's seminal book on typography "*The Elements of Typographic Style*".

All figures were produced by the author using TikZ.

[June 18, 2019 – final version – digital copy]